Electrocortical Activation and Human Brain Mapping

by

Erik Edwards

B.S. (University of California, San Diego) 1999

A dissertation submitted in partial satisfaction of the

requirements for the degree of

Doctor of Philosophy

in

Psychology

in the

Graduate Division

of the

University of California, Berkeley

Committee in charge:

Professor Robert T. Knight, Chair

Professor Frédéric E. Theunissen

Professor Jeffery A. Winer

Spring, 2007

Electrocortical Activation and Human Brain Mapping

by Erik Edwards

Abstract

Electrocortical Activation and Human Brain Mapping

by

Erik Edwards

Doctor of Philosophy in Psychology

University of California, Berkeley

Robert T. Knight, Chair

This thesis concerns the question of how to map the cerebral cortex on the basis of its electrical activity. A major question in neuroscience is the question of localization of function, and electrical means of functional mapping were attempted as early as 1875. By the late 1930s, a consistent pattern of "electrocortical activation" was identified and used for functional mapping in animal studies. Because this knowledge has been largely forgotten, an historical survey of these attempts is given in order to establish a firm empirical grounding for using this method of mapping. Such electrocortical mapping is of vital clinical interest in neurosurgical approaches to tumor and epilepsy treatment. Original studies are presented involving the recording of electrical potentials directly from the cortical surface in awake neurosurgical patients. These studies involve the reactions to simple auditory stimuli (tones and syllables) in tumor patients, as well as the performance of a complex language task (verb generation) in epilepsy patients. Time-frequency analyses of these data reveal the pattern of electrocortical activation, and consistently show activity in the frequency range ~60-300 Hz ("high-gamma") as the most specific and powerful sign of cortical activity.

This dissertation is dedicated to those who still believe in the sanctity of science;
and to my parents, Dale and Eva Edwards, for my original inspiration to seek truth;
and to my wife, Elizabeth A. Shaw, for her love and support.

Fundamentally all of us strive for the same goal: to learn to read the truth in the great book of nature of which man and his brain are but a part.

-Hans Berger (1936)

Contents

Acknowledgements

The following people are acknowledged for their contributions to the experimental work presented in this dissertation:

Nicholas M. Barbaro

Mitchel S. Berger

Ryan Canolty

Clay Clayworth

Sarang S. Dalal

Leon Y. Deouell

Richard Fechter

Heidi Kirsch

Scott Makeig

Sri S. Nagarajan

Maryam Soltani

Chapter 1: Introduction

Terminology and abbreviations

Electroencephalography (EEG) is the measurement of electrical voltages from the brain, or sometimes current, as in some older studies. The EEG in animals was independently discovered by three 19th century experimentalists (Caton 1875; Danilevsky 1877; Beck 1891), and Hans Berger (1929) first demonstrated the scalp EEG in humans. Because voltage is only defined with reference to two points in space, EEG requires the placement of at least two electrodes, with at least one in contact with the brain or a nearby structure such as the dura or scalp. The electrodes can range in size from microelectrodes with submillimeter contact area to the giant foil electrodes used occasionally by Hans Berger that covered some 70 cm^2 of the scalp. All of these recording methods will be referred to with the general term EEG. Sometimes "EEG" is used to refer to recordings only from the scalp, but I use "EEG" in the more general sense, and specify "scalp EEG" when appropriate.

Electrocorticography (ECoG) is EEG taken directly from the cortex, usually the cortical surface. ECoG was first performed in humans during the 1930s in Germany (Berger 1931; Tönnies 1934; Foerster and Altenburger 1935; Kornmüller 1935; Berger 1936) and England (Adrian and Matthews 1934b; Walter 1936). These are technically epipial recordings, since the pia is only a couple of cells thick and remains intact. Recordings from the dura have not earned a special term and will be referred to as "epidural EEG".

Local field potential (LFP) recordings entail electrical recordings with microelectrodes in contact with the extracellular space. These are referred to as LFP recordings only if frequencies below ~1 kHz are recorded. Recordings only for the purpose of detecting **action potential (AP)**

spikes typically filter the incoming data above ~0.3-1 kHz, and are not included under the terms "LFP" or "EEG".

Magnetoencephalography (MEG) is the measurement of brain magnetic fields, introduced circa 1970 (Cohen 1968; 1972; Brenner et al. 1975; Reite et al. 1976). MEG is typically done with sensors outside of the scalp in humans, although occasional MEG recordings have been done over the exposed cortex of animals.

Positron emission tomography (PET) is a functional imaging technique to measure blood flow or other metabolic parameters, introduced in the 1970s. Because the metabolic and hemodynamic responses of the brain are slow (on the order of seconds), PET has a poor temporal resolution compared to electromagnetic measures of the brain's activity.

Functional magnetic resonance imaging (fMRI) is a functional imaging technique introduced in the early 1990's (Ogawa et al. 1990; Bandettini et al. 1992; Kwong et al. 1992; Ogawa et al. 1992). Typically, this involves measuring the **blood oxygen level dependent (BOLD)** signal, the physics of which is based on the differential magnetic effects of oxygenated vs. deoxygenated hemoglobin in the blood. Although fMRI boasts excellent spatial coverage and resolution, its temporal resolution is poor due to the relative sluggishness of hemodynamic responses.

19th century origins of EEG

Perhaps the dominant question in the history of neuroscience has been the question of localization. To what extent are separate functions localized to separate areas of the brain? Can we make a map of the cortex? And if so, by what means? After the premonitory but forgotten ideas of the Swedish thinker Emanuel Swedenborg (1740-1741), it was the phrenologists of the early 19th century who first advanced a version of localizationalism. Led initially by the Austrians Gall and Spurzheim (1810-1819), the phrenologists used highly dubious methods, such as inferring cortical localization from cranial features. Although highly popular, phrenology quickly fell into disrepute amongst the scientists of the day. The eminent French scientist Flourens was the first serious critic of phrenology, and advanced instead a theory of cortical "equipotentiality" (Flourens 1824) whereby the cortex functions as a whole. However, following the work of French neurologists Bouillaud (1825) and Broca (1861) on patients with cortical lesions, cortical localization gained wide scientific acceptance. The electrical stimulation experiments of the German scientists Fritsch and Hitzig (1870) demonstrated the localization of motor cortex in dog with a somatotopic organization. The British experimentalist Ferrier (1876) improved stimulation methods and extended these observations to other systems and species. However, the doctrine of cortical localization was not universally accepted and the debate continued well into the 20th century. For example, Goltz (1892) criticized "the obvious shipwreck of the doctrine of small, outlined centers" and advanced instead a model of "mixed specificity". This was one of the earliest appearances of the contemporary viewpoint (also, Munk 1890; Lashley 1929; Luria 1973) – that basic sensory and motor functions are clearly localized, whereas more complex functions are distributed among interacting cortical networks with overlap of function within individual areas. See Finger (1994) for an excellent survey of this debate.

It was in the context of this debate on cortical localization that the English physician Richard Caton performed arguably the first functional neuroimaging experiment (Caton 1875).

Although prior studies had looked at the effects of lesions or electrical stimulation, his was the first to measure the activity of the intact brain for the purpose of localizing function. He placed non-polarizable electrodes on the cortical surface in monkey and rabbit, and connected these to a galvanometer for measuring electrical currents. This was also the first EEG (and ECoG) experiment. Amplification was achieved by a mirror connected to the galvanometer, which reflected a beam of light to a scale on the distant wall of the room. Caton concerned himself primarily with the localization of motor and sensory areas, and in particular he sought to use "negative variation" as a sign of local activity. This theme appeared throughout his work on the EEG (Caton 1875; 1877; 1887); here is an example from his first account:

> "The electric currents of the grey matter appear to have a relation to its function. When any part of the grey matter is in a state of functional activity, its electric current usually exhibits negative variation. For example, on the areas shown by Dr. Ferrier to be related to rotation of the head and to mastication, negative variation of the current was observed to occur whenever those two acts respectively were performed." –Richard Caton (1875).

Figure 1.1. Richard Caton. English physician who discovered the electrical activity of the cortex. Photograph from Brazier (1961).

The concept of negative variation originated with the renowned physiologist Emil du Bois-Reymond, whose famous laboratory in Berlin trained a long list of other famous physiologists. Du Bois-Reymond was a skilled instrument maker and introduced many technical advances, such as improved galvanometers and the use of non-polarizable electrodes (which do

not introduce an artificial current by virtue of their composition). Du Bois-Reymond (1848-1884) observed negative variation at the cut ends of animal nerves (now known to be an injury current) and during nerve activity (for which he is credited with the discovery of the action potential). Du Bois-Reymond's model for the negative variation turned out to be wrong - he was writing before electrons and modern electromagnetism were known – and is not covered here. However, the basic idea can be appreciated from a modern biophysical perspective, which emerged in the early 1900s (e.g., Bernstein 1912; Höber 1926; Berger 1932a). The resting intracellular potential of a nerve cell is negative, and excitation of the cell results in a depolarization of this resting potential. This is due to the net movement of positive charge carriers into the cell and/or a net movement of negative charge carriers outside the cell. With the excitation of a large population of cells, there will be a net increase in positivity in the intracellular compartment, and a corresponding increase of negativity in the extracellular compartment. LFP or EEG electrodes in contact with the extracellular compartment would then record a negative variation as a sign of excitation. Although dipolar theory (introduced into the EEG literature in the 1940s) would later show that negativity is not always a sign of activity, this concept remains useful. For example, gamma oscillations lock to the negative phase of slow oscillations, and AP firing locks in turn to the negative phase of gamma oscillations. This notion of negativity as activity persists today also in the prevalent convention of plotting negativity upwards in many EEG figures.

Two Eastern European scientists independently discovered the EEG and, like Caton, their main concern was localization of function. Also like Caton, they used the methods of du Bois-Reymond (galvanometer and non-polarizable electrodes) and worked with the notion of negative variation as a sign of activation. The first was the Ukrainian-born Vasili Danilevsky, who completed his university and medical training in Russia. His work on the EEG of curarized dogs appeared in his doctoral thesis (1877) and in a later, fuller account (1891). According to the historian Brazier (1961), "he too found a negative variation with various kinds of sensory

stimulation and observed that these effects were obtained from the posterior lobes of the brain and in most cases from the side opposite to the one in which the excitation had been applied."

The third independent discoverer of the EEG was a Polish doctoral student Adolf Beck. He was drawn to the study of the EEG by a prize offered by his teacher Napoleon Cybulski[1] and some others of the Krakow Medical Faculty in 1888. The theme for the prize was – "To determine whether it is possible to demonstrate a state of activity in nerve centres by using the so-called negative variation…" (translation from Brazier, 1961). Beck combined electrical recording and stimulation to test his assumption that "the development of electro-negativity in an area of cortex really indicates the creation of an active state in centres located there" (translation from Brazier, 1961). Some of Beck's other important observations are treated below.

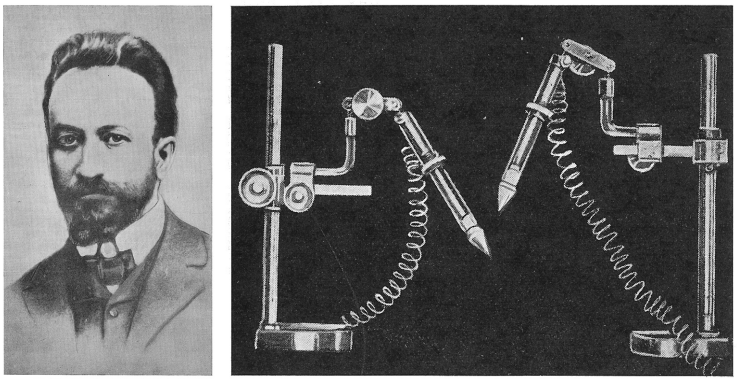

Figure 1.2. Left: Photograph of Adolf Beck at the time of his discovery of the EEG. **Right:** Photograph of the modified du Bois-Reymond, non-polarizable electrodes used by Beck. Both photographs from Brazier (1961).

[1] Napoleon Cybulski was born in Lithuania and trained in Russia under Tarkhanov before moving to Poland. Tarkhanov discovered of the galvanic skin response and suggested that the galvanic method could be used to study localizations in the brain. Tarkhanov, like many other European physiologists of his generation, had studied in Berlin under du Bois-Reymond.

Ultimately, the notion of using negative variation as a means of functional mapping in the cortex would be questioned. Danilevsky (1891) and subsequent investigators found that positive and mixed responses could also be obtained in response to stimulation, and so negativity could not be used as the exclusive indicator of activity. The rise of dipolar theory in the 1940s would also show that the interpretation of negativity at the cortical surface is more complicated. What aspect of the EEG can be used as a sign of activity? The answer would emerge in a second major theme to develop in the early investigations of the EEG – the existence of spontaneous fluctuations, or background rhythms, of cortical currents.

In his first report on the EEG, Caton (1875) noted that: "Feeble currents of varying direction pass through the multiplier when the electrodes are placed on two points of the external surface, or one electrode on the grey matter, and one on the surface of the skull." From this and other statements, he clearly measured the fluctuations of potential from the brain, and not only the D.C. currents[2]. According to Brazier (1961), Danilevsky (1877) "observed changes in the electrical potential of the brain that were independent of stimulation. He noted that the brain had its own "spontaneous" activity." Beck (1891) also described "rhythmic oscillations" in the EEG, and a subsequent chapter will show that he was the first to note their changes with sensory stimulation. These early investigators (and indeed modern investigators!) did not know how to interpret these spontaneous oscillations. This thesis concerns itself almost exclusively with these spontaneous brain rhythms, rather than the evoked changes in potential level, such as the negative variation. I will argue, and present data to show, that alterations in these background rhythms are a powerful means to realizing the 19th century goal of cortical localization. This goal is not only of long-standing theoretical importance, it is central to the clinical motivation of the research presented here.

[2] It is a misconception that galvanometers only measure D.C. current. I estimate the frequency response of Caton's galvanometer to extend up to at least 5 or 10 Hz. Later galvanometers, like the Einthoven string galvanometer, were quite sensitive and had frequency responses up to 100 Hz or greater.

Clinical Motivation

The research presented here is part of a collaborative project with neurosurgeons at the University of California, San Francisco. Our opportunity to record electrical activity directly from the cortical surface (ECoG) has its background in the radical resectionist approach to tumor management and the associated cortical mapping. In this approach, the cortex is exposed by craniotomy and the pathologic tissue is resected as fully and early as possible.

Within neurosurgery, there is a debate concerning what role craniotomy and resection should play, versus more "conservative" management techniques like chemo- or radio-therapy. Several findings support the radical resectionist approach. First, there is often no sharp boundary between tumor and normal brain. There is functional tissue even within the tumor nidus (Ojemann et al. 1996; Skirboll et al. 1996), and cancer cells are found intermingled with neurons surrounding the tumor. Consistent with this wide dispersion of tumor cells, the risk of recurrence decreases with an aggressive early procedure that removes as much tumor and surrounding tissue as possible (Berger et al. 1994). Aggressive tumor resection improves patient outcome in several ways: reduced chance of seizures, relief of dysfunction due to mass effects, reduced time to tumor progression, improved postoperative lifestyle (such as probability of caring for oneself and returning to work), and increased survival times (Berger 1995).

The drawback to maximal resections is that the risk of postoperative functional deficits increases. Thus, the radical resectionist must make special effort to spare as much functional ('eloquent') cortex as possible. Eloquent cortex consists of primary motor and language areas, lesions to which produce obvious postoperative behavioral deficits. To ameliorate such deficits, intraoperative brain mapping with electrical stimulation is used to identify functional cortex

(Berger 1996). This technique was developed in its modern form by Wilder Penfield and colleagues in the 1930s through 1950s (Penfield and Boldrey 1937; Penfield and Erickson 1941; Penfield and Rasmussen 1950; Penfield and Jasper 1954). This was primarily in the context of epilepsy surgery , and Penfield proposed a "radical" approach to epilepsy treatment (Penfield 1930). The data in this thesis comes from both tumor and epilepsy patients.

Unfortunately, electrical stimulation is invasive and can induce seizures. Indeed, the clinical rationale for ECoG electrodes is seizure monitoring. It has long been hoped that the ECoG recordings themselves, which are entirely passive and without risk to the patient, could be used for functional mapping. How can ECoG recordings be used to make functional maps of cortex? In performing a given task, is there any sign from a passive electrical recording that the underlying cortical tissue is active? My primary thesis is that there is such a pattern of cortical activation to be found in the ECoG. I term this pattern "electrocortical activation" or "EEG activation" (it is also present to some degree in scalp recordings), and show that it embodies a long tradition of empirical observations.

Chapter 2: EEG Activation

EEG activation: early observations

In the previous chapter, we saw that the three independent discoverers of the EEG (Caton, Danilevsky, and Beck) had each noted that the cortex exhibited spontaneous fluctuations of current. Although all three studied the effects of sensory stimulation, with a focus on the negative variation as a sign of local activation, only Beck (1891) noted the change of the spontaneous fluctuations consequent to stimulation. According to Brazier (1961), "in his very first experiment (on a rabbit) Beck found an oscillating potential difference between two electrodes placed on the occipital cortex. The fluctuations ceased when he uncovered the animal's eyes and lit a magnesium flare, and they also ceased with stimulation of the hind leg." Beck noted that "this phenomenon was not the consequence of light stimulation specifically for it appeared with every kind of stimulation of other afferent nerves." Thus, he had discovered the non-specific desynchronization of cortical activity (Brazier, 1961; the terms "non-specific" and "desynchronization" will be treated below). In a later discussion, Beck again notes that: "an important event which occurred in nearly all the experiments on stimulation of the cerebral cortex by any of the afferent nerves (and especially on stimulation of the sensory nerves of the skin) was the arrest of the intrinsic oscillations of the functional current" (Beck 1891; all translations from Polish by Brazier, 1961). Beck interpreted this arrest reaction as due to inhibition from other active areas. However, it will be seen later that the suppression of spontaneous activity is actually a counter-intuitive result of excitation and increased activity.

Between the three 19th century pioneers of the EEG and the discovery of the human EEG by Hans Berger (1929), a handful of studies appeared on the EEG of animals, mostly from Eastern Europe. For example, Beck's teacher, Napoleon Cybulski, made an early observation concerning the appearance of faster rhythms with peripheral stimulation (Cybulski and Jelenska-

Macieszyna 1914). By far the most noteworthy and influential student of the EEG during this period was the Ukrainian Vladimir Pravdich-Neminsky.

In a landmark study of 1913, in which he recorded EEG from dogs using non-polarizable electrodes and an Einthoven string galvanometer[3], Pravdich-Neminsky introduced several important advances and observations. First, he noted that "spontaneous current fluctuations can already be observed by derivation from the skull" (Pravdich-Neminsky's major reports were in German, and all translations here are my own). He monitored blood pressure and curarized the dogs (curare is a paralytic agent that eliminates voluntary muscle activity) to prove that his findings were not due to artifact. Hans Berger, who discovered the scalp EEG in humans, cited and acknowledged his debt to Pravdich-Neminsky for the idea of scalp recordings. Second, Pravdich-Neminsky was the first to report the frequency of the spontaneous fluctuations. He did this by counting the time intervals between successive peaks or troughs in the fluctuations, and taking the reciprocal (a method that persists in the animal EEG literature). With electrodes over the motor or visual areas, "the frequency of the fluctuations was in two cases calculated to be 12-14 per second," which may have been the dog alpha rhythm. Later he noted that they slowed to 4-7 Hz with asphyxia, and that the frequencies were as high as 35 Hz from the cortical surface. Third, he published the first photographs of the EEG (Figure 2.1). He confirmed and extended Beck's (1891) initial observation on the arrest of the spontaneous fluctuations with stimulation. He states that "if appreciable spontaneous fluctuations preceded the stimulation, then a diminishing effect [of the stimulation] was clearly noticed. Complete cessation of the fluctuations was not usually observed."

[3] Einthoven was the great Dutch pioneer of the EKG who introduced more sensitive galvanometers, known as Einthoven string galvanometers, with frequency responses of 100 Hz or higher. Pravdich-Neminsky was the first to use these sensitive instruments for the EEG.

Vladimir Pravdich-Neminsky
Ukrainian, 1879-1952

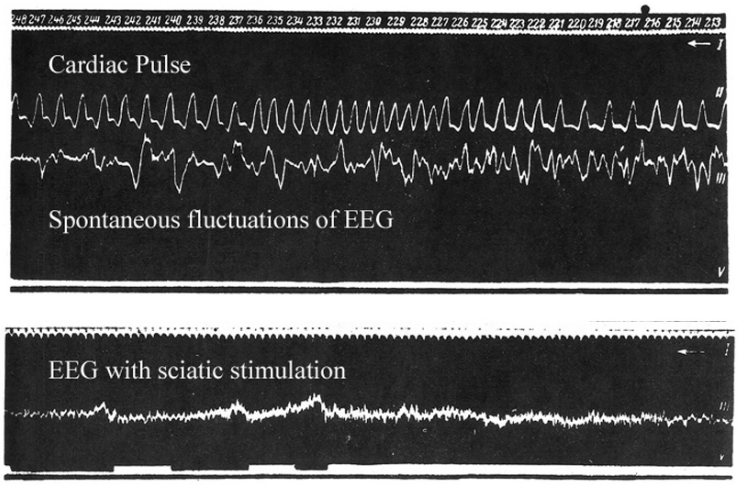

Figure 2.1. First published records of the EEG, from Pravdich-Neminsky (1913). These were made by reflecting a beam of light from the galvanometer to moving photographic film. In both photographs, time runs from right to left. **Top:** Spontaneous fluctuations of the dog EEG, which he reported to be around 12-14 Hz. The fluctuations can be seen to be independent of the cardiac pulse (top trace). **Bottom:** The dog EEG under conditions of sciatic stimulation. With each stimulus (bottom most trace), there is an upward deviation of the voltage. Although these appear as the traditional negative variation, he reported that both positive and negative, and multi-phasic, deviations occurred. Furthermore, the spontaneous fluctuations have been suppressed and appear to be replaced by fast activity (which appears at this time scale as essentially just a thickening of the trace). Photographs reproduced from Brazier (1961), with labeling added.

A final contribution was his attempt to categorize the EEG waves (Pravdich-Neminsky 1925, again studying dogs). His first two categories corresponded roughly to alpha and beta, and this was the first recognition that EEG fluctuations are a mixture of physiologically distinct processes separable at least in part by frequency. However, his lengthy discussion was difficult to understand in modern terms and is not discussed further.

Hans Berger on alpha and beta

In 1929, a little-known psychiatrist from Germany reported that electrical brain waves could be obtained from the human scalp (Figures 2.2 and 2.3). Although Pravdich-Neminsky (1925) had suggested the term "elektrocerebrogramm" for the EEG, Berger considered this term a "barbarism" as it combined Greek and Latin roots. He instead proposed "the name "electroencephalogram" for the curve which here for the first time was demonstrated by me *in man*" (all translations from Berger from Gloor 1969). The scientific world had not yet heard of the EEG, and Berger's 1929 report was largely ignored or greeted with skepticism. Berger remained cautious about his own findings for a time, and his first two reports concern themselves at length with the exclusion of respiratory, cardiac, muscle, and skin contributions to his recordings. With this motivation, he reported on a series of studies in 51 patients with skull defects, including recordings from needle electrodes inserted to the level of the dura in order to bypass skin and muscle. This same motivation led to the first human ECoG experiment, where Berger showed that electrical activity was generated in the cortical gray matter (Figure 2.4). Additional human ECoG results were presented in his 11th report (1936), with the purpose of proving that his "beta" waves were of cerebral rather than myogenic origin.

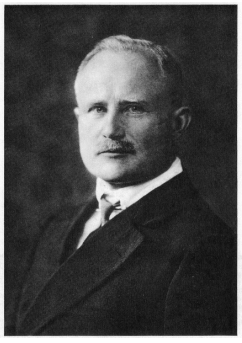

Figure 2.2. Hans Berger in 1925 at 53 years old, when he began his work on the human EEG. Photograph from Gloor (1969).

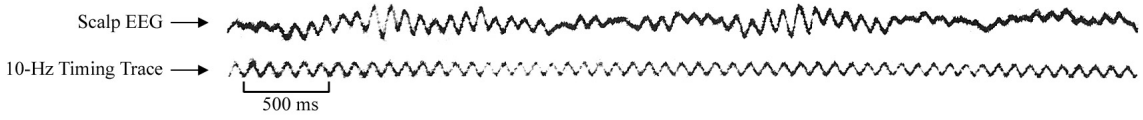

Figure 2.3 (previous page). First record of the human EEG, published in 1929. Berger recorded this in 1925, using a galvanometer and lead electrodes on the forehead and occiput. The subject was his 15 year-old son. Reproduced with labels added from Berger's 1st report, in Gloor (1969).

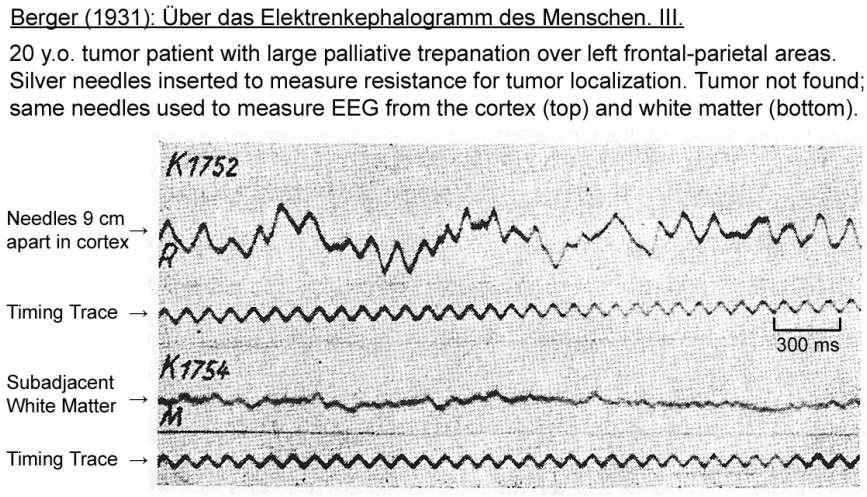

Figure 2.4. First human ECoG experiment, done with the primary motivation of showing that the scalp EEG was of cortical origin. Waves similar to the scalp EEG were found with needle electrodes in cortical gray matter, but the record was essentially flat from the subadjacent white matter. Reproduced, with labeling added, from Berger's 3rd report (1931) in Gloor (1969).

Berger went on to publish a series of 14 reports on the EEG (Berger 1929; 1930; 1931; Berger 1932a; Berger 1932b; 1933a; 1933b; 1933c; 1934; 1935; 1936; 1937a; 1937b; 1938), all with the same title "Über das Elektrenkephalogramm des Menschen" ("On the electroencephalogram of man"). These made many original theoretical and clinical contributions to electroencephalography and to neuroscience as a whole (Berger has been credited with the founding of *dynamical* neuroscience). I will only cover his distinction between alpha and beta, and his eventual distinction between the "passive" and "active" EEG.

In his 2nd report (1930), Berger introduced the Greek letters α and β to stand for waves with periods of ~90-120 ms and ~30-45 ms, respectively (corresponding to frequencies of ~8-11 Hz and ~22-33 Hz)[4]. The α waves (α-w) were best seen with the subject relaxed in the quiet with eyes closed. The α-w disappeared with sensory stimulation, replaced by β-w. This was first shown with a somatosensory stimulus (Figure 2.5), but also occurred for other stimuli. In experiments on reaction time with a warning signal, the EEG change would occur immediately after the warning signal. The EEG change would also habituate with repeated stimulation, suggesting a loss of interest in the stimuli. These and other observations led Berger (1930) to assert "that the directing of attention upon a stimulus causes these changes in the EEG." Berger confirmed this observation with sensory stimulation in subsequent reports, and remained with his interpretation that attention was the essential factor involved.

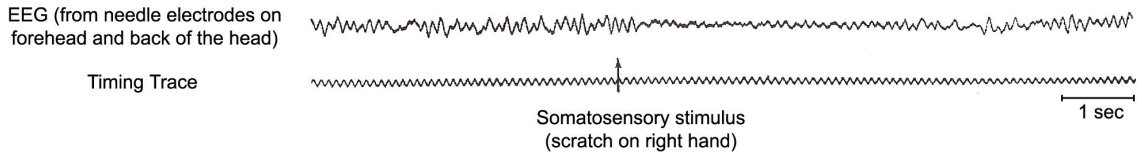

Figure 2.5. Disappearance of larger α-w with sensory stimulation, replaced by smaller β-w. Reproduced with labels added from Berger's 2nd report (1930), in Gloor (1969).

In his 3rd report (1931), Berger discusses recordings from the left frontal bone defect of a man doing mental multiplication: "The smaller β-w appear more often, replacing the α-w, as is usually the case with mental work." This observation was confirmed in two subsequent reports

[4] These pertained to scalp recordings, typically frontal-to-occipital, in normal subjects. Berger would come to use α to stand for any slow waves less than ~15 Hz (including frequencies that we would call "theta" or even "delta" today), and β to stand for any waves faster than ~15-20 Hz (including frequencies that we would call "gamma" today).

(1932a, 1937a). Figure 2.6 shows one example from his 16 year-old daughter doing mental arithmetic. Berger (1937b) found that caffeine or cocaine injections increased β activity. The β waves associated with stimulants or with mental work were said to go as high as 90 Hz, although his final report (1938) stated that he "hardly ever found β-w with a frequency above 50 Hz".

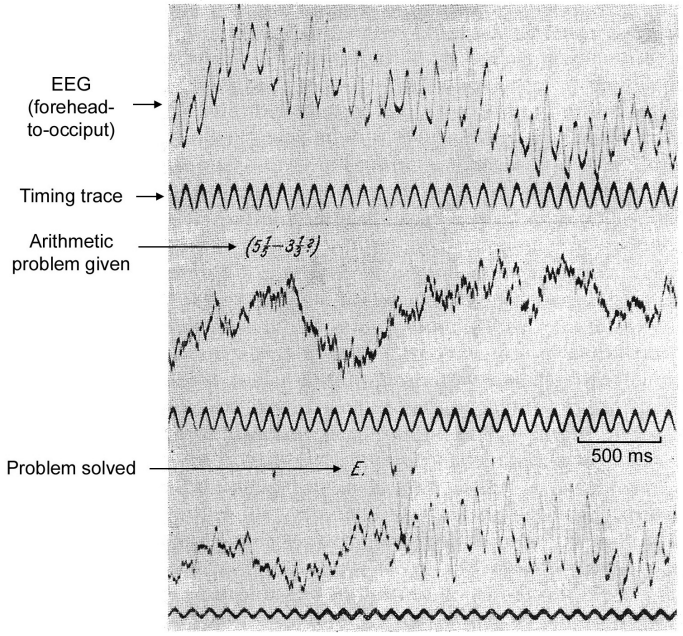

Figure 2.6. EEG changes with mental work. The α-w disappear when an arithmetic problem is given, replaced by smaller β-w, and return when the problem is solved. The slow drifts (~1 Hz and below) should be ignored. Reproduced with labels added from Berger's 12th report (1937a), in Gloor (1969).

From these results with sensory stimulation, mental work, and stimulants, Berger realized that the β-w represent a state of cortical activation. He states that β-w "represent concomitant phenomena of the psychophysiological activity of the cortex… they must be regarded as the material concomitant phenomena of *mental* processes!" (1937b). The α-w, on the other hand, are stated to be "concomitant phenomena of the automatic physiological cortical processes" (1938), what we today might term an "idling" process. In his final report (1938), he distinguishes between the *passive* EEG dominated by α-w, and the *active* EEG dominated by β-w. However, he rejected the notion that α-w reflect *vegetative* processes (Rohracher 1935); rather they reflect a different kind of activity, one of "undisturbed automatic cortical activity."

These opinions at the end of Berger's career are basically in accord with the modern view, but he did not always hold this view. He began with a particular fascination with the α-w and proposed initially that they represented active mental processes. Their disappearance with sensory stimulation was interpreted as reflecting an inhibitory process[5]. What caused Berger's rather sudden turn around in his 1937 reports? The answer was partly the accumulation of his own evidence, but his introductory and discussion sections make clear that the major factor was the appearance of experimental work from other investigators; Adrian and Matthews in England, Ectors and Bremer in Belgium, and Jasper in North America. Another factor was probably his acquisition in 1932 of an amplifier and oscillograph (see below), a much more sensitive system than his original galvanometer for studying the smaller, faster β-w.

Edgar Adrian and the desynchronization hypothesis

Sir Edgar Adrian, who worked at Cambridge in England, was one of history's great neurophysiologists and received the Nobel Prize in 1932 for pioneering work in nerve physiology and coding. Among his many contributions, he was the first to study action potentials of single nerve fibers (Adrian 1926; Adrian and Zotterman 1926) (prior studies, beginning with those of du Bois-Reymond in the mid-19th century, had looked at the compound action potentials of peripheral nerves composed of many individual nerve fibers). This work was largely the result of new advances in amplification technology, as Adrian himself acknowledged: "The history of electrophysiology has been decided by the history of electrical recording instruments" (Adrian 1932; cited in Finger 2000). Because this same technology was essential for the new EEG work done by Adrian and those in the subsequent sections, it is worth a brief digression to describe it.

---

[5] The specific sensory center would have shown an increase in α-w and would have inhibited much larger areas of cortex surrounding it, resulting in the overall flattening seen at the scalp. This is similar to Beck's (1891) interpretation, and both are related to the theory of *dominata* (initially developed in Russia by Ukhtomsky in the early 20th century), whereby active nervous centers come to inhibit, or dominate, surrounding areas.

Adrian's recording system consisted of vacuum tube amplifiers and a cathode-ray oscillograph. Vacuum tubes were developed during the First World War in radio applications, and were first used to build an amplifier for physiological research by Forbes (Forbes and Thacher 1920a; 1920b), a Harvard physiologist who had served as a naval officer. More amplification was required, and a three-stage amplifier was built by Gasser and Newcomer (1921) at Washington University in St. Louis. Adrian built his own amplifier after a visit from Forbes and based on instructions from Gasser. A much better display technology was also on the way, based on the cathode-ray tube invented by the German physicist Braun in 1897. This uses the deflection of a beam of electrons by an electric field, so there is no inertia and no moving mechanical parts (and therefore no practical limit on the frequency response of the system). The first cathode-ray oscillograph for physiological use was built by Gasser and Erlanger (1922), who would receive the Nobel Prize in 1944 for their technological achievements and work in peripheral nerves. Adrian used an improved oscillograph built in his Cambridge lab by Matthews (see Finger 2000 for an excellent survey of this period of technological advances).

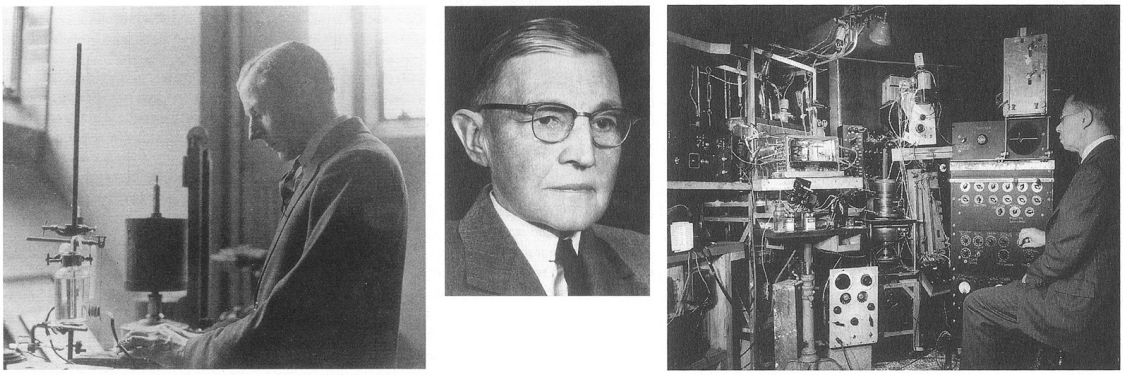

Figure 2.7. **Left:** Sir Edgar Adrian (English, 1889-1977). **Middle:** Herbert Gasser (American, 1888-1963). **Right:** Joseph Erlanger (American) in his Washington University laboratory. All photographs from Finger (2000).

Having just won the Nobel Prize, and using the best technology in the world, Adrian began a series of experiments on the EEG in 1934. He undertook both animal studies (treated below with respect to his desynchronization hypothesis) and human studies, where he confirmed some of Berger's main findings on the scalp EEG (Adrian and Matthews 1934b; Adrian and Yamagiwa 1935). A ~10 Hz rhythm was easily identified in vertex-to-occiput recordings that appeared/disappeared with eye closure/opening (Figure 2.8). This was referred to as "the Berger rhythm" (to Berger's chagrin), but I will continue to refer to it as α-w. Contrary to Berger's interpretation that emphasized the global effects of attention, Adrian and Matthews hypothesized a primarily occipital origin and emphasized the role of vision in α-w blocking. However, they also noted that the α-w was abolished with mental work and by non-visual stimuli that were unexpected or had an influence on affect or attention. These are clearly examples of non-specific α blocking, as opposed to a specifically visual perturbation. In any case, they clearly thought of the α-w as an idling rhythm: "It is true that, in our view, the rhythm shows the negative rather than the positive side of cerebral activity, it shows what happens in an area of cortex which has nothing to do, and it disappears as soon as the area resumes its normal work" (Adrian and Matthews 1934b). Thus, they were the first to propose the "idling" hypothesis for the α-w.

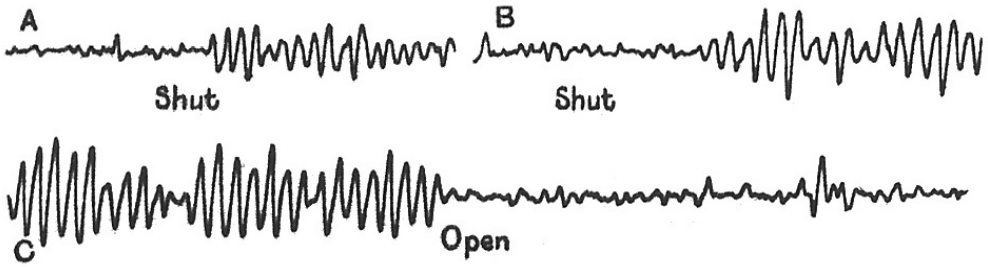

FIG. —The development of the rhythm in the absence of visual activity.
A. E. D. A. The rhythm appears when the eyes are closed.
B. B. H. C. M. Ditto.
C. E. D. A. The rhythm disappears when the eyes are opened.

Figure 2.8. The "Berger" rhythm of the scalp EEG, with eyes open/shut. From Adrian and Matthews (1934b).

Adrian and Matthews were also the first to propose the "desynchronization" hypothesis for α-w blocking. In the above study (1934b) they state: "The abolition of the rhythm by pattern vision represents the change from synchronous to asynchronous action; this would follow from the disturbing effect of a mosaic of excitations in the optic tract. In the same way the invasion of the beating area by widespread cortical excitations would prevent synchronous action although the visual field was uniform, and this would account for the effect of intense non-visual activities." Thus, this explanation was offered for both specific (visual) and non-specific (widespread) α-w blocking.

Adrian and Matthews (1934a) performed cortical surface recordings in lightly anesthetized rabbits and observed "that pinching the foot abolishes the slow rhythms and increases the prominence of the brief waves." The slow rhythms were at 3-4 Hz, and the brief waves at 25-40 Hz. This observation was revisited in a subsequent study (Figure 2.9), and Adrian (1934) noted that "a record from a human being with the eyes first closed and then open is in every way comparable with one from the rabbit's cortex when the foot is pinched." He clearly interprets this finding in rabbits as due to desynchronization rather than to inhibition.

Figure 2.9. Cortical surface recordings in lightly anesthetized rabbits, from Adrian and Matthews (1934b). The EEG trace is formed by the boundary between light and dark. "The large waves represent periods of widespread activity due, probably, to the spontaneous discharge of the cortical neurons. At the signal the foot is pinched, and with the arrival of afferent impulses the cortical beat breaks up into small irregular oscillations of high frequency – the sign of asynchronous action."

Given Adrian's fame and the large readership of the journals in which he published, his work led to widespread recognition and acceptance of Berger's findings and of the EEG in general. An explosion of EEG research followed in the second half of the 1930's, some of which is treated next as it pertains to the idea of EEG activation. We are now beginning to see how slow wave blocking with fast wave enhancement (a pattern I refer to as "EEG activation") might be the sought after pattern for mapping the cortex on the basis of its electrical activity. Léon Ectors, working with Frédéric Bremer in Belgium, would be the first to demonstrate this.

Léon Ectors and the discovery of gamma

One of the most famous early investigators of the EEG was Frédéric Bremer, a Belgian physiologist who did pioneering work on ascending brainstem influences on the cortex beginning in 1935. Bremer's laboratory in Brussels boasted the latest technology for electrophysiology – a multi-stage amplifier and a Matthew's oscillograph – a sensitive system for examining fast, low amplitude activity of the EEG. Working in the same laboratory was Léon Ectors, who would only publish one full study (Ectors 1936) and a preliminary report of the same data (Ectors 1935). Both Bremer and Ectors were well aware of the EEG work by Berger and Adrian, and they referred to slower waves as α or "ondes de repos" ("waves of rest") and faster waves as β or "ondes d'activité" ("waves of activity").

Ectors (1936) performed the difficult experimental work of recording ECoG from awake, behaving rabbits. Bipolar electrode pairs were implanted on the cortical surface through skull trephinations. After recovery from the surgical procedure the rabbits were unanesthetized and free to move about. As Ectors discusses, this was essentially the only contemporary study in unanesthetized animals, which was essential to his observations in the gamma band (>30 Hz, but the term gamma was not introduced until 1938 and Ectors continued to use β for all the fast frequencies >~20 Hz). Ectors major observation was that stimulation resulted in a suppression of

the α-w (3-9 Hz in his rabbits) and an augmentation of the amplitude and frequency of the β-w (30-50 Hz, which is the band termed "low gamma" today). This occurred in the appropriate sensory projection area and was demonstrated for olfactory, optic, acoustic, gustatory, and tactile stimuli. In cases of stimuli that were intense or particularly effective for emotional or attentional reasons, the β waves reached frequencies of 80-100 Hz (which is in the band termed "high gamma" today). A similar EEG activation pattern was observed in motor areas for motor actions.

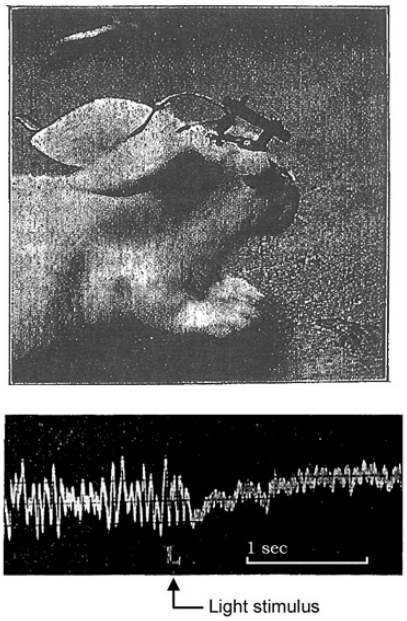

Figure 2.10. Outstanding early study of EEG activation and gamma (Ectors 1936). **Top:** ECoG recordings in unanesthetized rabbits free to move about. Bipolar electrode pairs place 4-5 mm apart on the cortical surface. **Bottom:** Example of ECoG response from the visual cortex, in response to a light stimulus. The larger, slower waves (α-w, ~3-9 Hz) of the baseline period are blocked and replaced with smaller, faster waves (β-w, ~30-50 Hz and higher).

Although prior studies had shown this EEG activation pattern, only Ectors (1936) performed the systematic mapping across modalities in awake animals and clearly showed gamma frequency range activity. For these reasons, I credit this study with the discovery of gamma and with the first demonstration of electrocortical mapping. It might be argued that Adrian and Matthews (1934a) should be credited with the discovery of gamma. However, they studied *anesthetized* rabbits, one sensory modality, and reported frequencies up to only 40 Hz. Berger's scalp EEG studies are another candidate, but most of his relevant observations occurred

after he read the reports of Adrian and Ectors. The term "gamma" was introduced in (Jasper and Andrews 1938).

Herbert Jasper on the "activation electrogram"

Herbert Jasper was a giant in the history of EEG and demands mention in this chapter because my concept and phrase "EEG activation" were originally based on his work. Born in Oregon, Jasper trained around the country and in Europe before settling at the Montreal Neurological Institute (MNI), where he did his major scientific work. He wrote many influential studies and reviews from the 1930s through the 1950s, including the first report from North America on the human EEG (Jasper and Carmichael 1935) and the introduction of the 10-20 system of scalp electrode placement (Jasper 1958). With Wilder Penfield, an American neurosurgeon who moved to Montreal and founded the MNI, he did pioneering studies of epilepsy and developed human ECoG to its modern form (Penfield and Jasper 1954).

Jasper's early work explored the relation of "cortical excitatory state" to EEG rhythms in both humans and cats. These concerned the appearance of higher frequencies in the EEG with specific sensory stimulation, motor activity, and with overall shifts in level of vigilance or emotional excitation. Summarizing in an early review (Jasper 1936), he describes the following sequence of "characteristic changes in both man and cat":

"1. *Extreme excitation*. No rhythmic brain potentials…

2. *Moderate excitation*. High frequency, low amplitude brain potentials…

3. *Moderate relaxation*. Fairly regular rhythms and beginning of irregularity…

4. *Further relaxation and drowsiness*. Slower rhythms and beginning of irregularity.

5. *Sleep*. Further decrease in frequency and regularity of brain potentials with definite increase in amplitude.

6. *Very deep sleep*. Very slow random potentials."

This sequence clearly describes the general inverse relation between excitation level and frequency of EEG rhythms. He would also use the phrase "activation electrogram" to describe the low-amplitude, high-frequency EEG pattern seen with excitation (Rheinberger and Jasper 1937), and it was based on these papers that I originally began calling the same pattern "EEG activation" (although Jasper never uses this exact phrase).

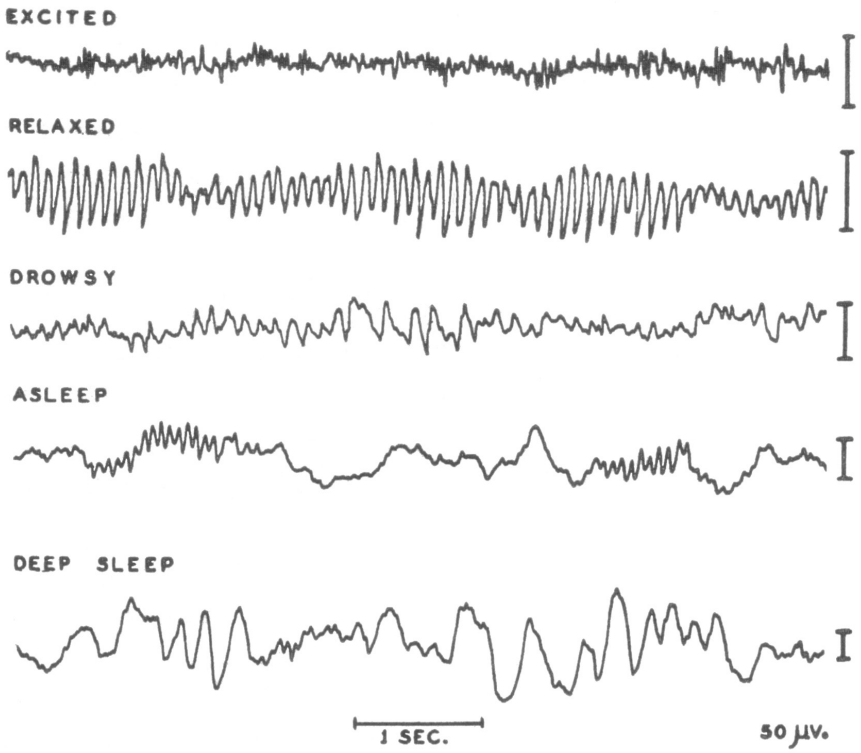

Figure 2.11. Sequence of cortical arousal level and the corresponding EEG patterns. The EEG shows slower waves of larger amplitude (note the changing μV scales) as the arousal level drops (from Jasper 1941, in Penfield and Erickson 1941).

Jasper's work of the 1930's was most often cited for his many observations on β activity. His studies of α and β wave blocking associated with motor activity are the original precursors to

the many contemporary studies of the "mu" rhythm. He recognized that lower frequency β waves (~15-25 Hz) were idling rhythms of the sensorimotor cortex given their consistent blocking with motor activation. But he also recognized that β waves, particularly at higher frequencies, were "waves of activity" and indicated cortical excitation. Thus, he saw the need for a division of the β band and introduced the term "gamma" in 1938. These were oscillations "of still higher frequencies (from 35 to 48 per second), which are usually obscured by the more prominent alpha and beta potentials" (Jasper and Andrews 1938). The term "gamma" was not often used in the literature for a many decades to follow, although Jasper (1948) states that: "The terms alpha, beta, gamma, delta, and even perhaps theta have a fairly definite meaning to most investigators."

Delta for dysfunctional states and deep sleep

Walter (1936) introduced the term "delta" for very slow oscillations (~2-4 Hz) seen in the scalp EEG over the vicinity of a tumor (Figure 2.12). The locations were later confirmed by post-mortem examination or during surgery, and in two cases he recorded ECoG. These recordings confirmed two earlier human ECoG studies (Foerster and Altenburger 1935; Kornmüller 1935) that the tumors themselves are electrically relatively silent. Thus, the δ waves arose from surrounding cortical tissue impaired by increased pressure. Walter (1936) also observed δ waves in other cases of raised intracranial pressure, and under general anesthesia.

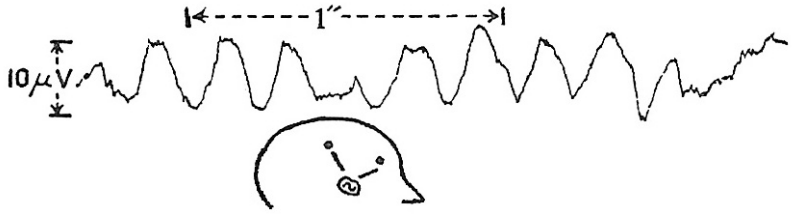

Figure 2.12. Illustration of δ waves (~2-4 Hz) from Walter (1936). His figure caption reads: "The first record taken from a patient with a cerebral tumor. Note the slow waves from an area which normally shows only the fast β waves."

Walter's 1936 study became highly cited and the term δ rapidly came into general use as other observations of δ accumulated. Subsequent studies confirmed the presence of δ waves in the vicinity of tumors (Walter 1937; Jung 1939). The first study of the EEG in coma found large, slow waves at ~3 Hz that resembled Walter's δ waves (Marinesco et al. 1937). δ waves at ~2-5 Hz were found with extreme hypoglycemia following insulin injection ("insulin coma", Hoagland et al. 1937; Davis and Davis 1939; Himwich et al. 1939; Hoagland et al. 1939; Davis 1941) and with oxygen deprivation to the point of fainting (Gibbs et al. 1935; Davis et al. 1938b; Davis and Davis 1939). A number of studies showed the presence of δ-range slow waves during deep anesthesia (Range 1935; Drohocki and Drohocka 1938; 1939a; Hoagland et al. 1939) (particularly with barbiturates, but other anesthetics can give quite different results). One study noted: "The more profound the anesthesia, the more the frequencies become slow" (Drohocki and Drohocka 1939b, my translation from French).

A major triumph of EEG during the second half of the 1930s was the unprecedented opportunity to objectively study sleep (Gibbs et al. 1935; Loomis et al. 1935a; 1935b) and the elucidation of sleep stages (Loomis et al. 1937). EEG remains indispensable for the study of sleep and for the clinical diagnosis of sleep disorders. With drowsiness and the transition to sleep, α waves can increase and there is a slowing of α or the appearance of "intermediate δ" (5-7 Hz) (Jung 1941). But as true sleep onsets, the α waves disappear and are replaced by δ (0.5-5 Hz) (Davis et al. 1937; 1938a). Although α waves will occasionally reappear during sleep, this happens most often with sensory stimulation or with spontaneous stirring of the subject, suggesting that α reappearance occurs with brief awakenings or near awakenings (Loomis et al. 1935a; 1936; 1937). Thus, from the perspective of sleep studies, δ is a sign of the deepest inactivity, and α is a sign of cortical arousal (!) relative to δ. In awake subjects, as reviewed in the above sections, α is a sign of resting or idling and γ is a sign of cortical arousal.

Figure 2.13. First illustration of slow waves during sleep (Gibbs et al. 1935). They state: "In all cases, as the subject becomes very drowsy the predominant waves become slower and show a greater amplitude… As the subject falls sound asleep, however, the predominant electrical activity becomes still slower and smoother, showing a characteristic frequency of from 3-5 Hz." This is in the δ range, although the term was not used in the sleep literature until 1937.

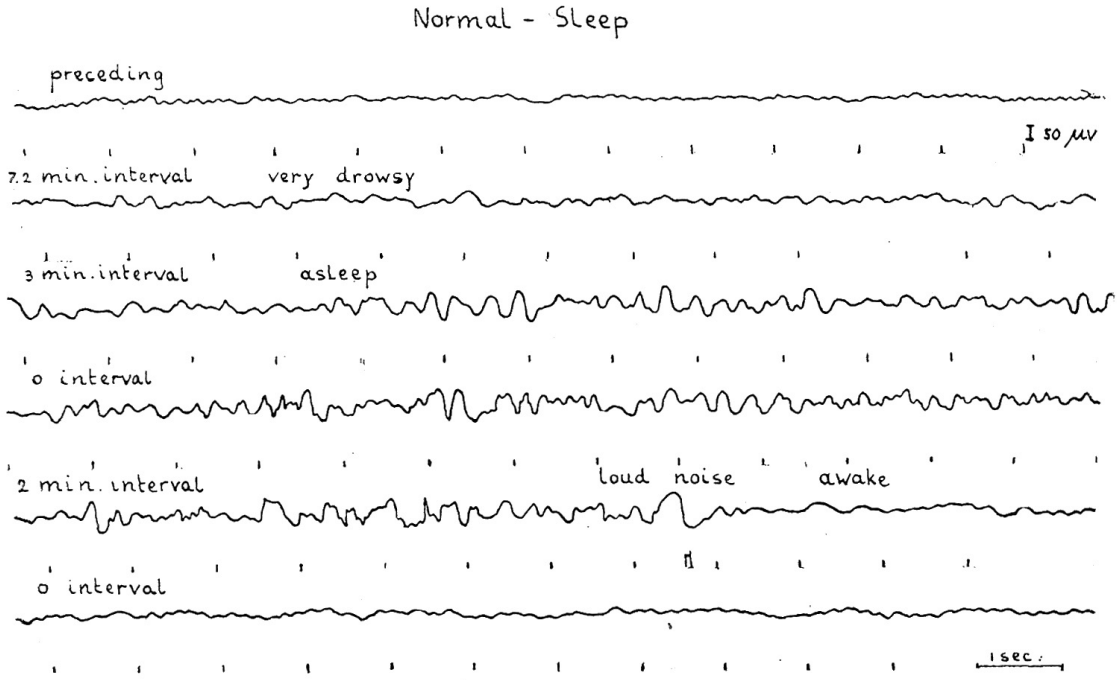

Chart 2.—Alteration of the electro-encephalogram with normal sleep. The increase in amplitude and decrease in frequency of the waves while the subject was asleep are obvious, as is the tendency for waves to appear in bursts.

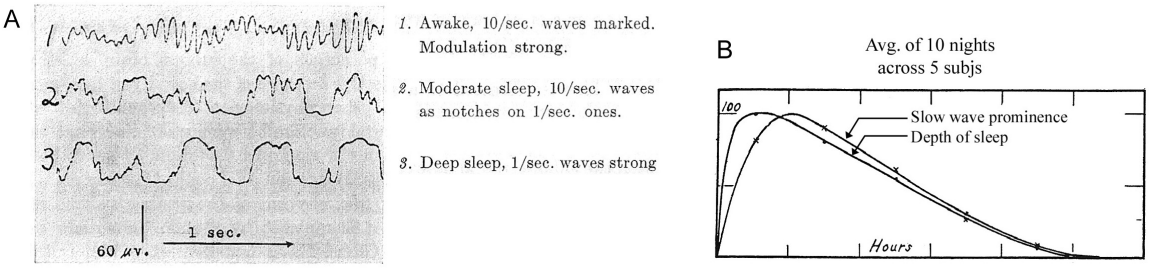

Figure 2.14. A. Transition from α to δ waves (0.5-3 Hz in this study) from awake to deep sleep. **B.** Strong correspondence between slow wave prominence and depth of sleep (assessed by movement, respiration, and ease of awakening). From Blake and Girard (1937) with text added.

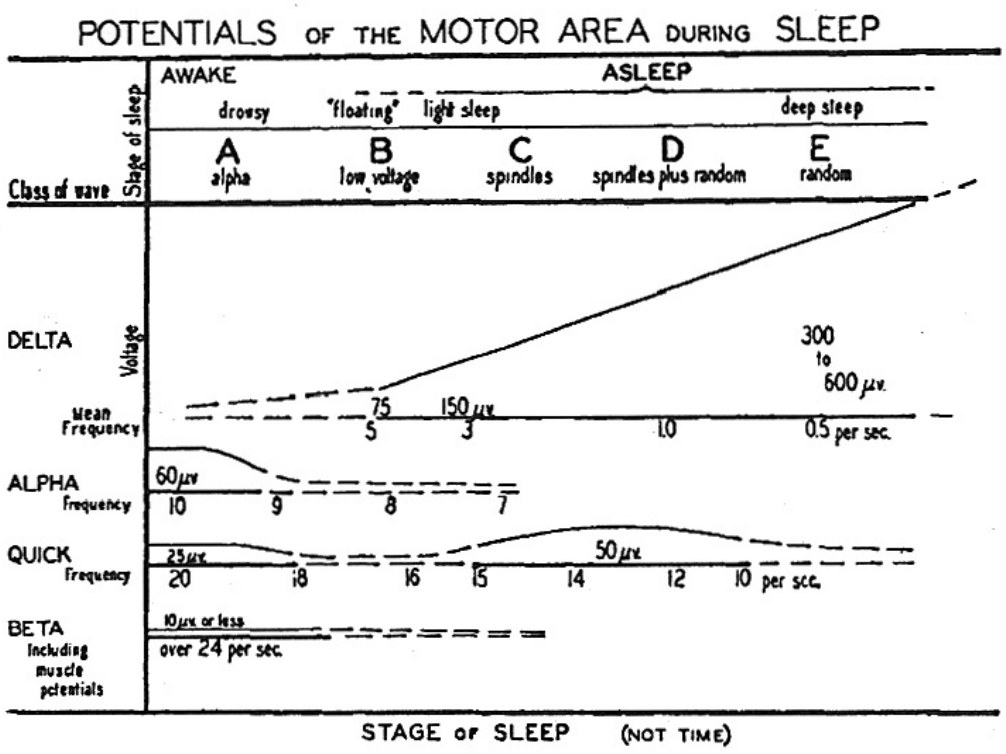

Figure 2.15. Excellent early illustration of sleep stages and EEG rhythms (Davis et al. 1938a). α rhythms decelerate and drop out with the onset of sleep. δ rhythms increase ~linearly with deeper sleep stages. They state: "In terms of potential patterns the index which seems *most nearly* to reflect the "depth of sleep" is the frequency and voltage of the slow, random "delta" waves."

In summary, slow waves in Walter's δ range were observed in a variety of states of deeply inactive or impaired cortical function. Particularly important were the pioneering studies of sleep and the EEG. These revealed δ waves to be the primary correlate of depth of sleep[6], and a sign of deeper inactivity than α, the awake idling rhythm.

[6] Note that this section has not treated sleep "spindles" in the β range or REM sleep, as the focus was on δ waves. REM sleep is considered its own state of consciousness with cortical arousal levels more similar to waking than deep sleep.

The EEG spectrum

There emerges from the above survey a progression of cortical arousal level in going from δ to α to γ. The slower the EEG rhythms (and the larger in amplitude), the less active is the cortex. This was summarized nicely by Jung (1941) (my translation from German): "The activation of the EEG thus runs through different conditions of the cortical activity in certain stages with a definite direction: from large, slow potential fluctuations (sleep EEG) to faster rhythmic processes (passive EEG) to small, high-frequency, non-rhythmic and little coordinated electrical phenomena (active EEG)." Whereas δ is a sign of deeply inactive or impaired cortical function, α is a sign of awake and healthy cortical function in a resting or idling state. β waves have a mixed set of connotations (confounded further by shifting boundaries for the β band), and γ fluctuations indicate a fully active state of cortical function. Figure 2.16 summarizes this state of the EEG spectrum in 1942. Although Jung's (1941) designation of "intermediate δ" (5-7 Hz) did not catch on in the literature, it is included because α rarely included the range 5-7 Hz by this time and because it is the precursor to today's theta band.

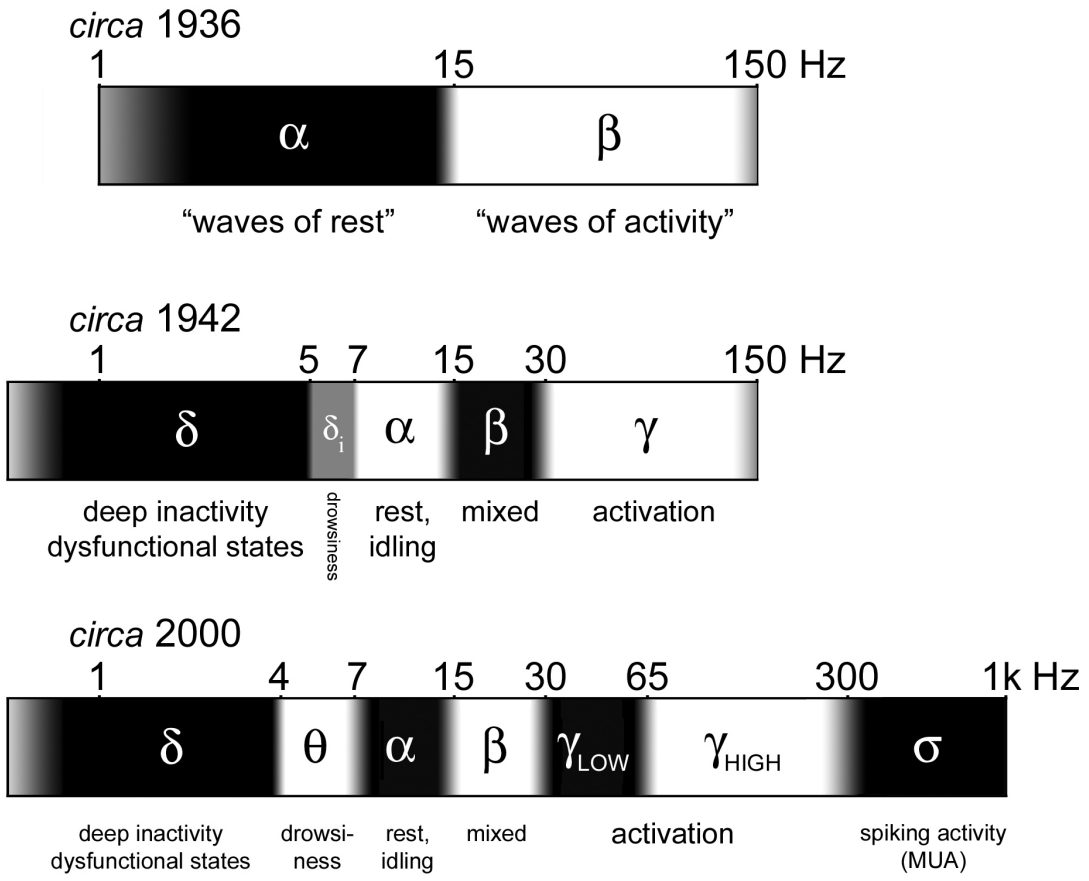

Figure 2.16. History of the EEG spectrum. All boundaries are approximate (indicated by gray transitional areas), due to different usages by different authors. The frequency scale is logarithmic. **Top** (*circa* 1936): Two frequency bands were distinguished with the division at ~15-20 Hz (Berger 1930). α was unbounded below but frequencies less than ~2 Hz were not studied. β was unbounded above but frequencies above ~150 Hz were not studied. **Middle** (*circa* 1942): δ (~0.5-5 Hz) and γ (above ~30-35 Hz) bands were introduced (Walter 1936; Jasper and Andrews 1938). Jung's (1941) "intermediate δ" band (5-7 Hz) is included. **Bottom** (*circa* 2000): The contemporary EEG spectrum includes the θ band (~4-7 Hz, Walter and Dovey 1944) and the division of the γ band into low (~30-60 Hz) and high (~65-300 Hz) regions (Crone et al. 1998). A set of phenomena above ~300 Hz are generated by summed multi-unit spiking activity (MUA) and is called here the σ band (after Curio 2000). Below the δ band is "infra-slow activity", but it is not represented here because it is rarely studied and does not fit neatly on the logarithmic scale.

Summary

In the first chapter, we saw that the earliest EEG studies sought to use negative variation as a means of cortical localization. Although ultimately a failed quest, another important theme was present in these early studies - the existence of spontaneous fluctuations of the EEG. This chapter has shown the early emergence of studies on these background fluctuations and their alterations with various manipulations. A consistent pattern, which I term "EEG activation", emerged in these studies and was first shown by Ectors (1936) to be useful for cortical localization. By the end of the 1930s, this pattern of slow wave blocking and fast wave enhancement was widely accepted as a sign of cortical activation. Indeed, it was so widely accepted that it was implicit in the discovery of the reticular activating system (RAS) (Moruzzi and Magoun 1949). That is, the RAS was shown to be an "activating system" because its stimulation led to the known EEG activation pattern in the cortex. From today's perspective, where the RAS is widely known and accepted, but knowledge of EEG activation is mostly forgotten (or just neglected in favor of sexier cognitive ideas about the EEG), the landmark study of Moruzzi and Magoun (1949) could be taken as a confirmation of the EEG activation pattern as a sign of cortical arousal.

Some today still analyze their data under the naïve assumption that greater overall amplitude in the EEG indicates greater underlying activation. Although this is usually the case in simple physical systems, it is the opposite of what is empirically found in the brain. For a field of inquiry to move backwards in progress must be considered a rare event in the history of science! Given this anomalous regression in the field of EEG due to a simple failure to know the literature, this thesis has devoted a chapter to recovering this original means of cortical mapping. Also, given the widespread disrespect in neuroscience for EEG as a method, I must be very careful to show that my proposed means of cortical mapping rests on a long tradition of empirical observation. The following chapters will complete the empirical demonstration of EEG

activation. The next chapter will introduce spectral analyses, and several confirmations will be found along the way. Chapters 4 and 5 will look at examples from the human auditory system. Chapter 6 will discuss the metabolic and hemodynamic correlates of EEG frequency bands, allowing comparison to other methods in neuroscience that are more widely accepted to yield images of cortical activation.

Chapter 3: Spectral analysis of the EEG

There is something misleading in using discrete Greek-letter frequency bands, as many authors have noted. A *continuous* representation is preferable in many respects, by which I mean the following. The difference between 29 and 31 Hz is not greater than the difference between 27 and 29 Hz simply because the former crosses a boundary between Greek-letter bands. Although there is a major change in the significance of 10 Hz vs. 40 Hz, there is not necessarily a sharp boundary where this change occurs. A preferable approach would be to test the whole continuum of frequencies and to report the range that exhibits some property (although this does require more space devoted to figures, as the dimension of frequency has been added). To do this, a method of spectral analysis is required. This chapter gives a brief historical survey of the development of spectral analysis of the EEG. Some important concepts and terms are introduced along the way in preparation for the time-frequency methodology I will use later.

Dietsch's Fourier analysis by hand

The original method of spectral analysis is the Fourier-transform, and Hans Berger immediately sought to apply this to his EEG data (Dietsch 1932). In collaboration with another professor in Jenna, G. Dietsch (at the "Technical-physiological Institute"), a laborious set of hand measurements and calculations was undertaken on segments of Berger's EEG data (Figure 3.1A). The "fundamental frequency" (f_0) was taken as 10 or 11 Hz, the frequency of the subject's α rhythm. f_0 determines the lowest frequency and the spacing between frequencies, and Dietsch tested the range 10-110 Hz or 11-121 Hz. The results were given in tables, from which I have made amplitude-spectrum plots (Figure 3.1B). With the lowest frequency at 10 Hz, we unfortunately do not get to see the α peak typical of scalp EEG (Berger usually recorded occiput-to-forehead). However, we do clearly see the so-called "1-over-f" relation of amplitude to

frequency (i.e., an inverse relation between amplitude and frequency). The flattening of the EEG with activation is a consequence of this rapid decline of amplitude with frequency. Although the higher frequencies are increased with activation, the lower frequencies that dominate the raw record are decreased and an overall flattening of the trace results.

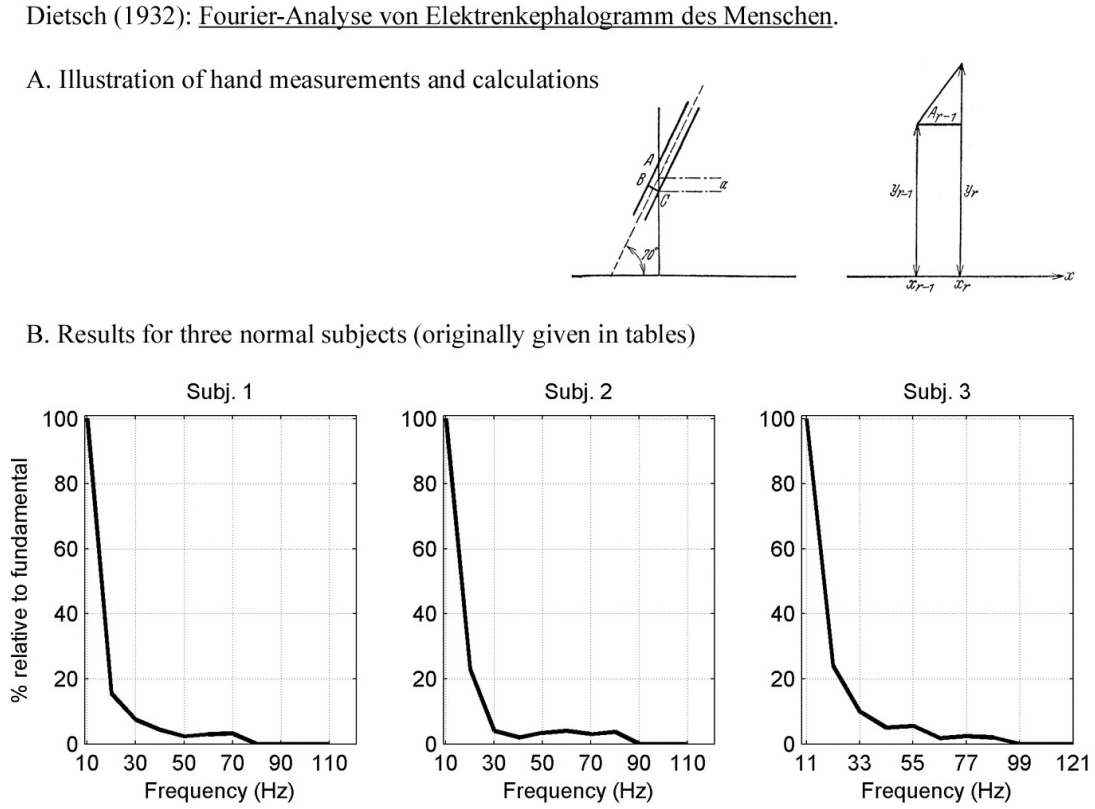

Figure 3.1. First spectral analysis of the EEG ("Fourier-analysis of the human EEG"). **A.** Illustration of hand measurements from Dietsch (1932). **B.** Plots made in Matlab using data presented in tables for 3 normal subjects. Amplitude falls off rapidly as a function of frequency.

Grass' automatic frequency analyzer

Laborious hand measurements are clearly not an effective means of obtaining a spectral analysis from the EEG, but even before the development of modern computers it was possible to do automatic frequency analysis using carefully designed electronic circuitry. Several such

devices were constructed in the history of EEG (Grass and Gibbs 1938; Drohocki 1939; Walter 1943). The first was by Albert M. Grass, the electrical engineer in the Dept. of Physiology at the Harvard Medical School, where the first North American EEG studies were done in the laboratory of Hallowell Davis. This device was described as a "mechanical-electrical integrator" (Figure 3.2A) and, with Frederic Gibbs of the Davis laboratory, it was used to produce the first plots of EEG amplitude spectra (Figure 3.2B, Figure 3.3).

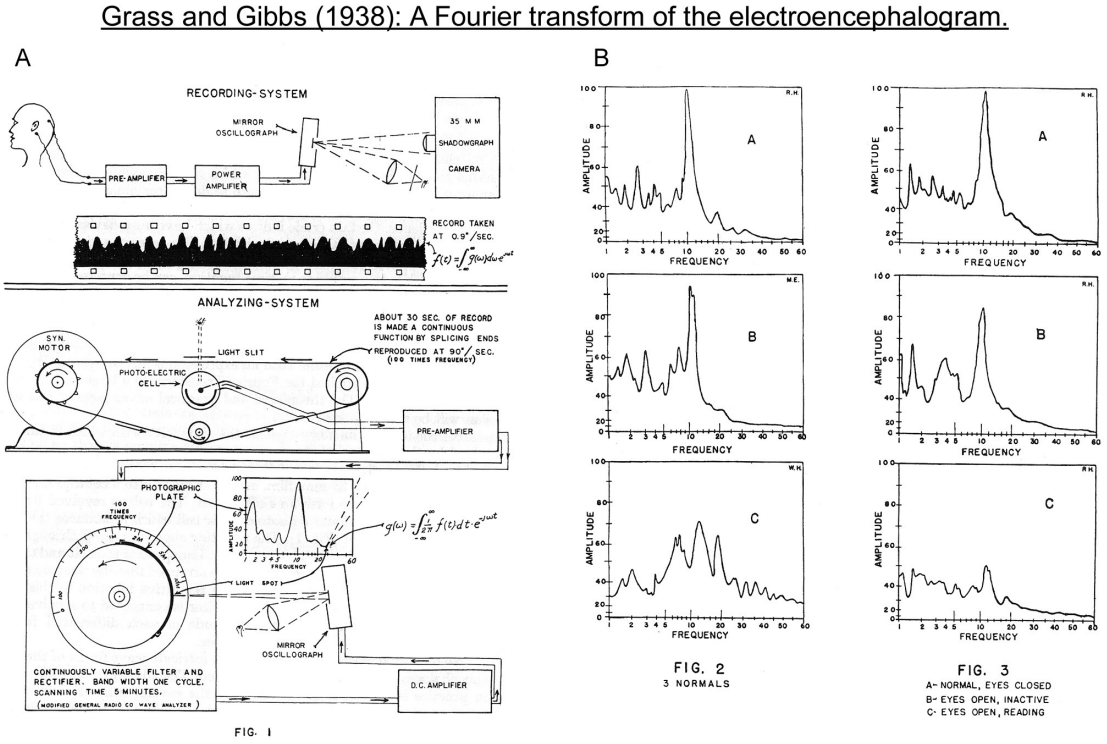

Figure 3.2. First plots of amplitude spectra of the EEG. **A.** Illustration of the "mechanical-electrical integrator", whereby the EEG is spliced onto a revolving belt, played through various bandpass filters, and the output of these rectified. **B.** The resulting amplitude spectra show clear α peaks. The frequency scale is semi-logarithmic (between linear and logarithmic).

Figure 3.3. From the above figure, the amplitude spectra on the right are put onto one plot. These show the amplitude spectra for one normal subject under three conditions. Blue: eyes closed, inactive. Green: eyes open, inactive. Red: eyes open, reading. Notice that the active condition (red) shows a reduction at the α and lower frequencies (below ~25 Hz), and an enhancement at the higher frequencies (above ~30 Hz) relative to the inactive conditions.

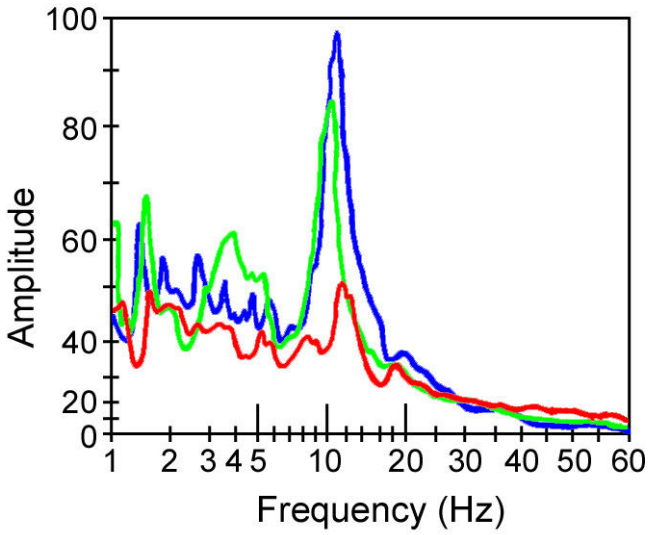

Motokawa's time-amplitude plots

The introduction of spectral analyses was a major advancement, but note that the above studies lack any *temporal* information. Although Grass and Gibbs (1938) stated that "the time element can be supplied in the form of consecutive analyses made at separate or continuous intervals of time", they did not present any results of this form. The time dimension would not be added to a frequency analysis until Japan's Koiti Motokawa (Motokawa 1941; Motokawa and Mita 1941), who would thus be the first to show time-amplitude plots (Figure 3.4). Motokawa was Japan's first EEG scientist, and his pioneering work will be revisited in the final chapter. However, Motkawa's frequency analysis still relied on a laborious set of hand measurements, he only analyzed the α band (roughly), and his time windows were separated quite far apart in time.

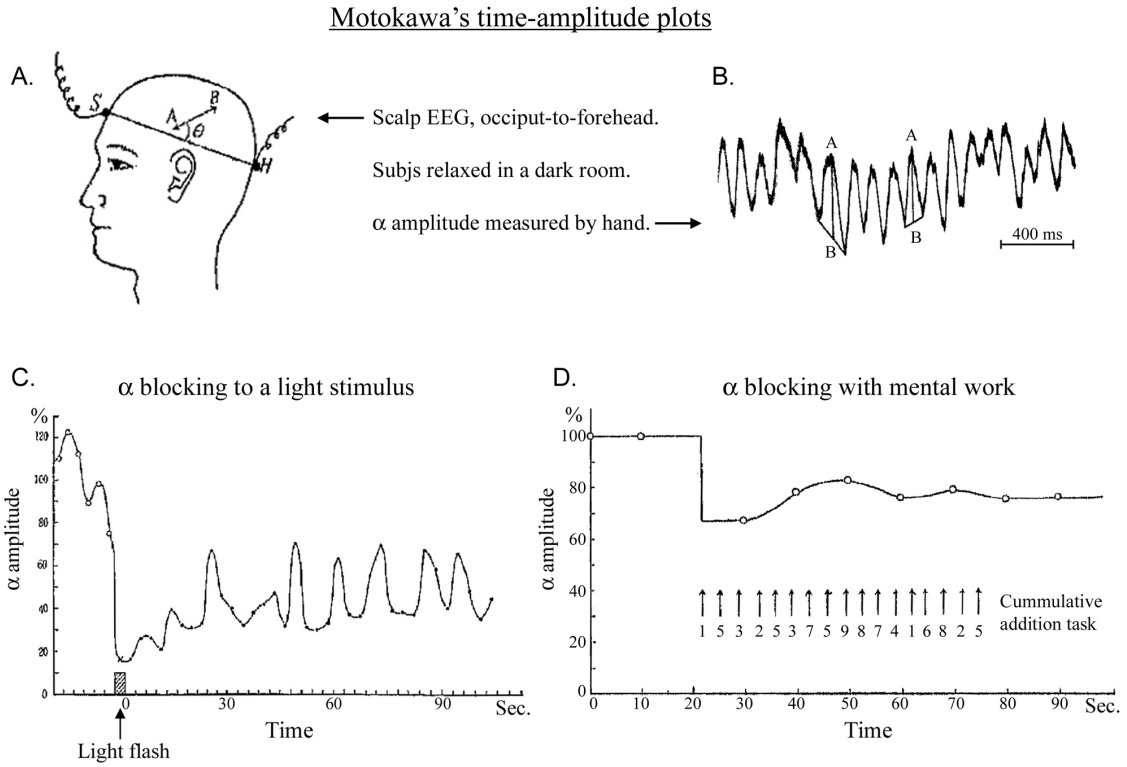

Figure 3.4. First published time-amplitude plots. **A.** Scalp EEG recorded occiput-to-forehead (from Motokawa and Mita 1942). **B.** α amplitude measured by hand ~peak-to-peak (from Motokawa 1944). Although this seems very crude, it actually gives a reasonable approximation to the envelope of the signal, and therefore to the analytic amplitude of the Hilbert transform that I will be using later (Appendix 2). **C.** α blocking to a light flash (from Motokawa 1941). **D.** α blocking with mental work (subjects were given numbers at the arrows to add cumulatively) (from Motokawa and Mita 1941). Minor labeling added to C and D for clarity.

Pfurtscheller's "Event-related desynchronization"

Motokawa's work was unknown or quickly forgotten outside of Japan, so it would be the well-known studies of Austria's Gert Pfurtscheller starting in the late 1970s (Pfurtscheller 1977; Pfurtscheller and Aranibar 1977; 1979) that would make time-amplitude plots known to most EEG scientists. Pfurtscheller used power rather than amplitude (power is amplitude squared), so these are "time-power" plots. Using a microcomputer, the Fast Fourier Transform (FFT, Cooley

and Tukey 1965) was applied to 1 s segments of data overlapping by 0.5 s. This is commonly called a "moving-window" or "short-term" FFT (ST-FFT). He studied the α band power (7-13 Hz) and the full band power (0-32 Hz, the upper limit determined by a 64 Hz sampling rate for these analyses). Results for visual and auditory stimuli are shown in Figure 3.5.

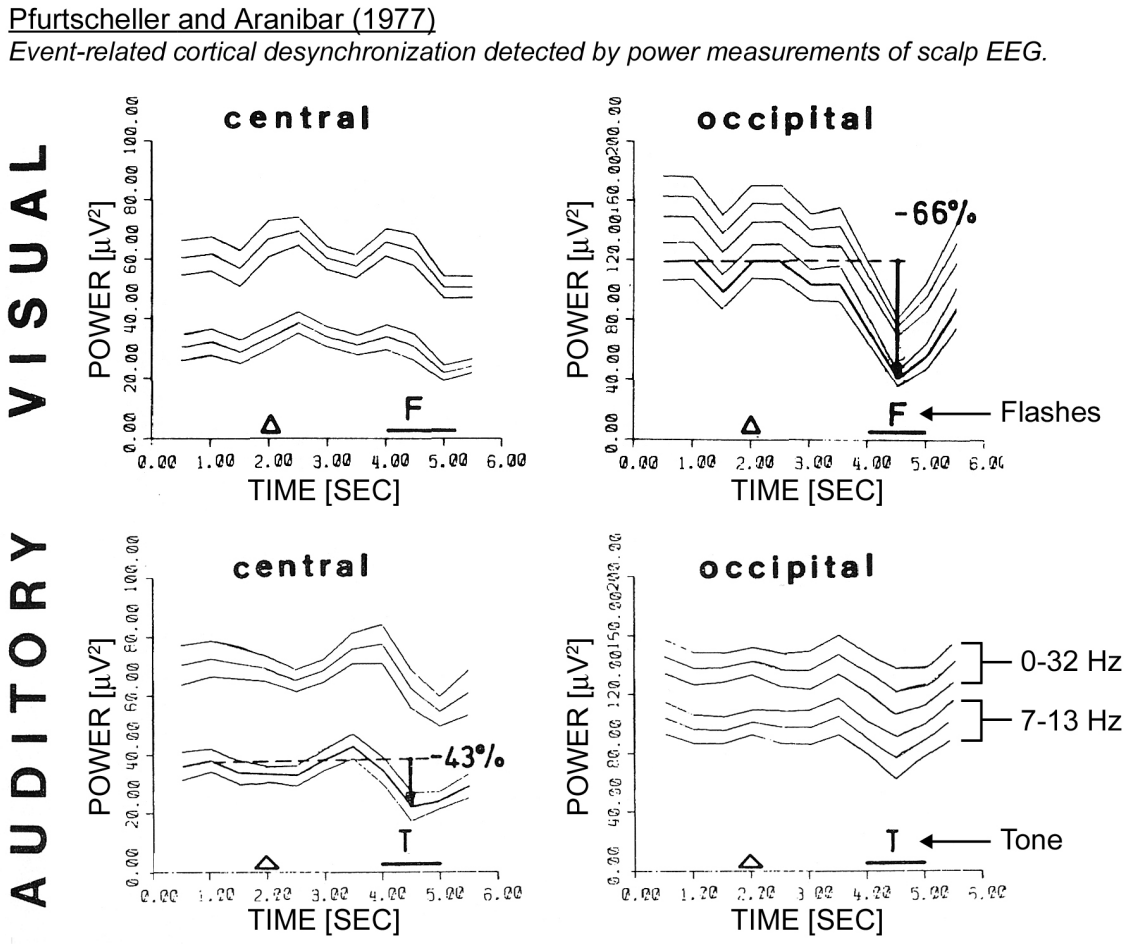

Figure 3.5. ERD of full-band (0-32 Hz) and α band (7-13 Hz) power in the scalp EEG. A warning click is played at the triangle, followed by flashes (top) or a tone (bottom). Occipital electrodes (O1, O2) show ERD to the flashes (power decrease of -66%). Central electrodes (C3, C4) show ERD to the tone (power decrease of -43%). Because of this topographical specificity, they argue that ERD is due primarily to specific thalamic input (as opposed to diffuse, non-specific input). From Pfurtscheller and Aranibar (1977) with minor labeling added.

Based on Adrian's widely-accepted desynchronization hypothesis for α blocking (Adrian and Matthews 1934a; 1934b), the flattened EEG during cortical activation was often called the "desynchronized" EEG. Based on this terminology (although he would not cite Adrian until many years later), Pfurtscheller referred to α or β blocking as "event-related desynchronization" (ERD). Later he observed power increases in the γ band (Pfurtscheller and Neuper 1992; Pfurtscheller et al. 1993), and referred to these as γ "event-related synchronization" (ERS) (Figure 3.6).

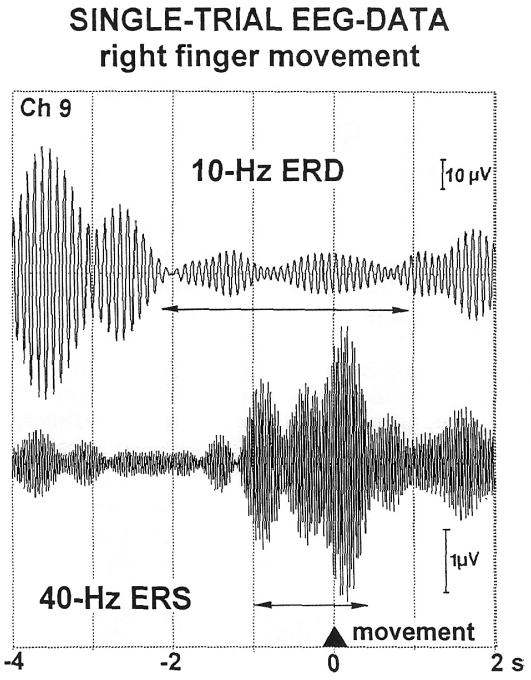

Figure 3.6. "Examples of 10 Hz ERD and 40 Hz ERS of band pass filtered EEG (10-12 Hz, 24-36 Hz) in one trial" (from Pfurtscheller and Neuper 1992). There is clear suppression of α amplitude beginning ~2 s prior to finger movement (10-Hz ERD), and clear enhancement of γ amplitude beginning ~1 s prior (40-Hz ERS). Note that these are just plots of filtered signals without any additional analyses. The envelope of such a filtered signal would be very similar to the "analytic amplitude" that I will use in my own analyses below.

"ERD" and "ERS" are highly loaded terms that have often resulted in unnecessary confusion. Had Pfurtscheller known the work of Motokawa, he would have known that there is a major alternative to the desynchronization hypothesis. Motokawa's challenge to the desynchronization hypothesis (Motokawa 1943b) and his proposed alternative will be covered in the final chapter. Pfurtscheller's terminology makes a confusing commitment to only one hypothesis for α blocking. However, Pfurtscheller's studies were otherwise very good, obviously a major technical improvement over Motokawa's analyses, and he brought these analyses into the mainstream of neuroscience. Thus, Pfurtscheller has made a noteworthy historical contribution to EEG spectral analyses and the terms "ERD" and "ERS" will continue to be used for some time (and occasionally in this manuscript).

Pfurtscheller is one of the few contemporary authors who writes of α suppression and γ enhancement as signs of cortical activation (although he has not always been clear on this point). For example, in a recent review (Pfurtscheller 1999): "Increased cellular excitability in thalamo-cortical systems results in a low amplitude desynchronized EEG. Therefore, ERD can be interpreted as an electrophysiological correlate of activated cortical areas… In contrast to the alpha band rhythms, the gamma oscillations reflect a stage of active information processing".

Makeig's "Event-related spectral perturbation"

A full time-frequency analysis did not finally appear in the EEG literature until the 1990's in the work of Scott Makeig at the University of California, San Diego (Makeig 1993; Jokeit and Makeig 1994; Makeig et al. 1995)[7]. The full "time-frequency plane" shows all three dimensions of time, frequency, and power (or amplitude) and therefore reveals the full spectral response to an event. Makeig named his plots "Event-related spectral perturbations" (ERSPs).

[7] Between myself and Scott Makeig (personal communication), we only know of 1 minor exception, which was a time-frequency analysis of an epileptic seizure with a long time-scale.

These usually show the power in each frequency band in units of decibels (dB) relative to the pre-event baseline. The power is obtained for each single-trial (typically by a ST-FFT) and then averaged across trials. Dividing by the mean baseline spectrum and taking the logarithm gives the ERSP. One example is shown here from a simple stimulus-response task (Figure 3.7) (the 1993 and 1994 studies cited above involved more complicated tasks with overlapping steady-state responses).

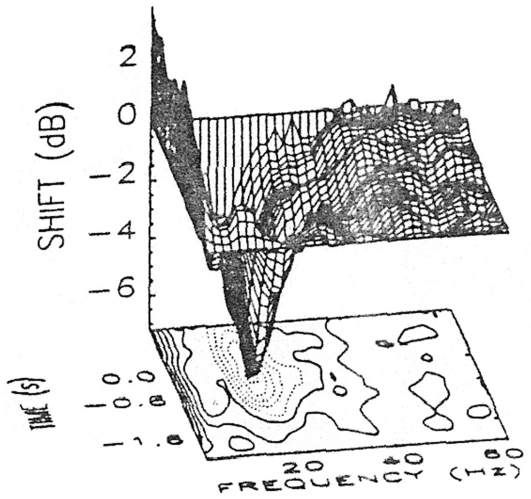

Figure 3.7. Early example of a full time-frequency analysis (from Makeig et al. 1995). MEG data from a sensor roughly over motor areas was analyzed with a short-time (moving-window) Fourier transform (ST-FFT). The resulting ERSP shows a strong suppression in the β and α bands peaking ~500 ms after the motor response. Cue and feedback stimuli were tones. The γ band does not show a response above noise level in this example.

Makeig and colleagues have made their analysis and visualization scripts publicly available in the widely-used EEGLAB toolbox (Delorme and Makeig 2004). My original time-frequency analyses were based on those in EEGLAB. Downloaded by hundreds of users, EEGLAB has contributed to the recent surge of EEG time-frequency studies in the literature.

Wavelets and the revival of gamma

Shortly after Makeig introduced the ERSP, a number of investigators, particularly in Europe, began using wavelets to analyze event-related EEG data (Sinkkonen et al. 1995; Tallon et al. 1995; Tallon-Baudry et al. 1996). This method became very popular and helped precipitate an outpouring of γ studies in the scalp EEG or MEG (Bertrand and Tallon-Baudry 2000). The great majority of these studies report an increase of γ band activity during some perceptual (usually visual) or cognitive task. This is compatible with the EEG activation hypothesis (increased cortical activation is expected in these situations), although a variety of explanations have been offered for these γ increases. In my opinion, these explanations have focused too much on the role of synchrony in binding and cognition at the expense of the simpler explanation that γ is a sign of cortical activation. As revisited in the final chapter, γ "ERS" does not require synchronization!

Competing methods of time-frequency analysis

The most commonly used wavelet is the "Morlet" wavelet, which is defined by its Gaussian-shaped tapering function. It turns out that convolving an EEG signal with a Morlet wavelet is mathematically identical to using a Gaussian filter bank with a Hilbert transform, and both of these methods are in turn equivalent to using the ST-FFT with a Gaussian-shaped windowing function (Flanagan 1980; Cohen 1995; Bruns 2004). The only caveat is that the parameters of the analysis (such as window length) must be carefully matched for each frequency band. There has arisen a sizeable literature comparing the relative merits of the ST-FFT, wavelet, and Hilbert approaches to time-frequency analysis. But once it is realized that they are equivalent and a unified perspective is seen (Cohen 1995; Bruns 2004), then this literature becomes moot. The question of which method to use becomes a question only of computational efficiency, and ease of programming and understanding. It is for these reasons that I will be using the Hilbert transform method in the following chapters (see Appendix 2 for more details).

Chapter 4: Examples in the human auditory cortex

In this chapter I present results from ECoG experiments in neurosurgical patients undergoing awake language mapping during tumor resection (see Appendix 1 for details). With electrodes over known auditory areas (as established briefly in the next section), a typical time-frequency response is obtained in response to simple auditory stimuli. This consists of a decrease of low frequency power (<20 Hz) and an increase in high frequency power (>25 Hz). These results, and other results surveyed in this chapter, provide additional confirmation of the EEG activation pattern discussed above.

Localization of human auditory cortex

David Ferrier localized the cortical auditory areas in monkey to the posterior and superior parts of the superior temporal gyrus (STG) on the basis of electrical stimulation (Figure 4.1A) and bilateral lesions (Figure 4.1B) (Ferrier 1875a; 1875b; 1886). Based purely on arguments of homology to the monkey brain, Ferrier (1886) localized the human auditory centers to the posterior half of the STG (Figure 4.2).

A. Electrical Stimulation (faradic current)

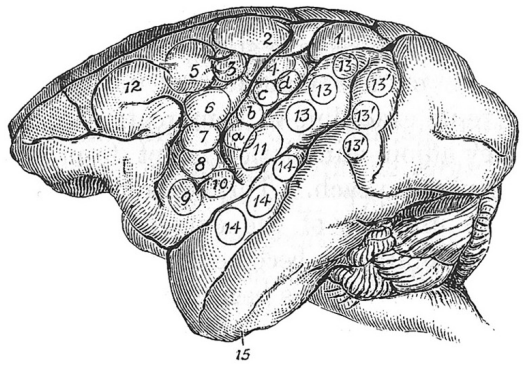

(14) → "Pricking of the opposite ear, head and eyes turn to the opposite side, pupils dilate widely."

B. Bilateral destruction of STG

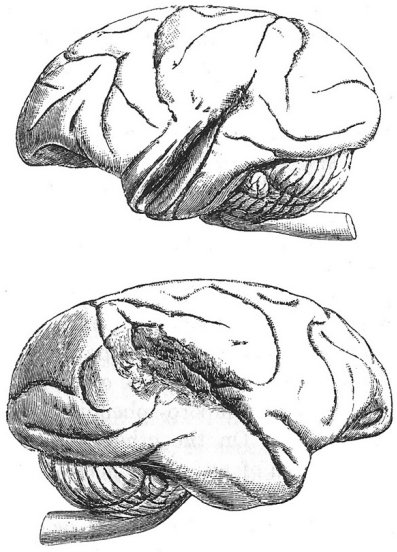

→ "complete deafness"

Figure 4.1 (previous page). Ferrier's localization of auditory cortex in macaque monkeys, from Ferrier (1886). **A.** Electrical stimulation at sites along the STG (circled areas 14) led to "pricking of the opposite ear, head and eyes turn to the opposite, pupils dilate widely." This was interpreted that the monkey heard a sound in the opposite side of space. **B.** Bilateral cauterization of the STG. This was Ferrier's famous "Monkey F", demonstrated at the widely-attended 1881 International Medical Congress. This monkey was considered by Ferrier to be completely deaf. "The animal was allowed to survive for more than a year, during which time, from the beginning till the end, it enjoyed perfect health and the full enjoyment of all its faculties and powers, with the single exception of hearing. No sign of hearing, or even twitching of the ears, could be elicited by sounds which invariably attracted the attention of other monkeys…" (Ferrier, 1886, p. 309-310).

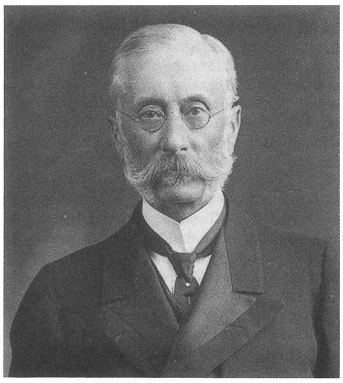

David Ferrier
British, 1843-1928
Functions of the Brain (1886)

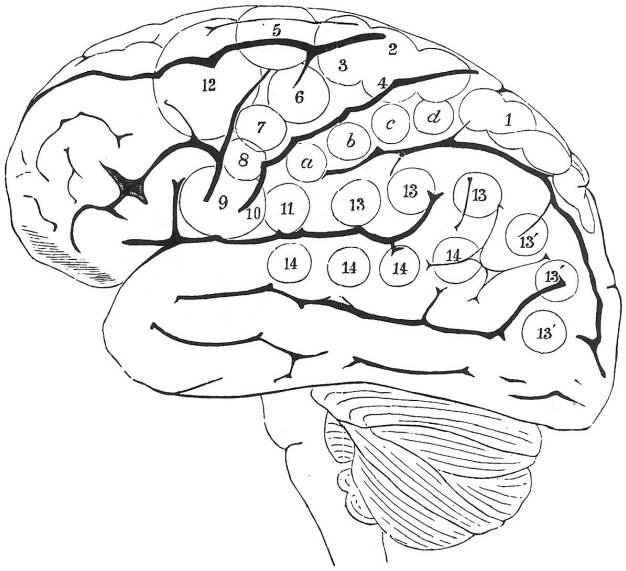

Figure 4.2. **Left:** Photograph of Ferrier (from Finger 1994). **Right:** Ferrier's suggested map of the human cortex based on arguments of homology to monkey cortex. Circled areas '14', along the posterior two-thirds of the STG, are the suggested auditory centers (from Ferrier 1886).

Ferrier's localization in humans, and the localization of primary auditory cortex to the superior temporal plane (STP), became accepted by further arguments of homology as evidence for the anatomical pathways from cochlea to cortex accumulated in both monkeys and humans. This localization also became accepted as clinical reports accumulated of cortical deafness in humans (Figure 4.3) (Mills 1891; Mott 1907; Bramwell 1927, reviewed in Finger 1994). The first functional demonstration of this localization in humans was done by recording the ECoG responses to clicks in neurosurgical patients. After some preliminary observations in frontal lobotomy patients (Chatrian et al. 1960), it was the extensive ECoG recordings of Gastone Celesia and colleagues in tumor and epilepsy patients (Celesia and Puletti 1969; Puletti and Celesia 1970; Celesia 1976) that firmly established the localization of auditory-responsive areas in humans (Figure 4.4).

Figure 4.3. First published illustration of cortical deafness in humans (from Mott, 1907). This was a case study of a 25 year old woman presenting with complete deafness (except perhaps to loud sounds) and partial aphasia. Post-mortem examination showed bilateral destruction of the posterior third of STG and the posterior portion of the STP, including the transverse gyri of Heschl.

Figure 4.4. Functional demonstration of auditory-responsive cortex in humans, from Celesia (1976). ECoG was recorded with electrodes on the lateral surface and depth probes on superior surface of the temporal lobe in 19 adult patients with partial seizures (15 local anesthetic; 4 under general halothane anesthesia). 60 dB clicks, and occasionally tones, were presented binaurally at 1/s. Auditory responses were obtained from two areas: 1) On the superior temporal plane corresponding to the anterior and posterior transverse temporal gyri (primary auditory cortex, or A_1). 2) On the lateral surface around the sylvian fissure.

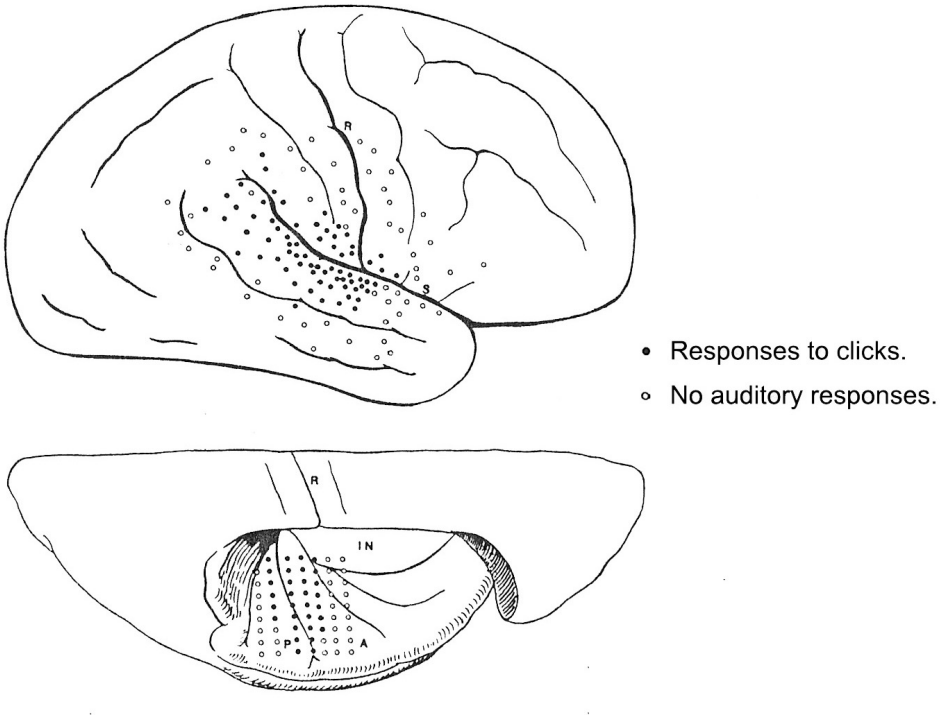

EEG responses to auditory stimuli

Suppression of α to auditory stimuli has been observed since the earliest days of scalp EEG. Hans Berger (1930) only showed a figure for α blocking to somatosensory stimuli (Figure 2.5), but stated that "sound stimuli worked just as well" and discussed several results with auditory stimuli. He used a variety of recording arrangements, most typically occiput-to-forehead, but none of these would be expected to image auditory cortex specifically. He also found

habituation to repeated stimulation, and concluded that attention was the critical factor: "When the same stimulus is repeatedly applied in one and the same session, the changes of the EEG appear less and less distinctly… There exists therefore for me no doubt, that the directing of attention upon a stimulus causes these changes in the EEG" (translation from German by Gloor 1969). Berger's finding of α suppression to auditory stimulation was confirmed in numerous subsequent reports using scalp EEG (Gibbs et al. 1935; Jasper 1936; Bagchi 1937; Davis 1939; Bancaud et al. 1953; Gastaut 1953; Perl et al. 1953) (Figure 4.5). Berger's observation of habituation with repeated stimulation was also confirmed (Durup and Fessard 1935; Darrow et al. 1957; Jus and Jus 1960; Kasamatsu and Hirai 1966) (Figure 4.6), and most or all authors concurred that the reaction was due to surprise, directing of attention, or affective reaction, rather than specific auditory function. Thus, auditory α blocking clearly includes a significant "non-specific" component.

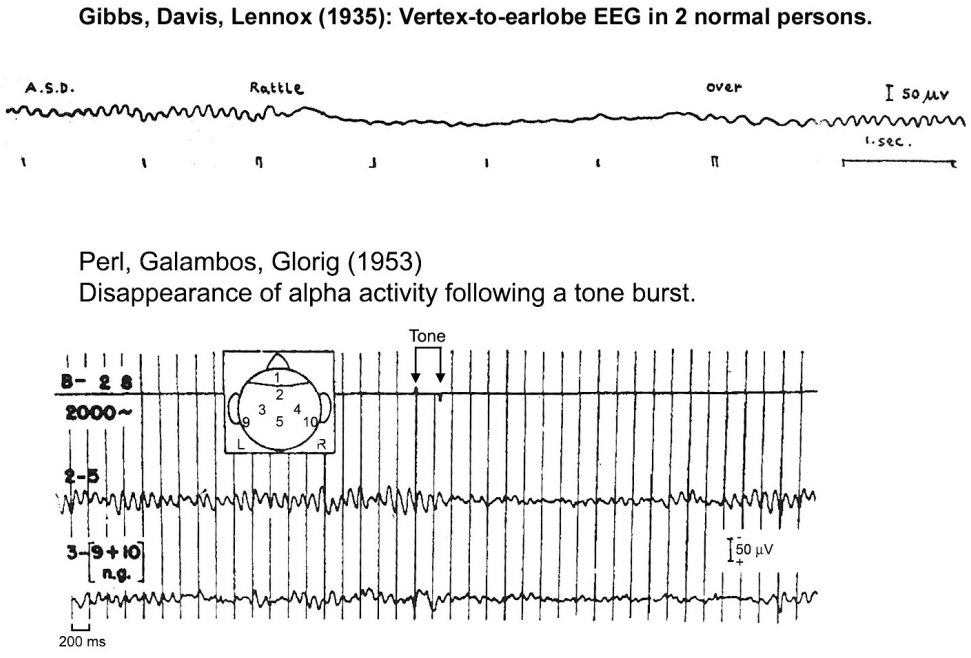

Figure 4.5. Examples of α blocking in the scalp EEG to auditory stimuli. **Top:** from Gibbs et al. (1935). **Bottom:** from Perl et al. (1953) with the stimulus label ("Tone") added.

Figure 4.6. Example of habituation of the α blocking response in the scalp EEG to repeated auditory stimuli.

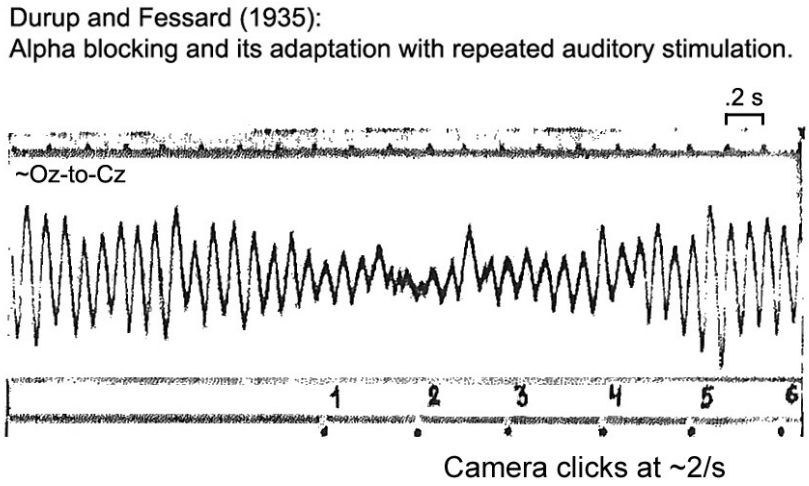

For completeness[8], it must be mentioned that α blocking has not always been observed for auditory stimuli. This seems to occur in situations where attention is not affected, as just discussed. But there have also been occasional reports of *increases* in α to auditory stimuli. This seems to occur in one of two situations. The first is when the subject is asleep or very drowsy. As discussed in the above section on δ and sleep, α is a sign of cortical *activation* relative to sleep or drowsiness on the edge of sleep. α is the idling rhythm of the awake cortex, and when the vigilance has dropped below this level, a sensory stimulus often has the effect of bringing the subject's α back. The second situation of auditory α increase is in switching of intermodal attention. α in the scalp EEG originates primarily from visual cortices (Adrian and Yamagiwa 1935; Jasper and Andrews 1936; Rubin 1938) and most authors report that visual stimuli are the most effective for α blocking. If the auditory stimulus takes attention away from the visual

[8] One often gets the impression in reading reviews that the half of the literature that supports the author's view is being selected at the expense of the disconfirming half. I want to be clear that, in addition to the abundance of confirming examples, there is an impressive absence of disconfirming examples to be found.

modality and visual cortices are *deactivated*, an overall increase in scalp α is certainly expected. However, α suppression more locally in the auditory areas would still be expected.

A final confound involves the auditory evoked potentials (middle-latency, MAEPS: Pa-Na-Pb-Na; long-latency, LAEPs: P1-N1-P2-N2), which occupy the α and surrounding bands in terms of their spectral energy. Electrodes showing these evoked potentials will show an increase in α power during this interval (~30-350 ms), which is often followed by suppression of the spontaneous α rhythm relative to the baseline. Examples of this will be shown from the ECoG data below.

In addition to α suppression, Berger (1930) reported an increase in β activity at ~22-33 Hz to auditory stimuli. Rohracher (1937) reported the appearance of "smaller, faster oscillations" (my translation from German) to sharp, isolated stimuli, and Abe (1954) reported an increase in β waves to clicks and brief tones. But Jasper and Andrews (1936; 1938) found that the precentral β rhythm (~25 Hz) was blocked by intense auditory stimuli, and Davis (1939) found increases, decreases, or no changes in the β band depending on the subject. It appears (as will be seen again in Chapter 6) that β fluctuations in the range ~20-30 Hz are not a decisive sign of activation or inactivation.

In the late 1950s through the 1970s studies of evoked potentials came to dominate EEG work with sensory stimuli, and only a handful of reports of auditory α suppression appeared during this period (Pillsbury et al. 1967; Giannitrapani 1970; Putney 1973; Milstein 1974). One of these deserves special mention, however, as it was the first report of spectral analysis of the EEG under auditory stimulation (Figure 4.7).

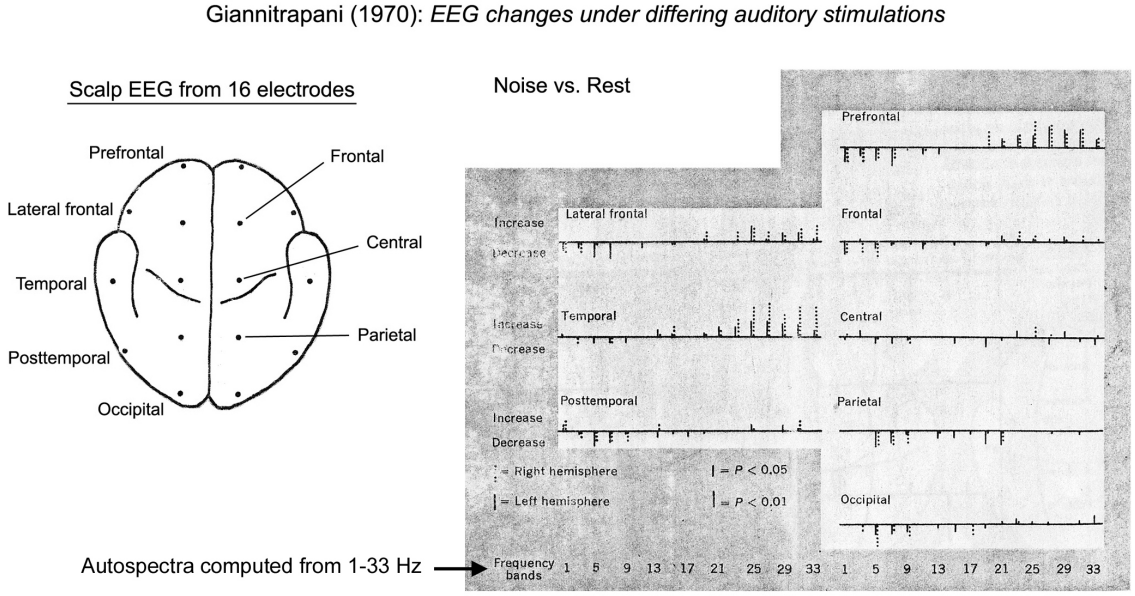

Figure 4.7. First report of spectral analysis of EEG with auditory stimulation (from Giannitrapani 1970, with labeling added). 8 sec segments of data were taken from each condition and autospectra were computed from 1-33 Hz (16 bands, each 2 Hz wide). This example shows log power of the noise condition relative to the rest (silence) condition. Careful scrutiny of the figure reveals that most electrodes show suppression in the bands 1-17 Hz. The temporal and frontal electrodes also show enhancement in the bands ~ 25-33 Hz.

ECoG responses to auditory stimuli

Although I know of over 50 human intracranial studies involving the auditory system, there is only 1 study prior to the year 2000 that looked at the responses of EEG rhythms or frequency bands to auditory stimuli! This is a consequence of the above-mentioned focus on ERPs in the sensory EEG literature from the late 1950s to the 1990s. This single study (Jacobson et al. 1998) appeared in an obscure journal and reported on 2 epilepsy patients. Using a band-pass filter from 24-48 Hz, they found increased γ power in response to tones presented every ~2 s. This occurred in known auditory areas, but the topography was found to be different from the N1

of the auditory ERPs. We have found a similar dissociation between γ and ERPs in many of our patients.

After this study, only a couple of additional studies have appeared with spectral analyses of auditory ECoG data (Crone et al. 2001a; Edwards et al. 2005). Crone's important study (Crone et al. 2001a) will be treated in the next chapter and data from the patients in (Edwards et al., 2005) is treated next. Crone's ECoG group has also given incidental auditory results in a language paper (Crone et al. 2001b) and a methods paper (Ray et al. 2003). Thus, there have been at most 4 other reports of spectral responses in human cortical recordings, and so the following studies are a highly unique contribution to the literature.

Experiment 1: ECoG responses to tones in tumor patients

Further examples are now shown from human ECoG data collected by myself and other students in human neurosurgical patients. The patients in this section (N=8) were all cases of left-hemisphere gliomas undergoing awake language mapping prior to resection. ~4-10 ECoG electrodes (3 mm contact diameter) were in place on the cortical surface as part of this procedure, with reference and ground electrodes at the margin of the craniotomy. At the end of the language mapping procedure and with the patient still awake, we presented several minutes of auditory stimuli. Further details of this collaborative project and the recording methodology are found in Appendix 1.

Tone stimuli were presented via loudspeakers in 2-3 blocks lasting ~3.5 min each. The first block type was a mismatch-negativity (MMN) paradigm, with standard and deviant tones. However, these results are not covered here as the MMN and deviancy processing are not the focus of this thesis. Instead, the results are presented from the second block type involving simple presentation of tones (550 Hz, ~70 dB SPL, 180 ms duration with 10 ms rise-decay). 100 tones

were presented with a stimulus onset asynchrony (SOA, which is the onset-to-onset interval) of 2.8 s ± 1.2 s. There was no task or response required of the patient, and he or she was asked to observe a slideshow of photographs for distraction. This protocol provides a very simple look at the passive reaction of auditory cortex to a simple stimulus.

Time-frequency analyses were done on the ECoG from each electrode. I originally (Edwards et al. 2005) used the methods of Makeig and colleagues described above (ERSP, Figure 3.7). However, I have since developed my own set of time-frequency methods using a Gaussian filter-bank and the Hilbert transform. As discussed above, these two methods can be made equivalent if the settings (e.g., filter width or window length) are carefully matched. The details of my method are given in Appendix 2, including the method of assessing statistical significance in the time-frequency plane. Because I use amplitude rather than power, I refer to the resulting time-frequency plane as the "event-related spectral amplitude" (ERSA). Here, "amplitude" is the analytic amplitude of the Hilbert transform. This is the envelope of the filtered signal and is in units of μV. However, given the large drop in amplitude with frequency (the "1-over-f" relation described above), the ERSA cannot be *displayed* in units of μV. For display purposes only, the units are changed to percentages relative to the mean amplitude in the pre-stimulus baseline (defined as 100%). This is done for each frequency band separately and so each frequency band is shown relative to its own mean. The plotting conventions for ERSAs are given in the figure legend for Figure A2.3 in Appendix 2.

The results from three patients showing good time-frequency responses are shown in the Figures 4.8-4.10. Figure 4.8 shows an example electrode from each of the three patients. These electrodes exhibit three features in common.

First, there is an increase in the θ band from ~50-300 ms that is due to the LAEPs or other slower AEPs. This is confirmed by plotting ERPs and by doing inter-trial coherence (ITC) analyses for these electrodes. These analyses are not shown here, as ERPs are not within the scope of this thesis. However, they have been examined in Edwards et al. (2005) and show strong ITCs for these electrodes in this time-frequency region. By definition, this guarantees that the increase in amplitude seen in the ERSA is contributing to the ERP. Patient 8 also shows an early increase in the γ_{low}, β, and α bands that is also strongly coherent across trials. This increase is associated with the MAEPs and early LAEPs (Edwards et al., 2005). Note also that the θ increase lasts for only 200-300 ms, barely enough time for one complete θ cycle. This also indicates that this increase is due to a distinct, ERP-related process rather than to an increase of ongoing θ oscillatory activity. These ERP-related increases are not discussed further except to note that this is one of the disadvantages of working with the lower frequencies, where "evoked" (ERP-related) activity makes a major contribution.

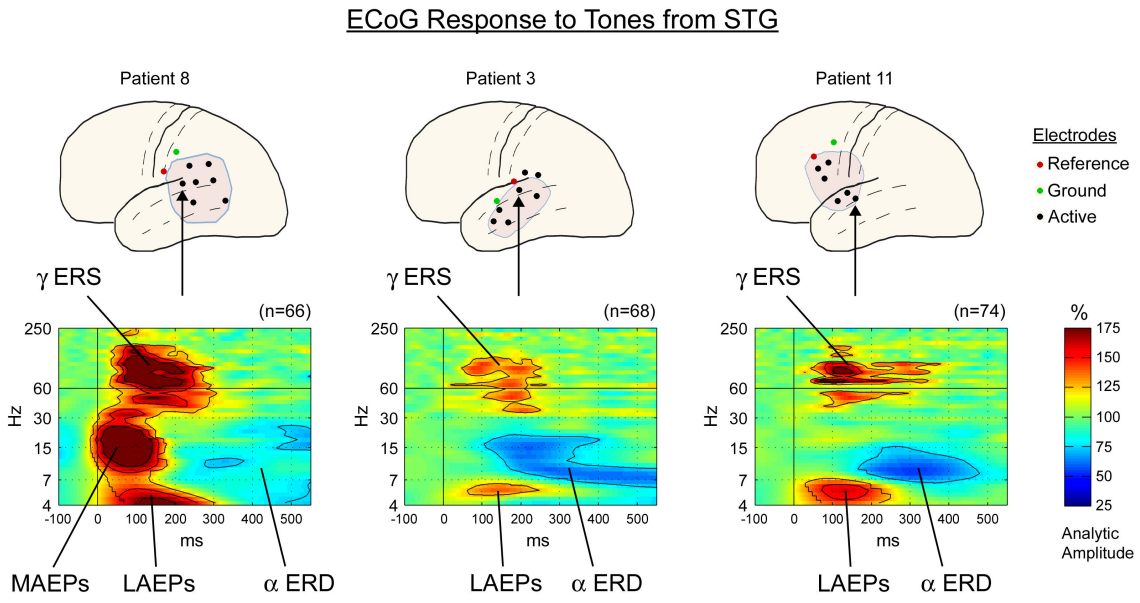

Figure 4.8. ERSAs are shown from 3 electrodes on the STG from 3 separate patients. The template brains in the top row show the locations of the craniotomies and electrodes.

The second consistent feature of the ERSAs in response to tones is the prominent increase in γ_{high} analytic amplitude from ~30-300 ms. As shown by the ITC analyses in Edwards et al. (2005), the γ_{high} increase is purely "induced" (shows very little or no ITC) and no ERP-associated activity has been found in the γ_{high} band. For example, filtering the signal below the γ_{high} band has no discernible effect on the resulting ERP. In the electrodes showing the strongest γ_{high}, the increase usually spreads into the γ_{low} band (~30-60 Hz). However, γ_{low} and γ_{high} do not always occur together, as figures 4.9 and 4.10 show.

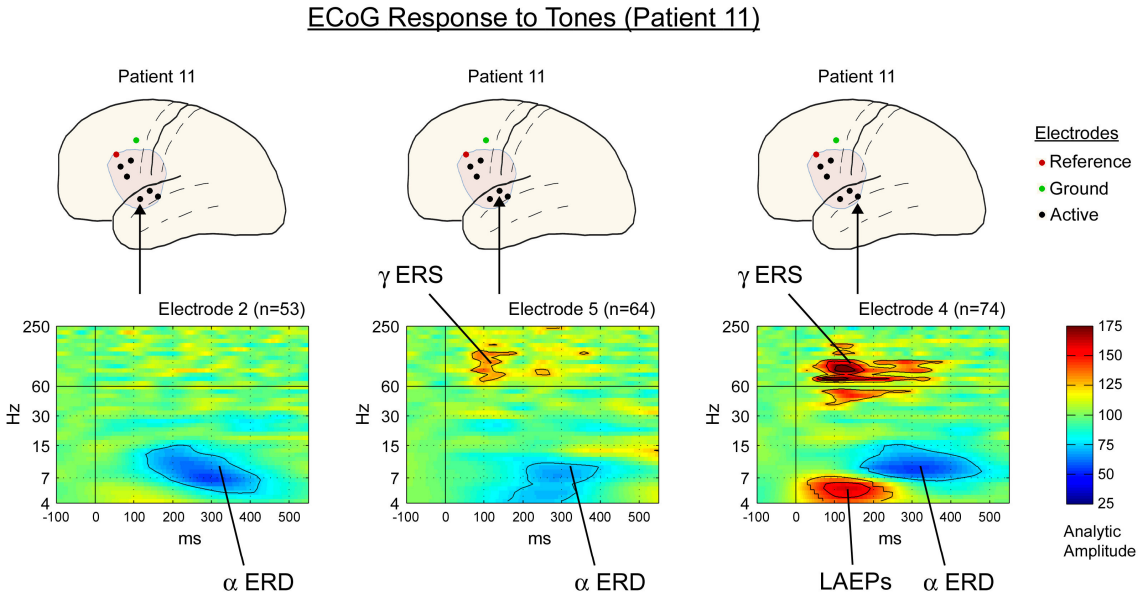

Figure 4.9. ERSAs from 3 different electrodes from the same patient (Patient 11). These are arrayed in an anterior-to-posterior sequence along the STG. The posterior-most electrode (right) is the same as in Figure 4.8 above. In moving from this electrode to the one anterior to it (middle), the evoked θ associated with the LAEPs is lost. Also, the γ_{low} is lost and the γ_{high} ERS becomes weaker. In the anterior-most electrode (left), the γ ERS is almost entirely absent, while the α ERD persists. This illustrates that these different features of the spectral response are dissociable, and that the α ERD is more widespread. The three frontal electrodes for this patient did not show any significant event-related responses.

The third consistent feature of the ERSAs in response to tones is the suppression of lower frequencies (<25-30 Hz) beginning as early as ~75 ms and lasting for several hundreds of ms, occasionally for a second or more. The most important feature of this low frequency ERD is that it is spatially very widespread. For example, it is seen in Figures 4.9 and 4.10 to occur without the γ ERS in electrodes at some distance from the main posterior-Sylvian auditory areas. The low frequency ERD is even seen in many frontal electrodes (Figure 4.11), constituting the only event-related response seen in the great majority of frontal electrodes for passive listening.

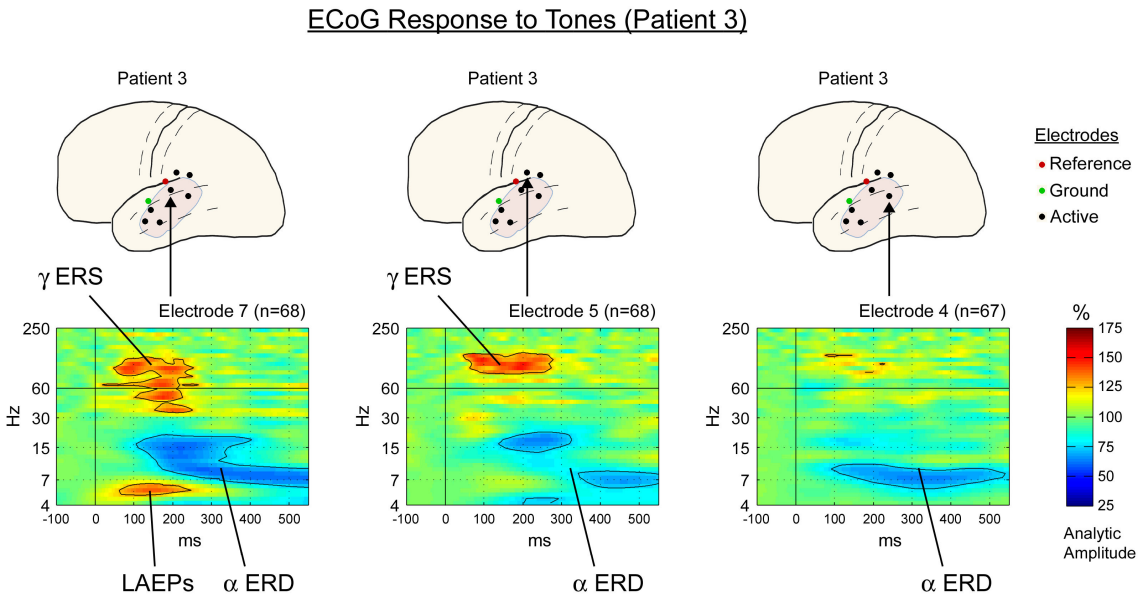

Figure 4.10. ERSAs from 3 different electrodes from the same patient (Patient 3). The electrode on the left is the same as the one in Figure 4.8 above. An electrode just above it (middle) does not show the evoked θ associated with the LAEPs. Also, the low-γ is much weaker. In the electrode on the posterior MTG, the γ ERS is almost entirely absent, while the α ERD persists. This illustrates again that these different features of the spectral response are dissociable, and that the α ERD is more widespread.

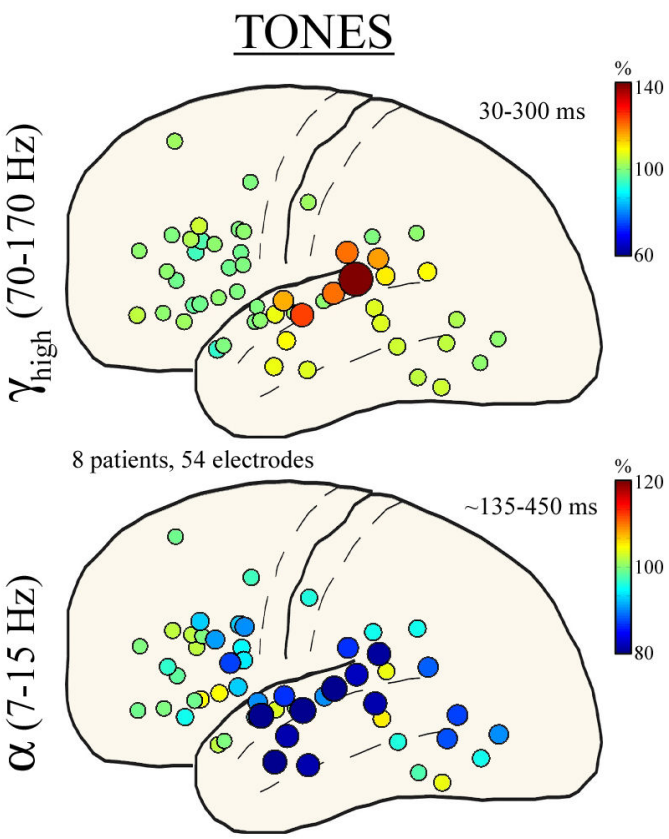

Figure 4.11. Summary of ECoG response to tones in 8 tumor patients, over 54 electrodes total. **Top:** γ_{high} ERS (mean from 30-300 ms, 70-170 Hz) is only found in the STG, concentrated around the posterior extent of the Sylvian fissure. **Bottom:** α ERD (mean from ~135-450 ms, 7-15 Hz) is strongest in the temporal lobe, but also present in frontal electrodes (particularly posterior IFG) and occipito-temporal electrodes.

Overall, the results are consistent with the EEG activation pattern discussed in Chapter 2. In known auditory areas of the temporal lobe, and particularly around the posterior extent of the Sylvian fissure (at the level of Heschl's gyrus, but our recordings do not enter into the Sylvian), auditory stimuli cause an increase in high frequency (>30 Hz) and a decrease in low frequency (<25 Hz) amplitude. The observations of α suppression in widespread cortical areas is consistent with the scalp EEG studies surveyed above, where α suppression was observed with a wide variety of electrode placements. Given the relatively focal distribution of γ enhancement, the low absolute amplitude involved, a very low coherence across ECoG electrodes (not shown here), and the presence of large muscle artifact at the scalp, it is easily understood why γ increases are less

consistently seen in scalp EEG studies. There are no scalp EEG studies that show the increase in the γ_{high} band that is seen very consistently in the ECoG.

The widespread suppression of lower frequencies relative to the more focal γ increases is consistent with the notion that low frequency ERD is a more "non-specific" response. This follows partly by definition, as "non-specific" and "spatially-diffuse" are inextricably linked. The dichotomy should not be taken too literally, as there is a continuum of spatial scales over which thalamo-cortical projections and coherent processes operate. Nonetheless, there appears to be a clear physiological difference between γ ERS and α ERD captured at least in part by the distinction between "specific" and "non-specific".

Three advantages of the γ_{high} band were observed already in this simple study. First, it is spatially more focal than the low frequency ERD. Second, it shows the best signal-to-noise ratio of any frequency band (strongest changes relative to the baseline). Third, it is not confounded by the presence of "evoked", ERP-associated activity. These and other advantages are seen again in the following chapters. To anticipate one of the main conclusions of this thesis, the γ_{high} band is emerging as the best electrocortical measure of activation to use for mapping.

Chapter 5: Auditory responses to simple speech stimuli

Chapter 4 discussed the basic localization of auditory cortex in humans and showed responses to simple auditory stimuli (tones). This chapter will delve further into mapping the human auditory system and bring us one step closer to language by looking at the auditory responses to simple speech stimuli (syllables). A strong EEG activation response is seen in the mid-STG, consistent with results from other imaging modalities.

Experiment 2: ECoG responses to syllables in tumor patients

As in Experiment 1, the patients in this study (N=8) were all cases of left-hemisphere gliomas undergoing awake language mapping prior to resection. The methods were identical to those of Experiment 1 (see also Appendix 1), but with a new set of auditory stimuli. These consisted of the 5 syllables /pa/, /ba/, /wa/, /aa/, and /uu/ spoken 5 times each by 4 male speakers (giving $5 \times 5 \times 4 = 100$ unique sound files total). The SOA (onset-to-onset) was 775 ms ± 50 ms. Onsets and offsets of each sound were identified by a simple moving-window root-mean-square (RMS) calculation. By this criterion, the sounds were ~250 ms long (200-284 ms), resulting an effective ISI (offset-to-onset) of ~525 ms ± 50 ms.

The sounds were presented in two blocks, where one was a mismatch block with 80% standards (/aa/) and 20% deviants (/uu/). This block was obtained for all patients. For the patients that completed two blocks, the other block included all 5 syllables with 20% probability for each. As in Experiment 1, mismatch responses and deviancy processing are not the focus here. The ERSAs shown combine the response to all syllable types across all blocks. The main result is to show the strong response to speech sounds from the mid-STG, and the differentiation of stimulus subcategories does not concern this goal. Also, in preliminary analyses no striking differences were seen between syllable types, except for standards vs. deviants in the ERPs.

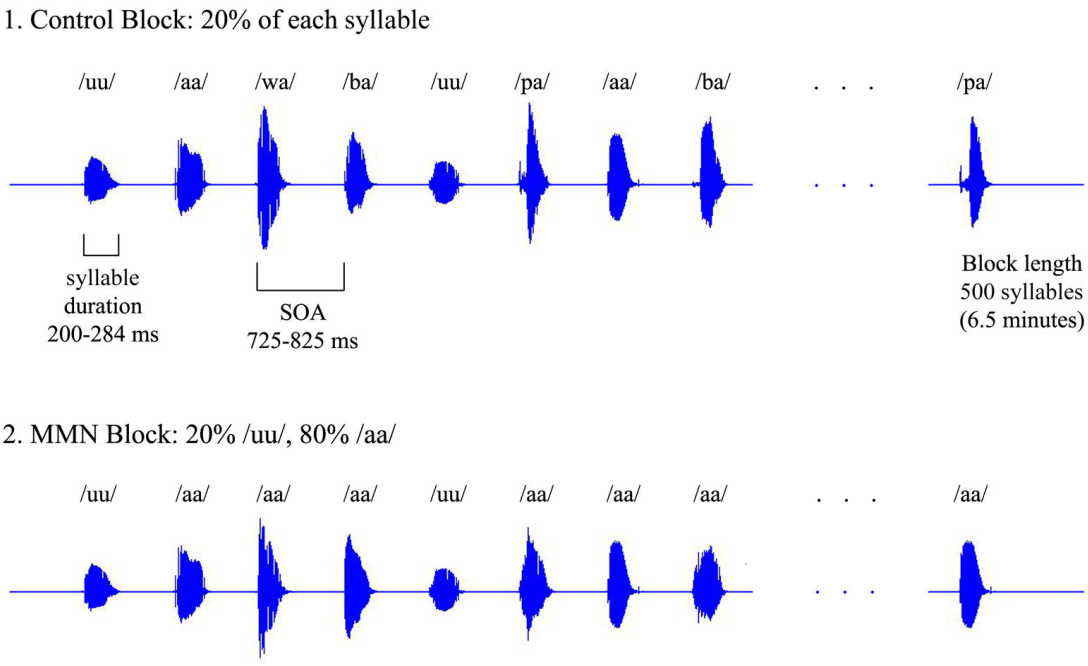

Figure 5.1. Design of Experiment 2 (syllables). Details given in text.

The main result was a γ_{high} increase found in three patients with electrodes on the mid-STG. Furthermore, these were the only three electrodes showing a strong γ_{high} response. Unfortunately, there were not any subjects with exposure of the posterior peri-Sylvian auditory areas, which undoubtedly would have also shown a response. In addition to the γ_{high} response, suppression of α and lower frequencies was also seen. This suppression was seen at widely dispersed electrodes, including frontal electrodes.

ERPs (again not shown) were seen at various temporal electrodes with a somewhat different topography than the γ_{high} response. An ERP-associated increase in α and θ bands is seen in the ERSA for Patient 26. However, ERPs were again absent at frontal electrodes.

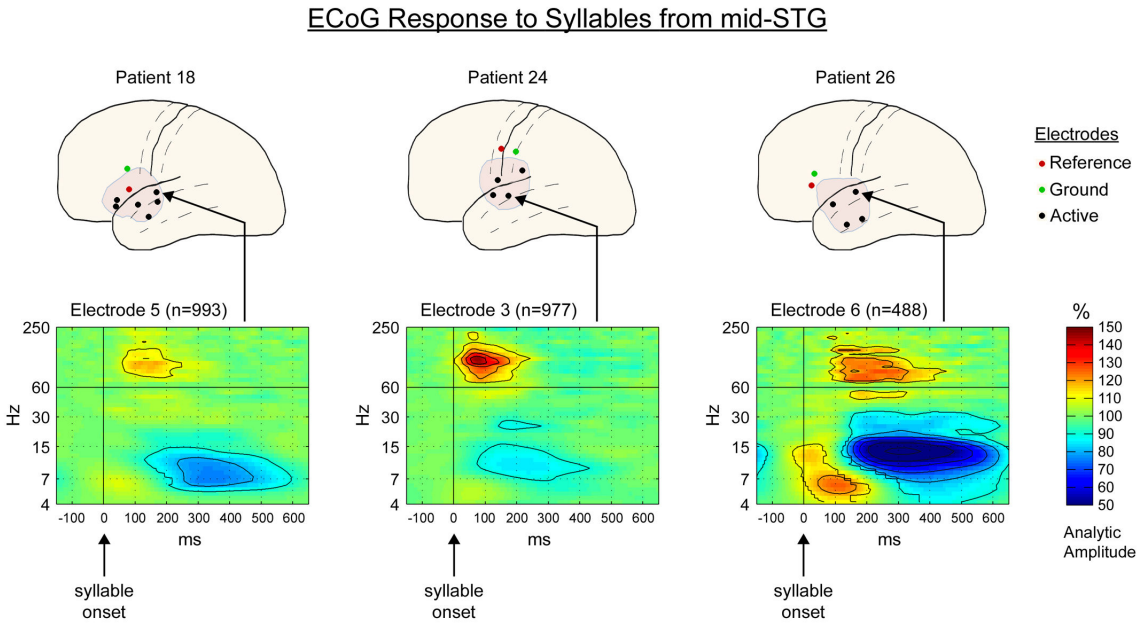

Figure 5.2. Time-frequency responses to syllables from the mid-STG. Methods and plotting conventions are given in detail in Appendix 2 (Figure A2.3). Three electrodes are shown from three separate patients. The main result is the γ_{high} (>60 Hz) increase from ~30-300 ms. Only weak increases are seen in the γ_{low} band (30-60 Hz), except perhaps in Patient 26. A decrease is seen in the θ, α, and β bands at these and other electrodes. This is particularly strong in Patient 26, where the α ERD persists for virtually the entire ISI (~525 ms) and shows up in the ERSA baseline ramping upward as it recovers from the previous trial. Thus, the significant pixels here in the baseline are not an error. This patient also shows an ERP-associated response in the θ and α bands peaking at 100 ms. Note that the precise onsets and offsets in these frequency bands are difficult to determine given the low temporal resolution at low frequencies (Appendix 2).

As in Experiment 1, there was almost a complete absence of response from frontal electrodes other than a couple of electrodes showing the widespread low frequency ERD (Figure 5.3). It would appear that the frontal lobe is uninterested in rudimentary sensory stimuli of no

behavioral consequence (passive listening). In subsequent experiments in epilepsy patients using active tasks (including with these very same stimuli), we have found frontal auditory activations. Frontal lobe activation for active but not passive tasks is also generally reported in the PET and fMRI literature (Démonet et al. 1992; Zatorre et al. 1992; Fiez et al. 1995; Binder et al. 1996; Zatorre et al. 1996). The activation of the mid-STG for speech stimuli is also consistently reported in the imaging literature, as discussed below. First, other intracranial studies are briefly shown that also implicate the mid-STG as the critical area for acoustic-phonetic processing.

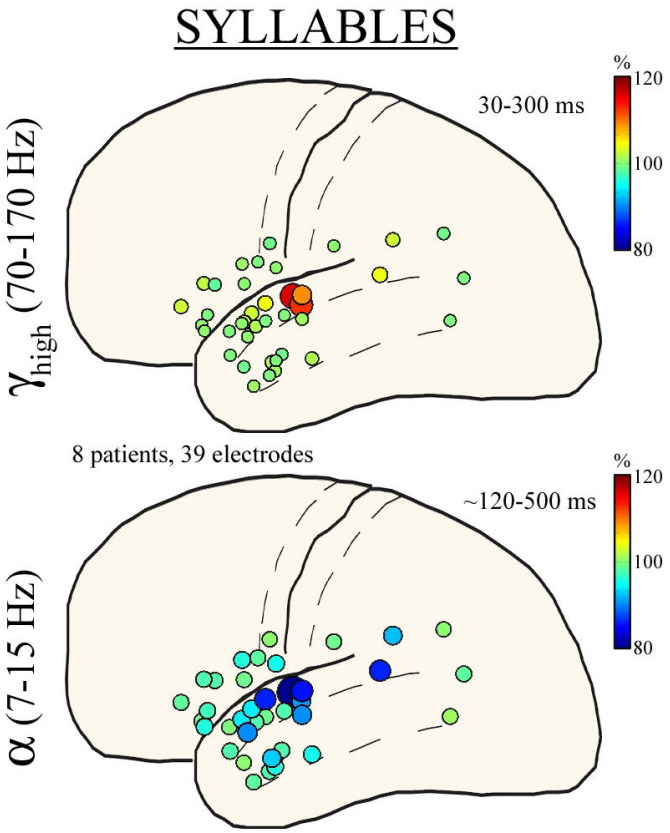

Figure 5.3. Summary of ECoG response to syllables in 8 tumor patients, over 39 electrodes total. **Top:** γ_{high} ERS (mean from 30-300 ms, 70-170 Hz) is only found in the mid-STG, (however exposure of the posterior extent of the Sylvian fissure is lacking). **Bottom:** α ERD (mean from ~120-500 ms, 7-15 Hz) is strongest in the temporal lobe, but also weakly present in frontal electrodes.

Other intracranial evidence

Other intracranial studies in human neurosurgical patients consistently implicate the mid-STG in acoustic-phonetic processing. These are briefly discussed here, and include evidence from single-unit recordings (Creutzfeldt et al. 1989), electrical stimulation mapping (ESM) (Boatman 2004), and ECoG recordings in epilepsy patients (Crone et al. 2001a). The single-unit and ESM evidence is shown in Figures 5.4 and 5.5, and discussed in the figure captions.

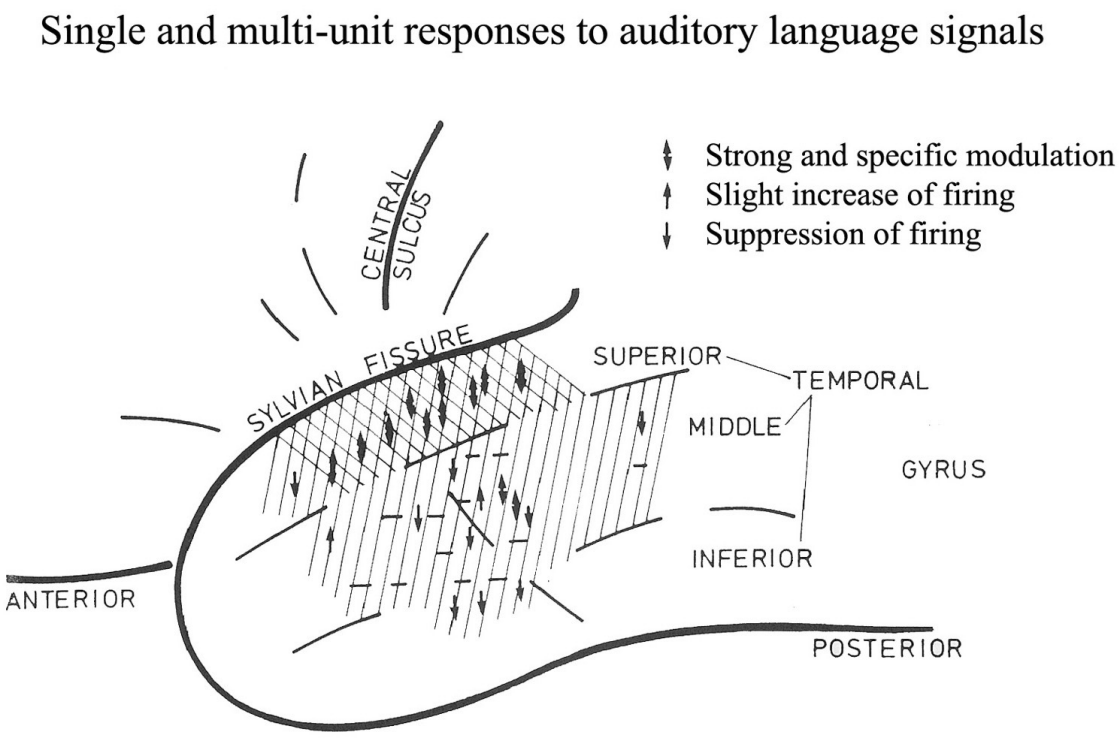

Figure 5.4. Single- and multi-unit recordings using microelectrodes were done in 34 human epilepsy patients during auditory presentation of words and conversational speech (from Creutzfeldt et al. 1989). The striped area shows areas found to be responsive to speech sounds, with the strongest responses found in the double-striped area of the STG. "Strong and specific modulation" of firing was found almost exclusively in the STG, centered below the central sulcus and post-central gyrus (this would fall approximately between the AC and PC lines of the imaging studies treated below, and is what I refer to as the mid-STG).

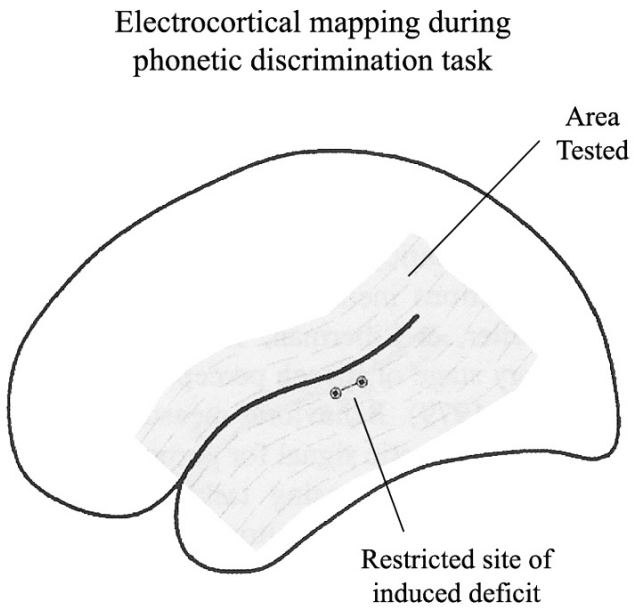

Figure 5.5. ESM during a phonetic discrimination task identifies a restricted site of induced deficit in the mid-STG (from Boatman 2004). The author concludes: "Acoustic-phonetic processing, as measured by auditory discrimination of phonetic features, is associated with a relatively circumscribed, local network within the middle-posterior region of the left STG. This was the only region associated with acoustic-phonetic processing during electrocortical mapping."

Further confirmation comes from the important ECoG study by Crone et al. (2001a) which also demonstrated several advantages of the γ_{high} band[9]. This study looked at an active phoneme discrimination task in epilepsy patients. Recording from the left STG, he found α suppression and γ_{low} and γ_{high} enhancement to phoneme stimuli. This is consistent with the EEG activation pattern, and with the results of Experiment 2. The two phonemes were presented with an SOA of 745 ms, and only the γ_{high} band showed two distinct response peaks. This illustrates the greater temporal resolution of the γ_{high} band for tracking cortical activation, in the sense that

[9] The γ_{high} band was discovered in the human ECoG and named as such by a prior study in the somatomotor system from Crone and colleagues (1998).

modulations of its envelope occur with greater rapidity than other frequency bands. This study also illustrates the excellent signal-to-noise (SNR) of the γ_{high} band, with power increases relative to the baseline reaching over 400% in some cases. Finally, the γ_{high} ERS was the most focal topographically.

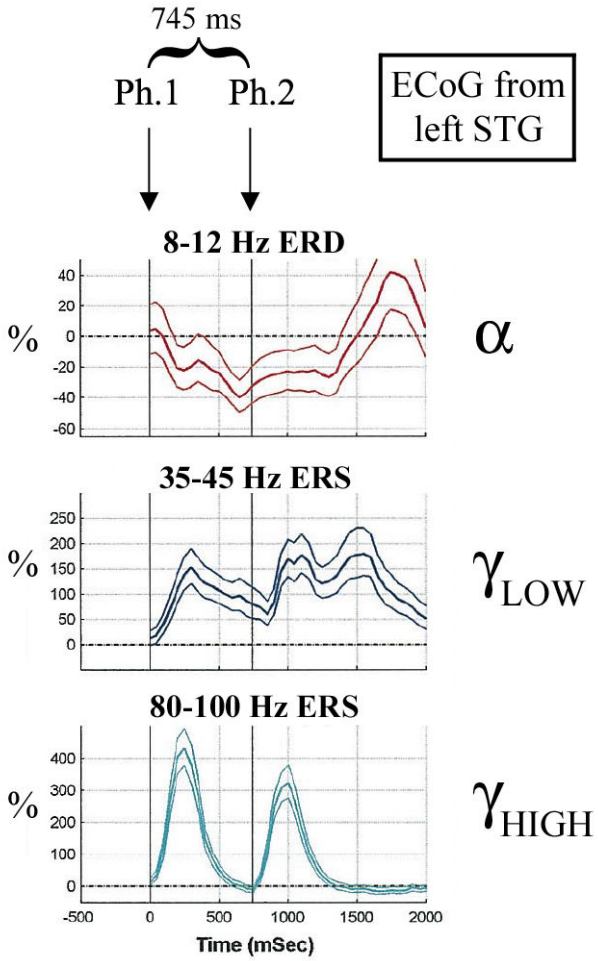

Figure 5.6. ECoG responses from left STG in epilepsy patients during a phoneme discrimination task (from Crone et al. 2001a with labeling added). Two phonemes were presented in rapid succession (745 ms SOA) and time-frequency analysis of the ECoG was done. Only the γ_{high} band showed two distinct response peaks in response to the two phonemes. Notice the high SNR of the γ_{high} band, reaching a power level of >400% relative to the pre-stimulus baseline. The α band shows a ~25% decrease, the γ_{low} band a ~150% increase.

PET and fMRI evidence

PET and fMRI studies of auditory speech processing consistently find activation of the STG, in accord with the γ_{high} ERS focus above. These include the auditory areas of the STP and posterior peri-Sylvian areas close to primary auditory cortex, as is the case for all auditory stimuli. But for speech stimuli in particular, the most consistent finding is activation of the mid-STG and neighboring cortex within the superior temporal sulcus (STS) (Démonet et al. 1992; Fiez et al. 1995; Binder et al. 1996; Binder et al. 2000; Tervaniemi et al. 2000; Indefrey and Cutler 2004; Liebenthal et al. 2005). For active tasks (auditory target detection, working memory, etc.) areas of the inferior frontal lobe (IFG, ~Broca's) are additionally activated (Démonet et al. 1992; Zatorre et al. 1992; Fiez et al. 1995; Binder et al. 1996; Zatorre et al. 1996). When lexical or semantic processing is involved, activations of the MTG and some additional language areas are commonly found (see meta-analyses of Binder et al. 2000; Indefrey and Cutler 2004).

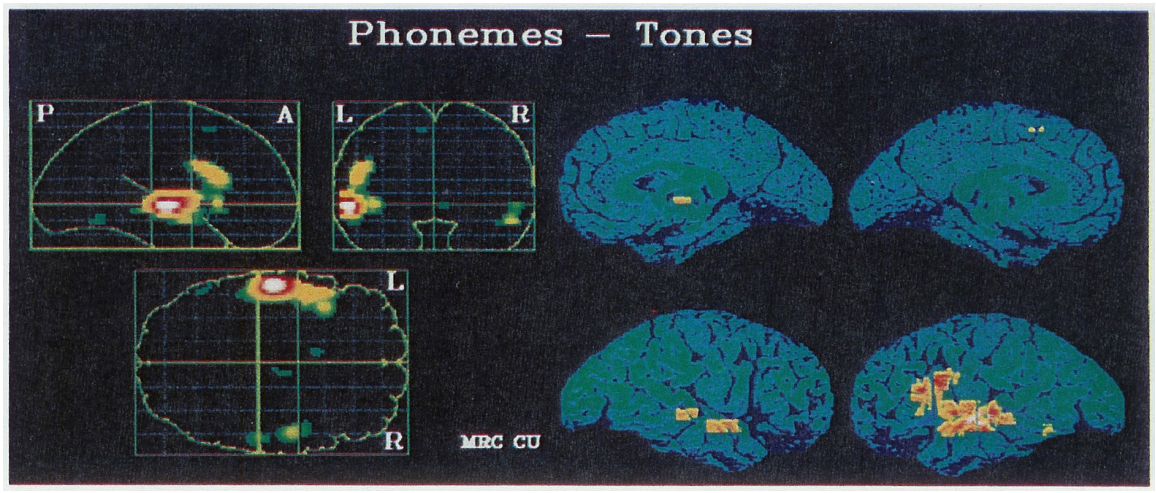

Figure 5.7. PET activation of the mid-STG to phoneme stimuli (from Démonet et al. 1992). The peak of the activation (phonemes minus tones) is in the mid-STG, between the anterior and posterior commissure lines (AC and PC lines). The activation is greater in the left hemisphere. The task was an active target detection task, and accordingly IFG activations are also seen. For a semantic decision task with words, additional MTG activation was found (Démonet et al. 1994).

Figure 5.8. fMRI activation for passive vs. active processing of auditory stimuli (from Binder et al. 1996). **Left (Passive):** For passive listening to speech stimuli vs. tones, the peak activation was in the mid-STG between the AC and PC lines. Tones showed greater activation at posterior peri-Sylvian sites. A similar pattern is seen in our γ_{high} activations comparing Figure 4.11 (tones) vs. Figure 5.3 (syllables), although we lack the systematic spatial covered to reach a strong conclusion. **Right (Active):** For active processing of words, the IFG, MTG, and angular gyrus are activated.

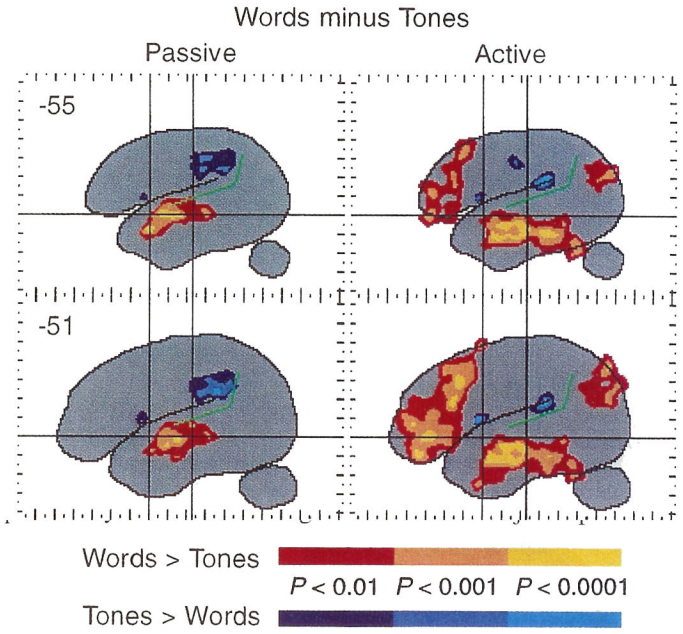

The γ_{high} results are consistent with the neuroimaging literature, keeping in mind that our ECoG studies involved only passive listening. For active tasks, a wider set of areas is implicated in the imaging studies. Interestingly, our α ERD results seem to be found preferentially in this wider set of areas found for active processing of speech sounds. It is almost as if some sort of preparatory, sub-threshold activation of these areas occurs for passive tasks, which is reflected in the perturbation of α in these areas.

Summary

In this chapter we have seen again that the γ_{high} ERS is more spatially focal than the α ERD. The γ_{high} results are found to align very well with the results from stimulation mapping, single-unit studies, and PET and fMRI studies. Several of our subsequent studies in epilepsy patients also find good alignment of the γ_{high} results with PET and fMRI studies. We must begin to ask: why does γ_{high} align with measures of blood flow and metabolism? Is there direct evidence that γ_{high} in the ECoG is correlated with hemodynamic or metabolic measures? The next chapter addresses these fundamental questions.

Chapter 6: Metabolic and hemodynamic correlates of the EEG

Now it is time to consider a direct test of the EEG activation hypothesis (that increased γ and decreased α and lower frequencies indicated cortical activation). When a patch of cortex exhibits EEG activation, it should show an increase in blood flow. Cerebral blood flow and metabolism are ~linearly coupled over a wide dynamic range (Hoge et al. 1999). Although blood flow and metabolism can become temporarily uncoupled during spurts of strong activity (Fox et al. 1988), this doesn't change a positive correlation into a negative one. It merely makes the relationship non-linear. Thus, in the following survey of the hemodynamic correlates of the EEG, positive correlations with blood flow almost certainly indicate positive correlations with metabolism. The only major caveat is to carefully consider the spatial extent of cortex to which a measure of blood flow, metabolism, or EEG activity applies. For example, scalp EEG would measure from a much larger extent of cortical tissue than ECoG, and there are a variety of blood flow measures that differ in their spatial resolution. Ideally, ECoG would be obtained from the same cortical area as some measure of blood flow, as was done in the outstanding early study considered next.

Pioneering study by Darrow and Graf

Studies of EEG correlations with brain metabolic factors (temperature, pH, glucose, etc.) and with autonomic measures of arousal (pupil dilation, GSR, etc.) were common in the 1930s and 1940s. These were generally confirmatory of the EEG activation hypothesis (for example, α is negatively correlated with autonomic measures of arousal), but these do not provide the direct test that we seek. The American researcher Chester W. Darrow, who began his research on EEG/autonomic correlates, would be the first to directly correlate EEG frequency bands with blood flow (Darrow and Graf 1945).

The study by Darrow and Graf (1945) was an experimentalist tour de force that has been unmatched until contemporary times. They simultaneously measured scalp EEG, surface ECoG, EKG, and blood flow in the parietal cortex of cats. The cats were lightly anesthetized with ether or curarized. As in the Ectors (1936) study above, the absence of heavy anesthesia may have been important for the results in the γ band. To measure blood flow, they used an early form of optical imaging ("photometry") and for this alone this was an outstanding experimental paper. The photometry was done through a small cranial window, essentially using a microscope and a camera to observe the diameter of blood vessels, waves of constriction passing along the vessels, and changes in the color through specially designed filters. The change in color indicates blood flow level, where darkening indicates more blood and paling indicates less blood. These effects are primarily due to changes in blood volume, which translates into the area occupied by vasculature of the cortical surface. The dilation of millions of capillaries darkens the cortical surface, and their constriction elicits paling. Blood oxygenation levels, with fresh blood flow being more oxygenated, also contributes, and filters enhance the color differences between oxygenated and deoxygenated blood.

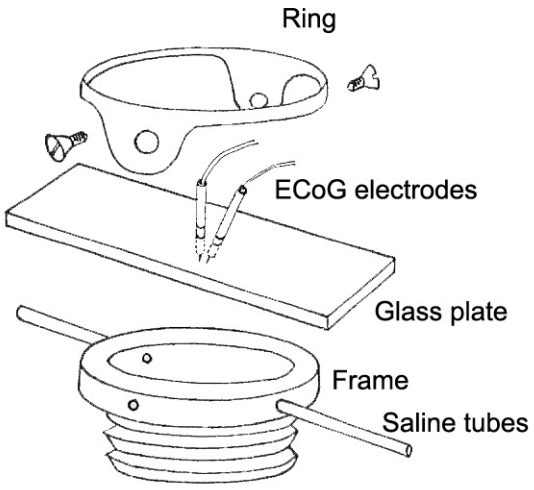

Figure 6.1. Illustration of cranial window technique for simultaneous ECoG and photometery (from Darrow and Graf 1945, with labeling added).

The surface ECoG was done with bipolar pairs of electrodes inserted through small holes in the glass covering the cranial window. Thus, the ECoG measures were obtained simultaneously and from the same cortical region as the photometry. On the ECoG data, they performed a spectral analysis using a laborious set of hand measurements. Given the rarity of spectral analyses at this time (Chapter 3), this is another impressive methodological aspect of this study. Although crude by contemporary standards, it provided amplitude in the frequency bands 4-8 Hz, 8-16 Hz, 16-32 Hz, 32-64 Hz, and >64 Hz (corresponding roughly to θ, α, β, γ_{low}, and γ_{high}). They state: "With photometrically observed paling there is a rather consistent shift toward the slow end of the spectrum with a tendency for the microvoltage of slower frequencies to increase, whereas with photometrically observed flushing there is a tendency for faster activity to increase and for the microvoltage of slower waves to decrease." That is, increased blood flow correlates with higher ECoG frequencies, and decreased blood flow with slower ECoG frequencies. This is precisely what is expected by the EEG activation hypothesis.

Darrow and Graf (1945) presented two large tables giving quantitative measures of blood flow and each of the ECoG frequency bands across a variety of manipulations of temperature and ventilation. A careful look at these tables reveals an inverse correlation between blood flow and slow ECoG frequencies(4-8 Hz and 8-16 Hz) and a positive correlation between blood flow and fast ECoG frequencies (32-64 Hz, >64 Hz). The β band (16-32 Hz) showed weaker positive correlations. To illustrate this data given in tables, I have entered the numbers into Matlab and obtained a simple Pearson's correlation coefficient (r) for each ECoG frequency band with blood flow (Figure 6.2).

Figure 6.2. Correlations between blood flow and amplitude in each of 5 frequency bands of the ECoG (data originally presented in tables in Darrow and Graf 1945). I have deliberately made the figure in the style of Mukamel et al. (2005) in order to facilitate a quick comparison (Figure 6.7 below). Darrow and Graf (1945) were clearly the first to demonstrate this ECoG/hemodynamic relationship, and their study provides the first strong confirmation of the EEG activation hypothesis by comparison across techniques.

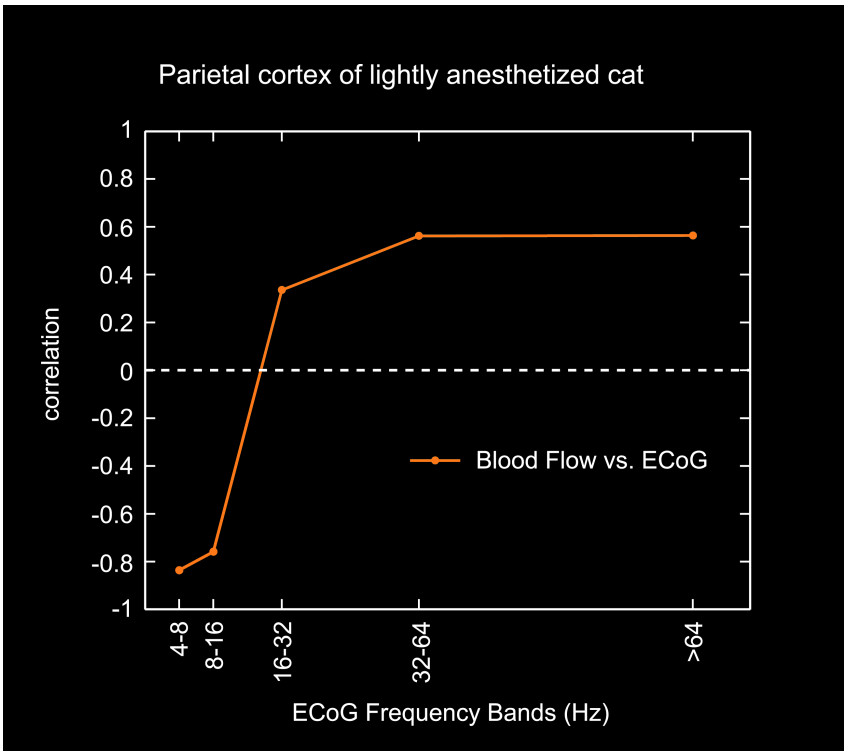

Simultaneous EEG and PET

With the development of PET in the 1970s it became possible to measure blood flow and metabolism in humans. Combined with simultaneous scalp EEG, this offered a new means of testing the EEG activation hypothesis. Unfortunately, only a small number of studies have combined PET and EEG measures, and most of these suffer from a methodological confound. The first such study was by Buchsbaum et al. (1984), who used injections of 2-deoxyglucose ^{18}F

(FDG-PET) to measure regional cerebral metabolic rate of glucose consumption (rCMRglu)[10]. α at the occiput (Oz) was negatively correlated (r = -0.76) with rCMRglu in the underlying section of the PET scan in the occipital cortex. However, these correlations were run *across* subjects, which is an unfortunate methodological flaw that considerably decreases the power of the study. A number of other EEG-PET studies made the same methodological error. For example, a recent study by Oakes et al. (2004) also found negative correlations of rCMRglu with α, as well as positive correlations with γ (Figure 6.3), but made the same methodological error. Only one study in this genre ran correlations *within* subjects (Sadato et al. 1998). This was a very good study using ^{15}O-labeled water to measure regional cerebral blood flow (rCBF), and negative correlations between occipital α and occipital rCBF were consistently found. Overall, the evidence from the PET-EEG literature has been consistent with the EEG activation hypothesis, but a sound study of rCMRglu using correlations within subjects is still lacking.

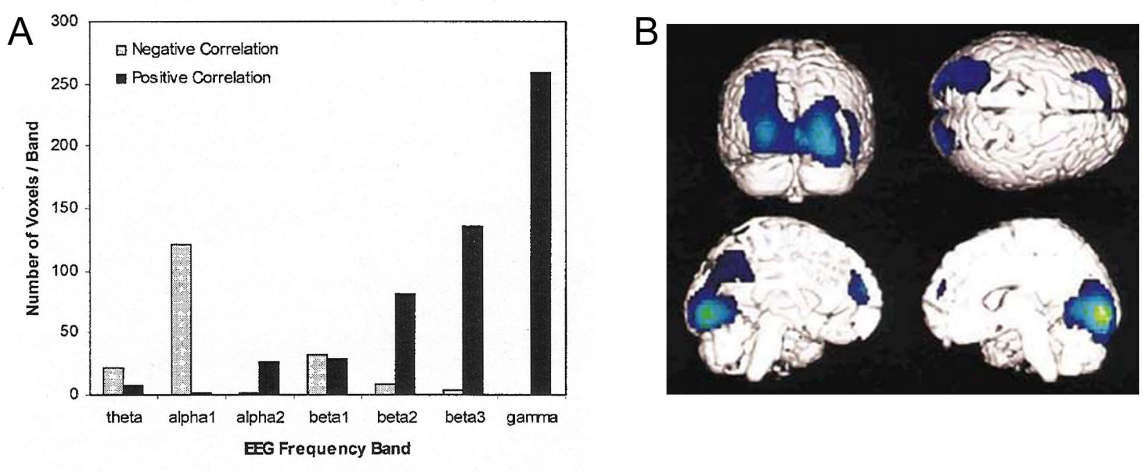

Figure 6.3. A. Correlations between rCMRglu and different EEG frequency bands (from Oakes et al. 2004). γ and higher frequencies show many positive correlations, whereas α and lower frequencies tend to show negative correlations. Unfortunately, these correlations were run *across* subjects. **B.** Negative correlations between rCBF and α over the posterior 1/3 of the scalp (from Sadato et al. 1998). This was a good study that ran EEG-PET correlations *within* subjects.

[10] The brain's metabolism relies almost exclusively on glucose as the source of energy.

Simultaneous EEG and fMRI

The advent of fMRI in the 1990s was a major event in the history of neuroscience and brought the 1800s quest for cortical localization back to the dominant foreground of neuroscience[11]. Recording EEG simultaneous with fMRI is technically very challenging due to the immense magnetic fields of the MRI scanner. Nonetheless, several studies have correlated the fMRI BOLD signal (a blood flow measure) with EEG α (Goldman et al. 2002; Laufs et al. 2003; Moosmann et al. 2003; Feige et al. 2005). These studies consistently find that occipital α and occipital BOLD are inversely correlated (Figure 6.4). One of these (Moosmann et al. 2003) also confirmed the negative correlation of α with blood flow using near infrared spectroscopy (another measure of blood flow based on sensitivity of infrared reflection levels to the oxygenation vs. deoxygenation of blood hemoglobin).

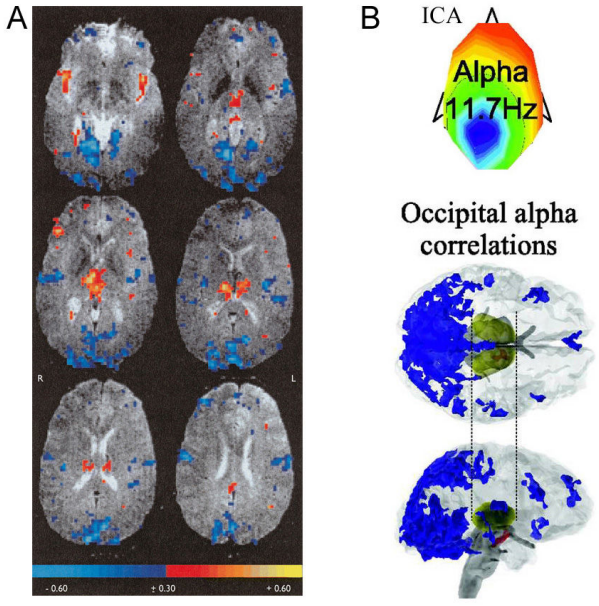

Figure 6.4. Simultaneous EEG-fMRI studies in humans showing negative occipital BOLD/α correlations. **A.** from Goldman et al. (2002). Positive correlations are found in the thalamus and other areas thought to *modulate* α power, but negative correlations are found in the occipital areas that *generate* the α under consideration. **B.** from Feige et al. (2005). Independent components analysis (ICA) was used to isolate a cleaner signal for the occipital α.

[11] Indeed, some comment that fMRI has led to an era of "neo-phrenology".

Only one simultaneous EEG-fMRI study in humans has looked at the γ band (Foucher et al. 2003). γ and BOLD showed good correspondence of changes across stimulus types, but the P300 and BOLD did not follow each other. Since the P300 occupies roughly the θ band, they conclude that "the BOLD signal is better correlated with high- than with low-frequency oscillations". The famous study of γ and BOLD is treated next.

Logothetis on the neural basis of BOLD

We now return to animal studies and look at the most commonly cited study of BOLD correlations with EEG (in this case, LFPs) (Logothetis et al. 2001). Simultaneous fMRI and microelectrode recordings were done in anesthetized monkeys, with the microelectrodes providing both local field potentials (LFPs, activity below ~300 Hz) and multi-unit spiking activity (MUA, activity above ~300 Hz). Results of this study are given in Figure 6.5.

Logothetis et al. (2001)

Neurophysiological investigation of the basis of the fMRI signal.

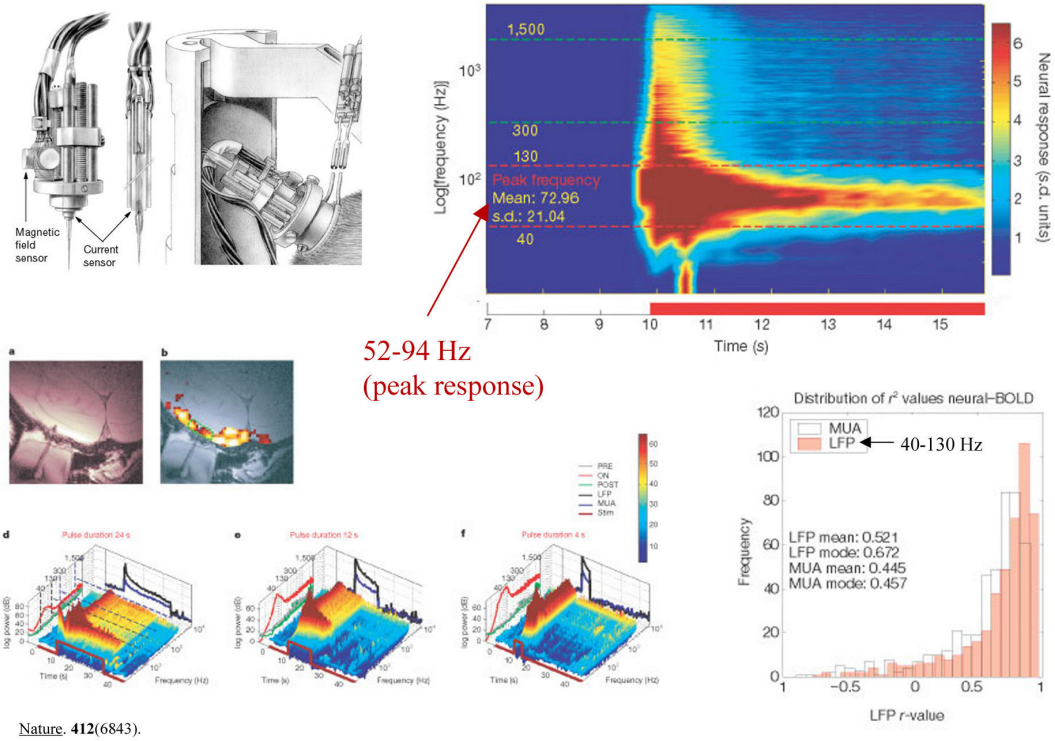

Nature. **412**(6843).

Figure 6.5 (previous page)**. Top left:** Simultaneous fMRI (BOLD) and microelectrode (LFP and MUA) recordings in monkey primary visual cortex (V1). **Top right:** Time-frequency response of LFP to reversing checkerboard stimulus (indicated with red bar on the time axis). A larger power increase was found in the frequencies above 30 Hz (γ), with the peak of the response at 52-94 Hz (mostly in the γ_{high} range). Close examination of other time-frequency plots (**lower left**) shows also a suppression (blue colors) in the lower frequencies. **Bottom right:** Distribution of correlation values for LFP γ (40-130 Hz) and MUA. On average, LFP γ gave a better estimate of BOLD responses than MUA (mean r-squared values of 0.521 vs. 0.445, described as a small but significant difference).

The Logothetis (2001) study is sometimes cited as showing that LFPs drive the BOLD response. But it must be clearly noted that only the γ range of the LFPs was used for the correlations. Thus, a better concluding summary would be that γ drives the BOLD response. In particular, the peak γ activity was mostly in the γ_{high} range (note that the traditional "40 Hz" frequency band is relatively inactive compared to γ_{high}). Thus, it appears that γ_{high} drives the BOLD response with a smaller contribution from γ_{low}. However, the MUA activity was nearly as good a predictor, and this study incidentally shows the positive correlation between γ and spiking activity.

Optical imaging and LFPs

As mentioned for the "photometry" study of Darrow and Graf (1945) above, optical imaging was an early method for measuring cerebral blood flow. Only one recent study has returned to the examination of EEG or LFP measures with optical imaging (Niessing et al. 2005). Simultaneous optical imaging (blood flow) and microelectrode recordings (LFPs and MUA) were made in visual cortex of anesthetized cats. Stimuli (drifting gratings) were presented at different

contrast levels, and correlations of blood flow and LFPs and MUAs were obtained across trials. As in Logothetis et al (2001), both MUA activity and LFP γ activity were correlated positively with blood flow, with slightly stronger correlations for LFP γ (Figure 6.6). As in Darrow and Graf (1945), negative correlations were found for lower frequencies (<15 Hz). They conclude that "there is a particularly tight correlation between hemodynamic responses and LFP oscillations in the high gamma frequency range".

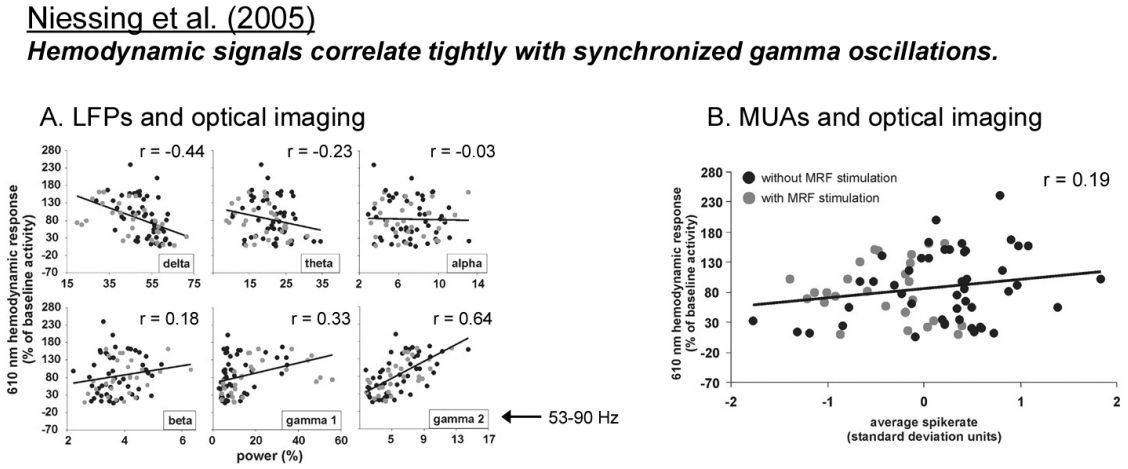

Figure 6.6. Simultaneous optical imaging (blood flow) and microelectrode (LFPs and MUA) recordings in visual cortex of halothane-anesthetized cats. **A.** Lower frequencies of the LFP (δ, θ, and to a lesser extent α) correlate negatively with optical measures of blood flow. Higher frequencies (β, γ_{low}, and in particular γ_{high}) show positive correlations. **B.** MUAs show a positive correlation with blood flow, but the correlation is weak compared to γ_{high} (r = 0.19 vs.0.64). This scatter plot was for only one stimulus type, however, and the correlations across all stimuli were more equivalent (r = 0.53 vs. 0.6 for MUAs vs. LFPs).

Correspondence of fMRI with human intracranial recordings

Appearing in the same issue of *Science* as the above optical imaging study was a study of human LFP correspondence with fMRI (Mukamel et al. 2005). LFP recordings were obtained from microwires in primary auditory cortex (A1) of two unanesthetized epileptic patients viewing a popular film. fMRI recordings were from a separate cohort of normal subjects watching the same film, and the A1 ROI was extracted for analysis. The ongoing BOLD signal was correlated with the ongoing ECoG activity in different frequency bands (convolved with a hemodynamic response function). MUA was recorded from the same microwires, and a similar positive correlation was obtained for MUA and BOLD. The results are presented in Figure 6.7, and show a nice confirmation of the Darrow and Graf (1945) study. Importantly, they also reported strong positive correlations (*within* subjects) between MUA spiking activity and LFP γ activity (blue trace in Figure 6.7). This provides one of the best demonstrations of this fact, and the only one in humans. Low LFP frequencies (<20 Hz) were negatively correlated with MUA spiking activity.

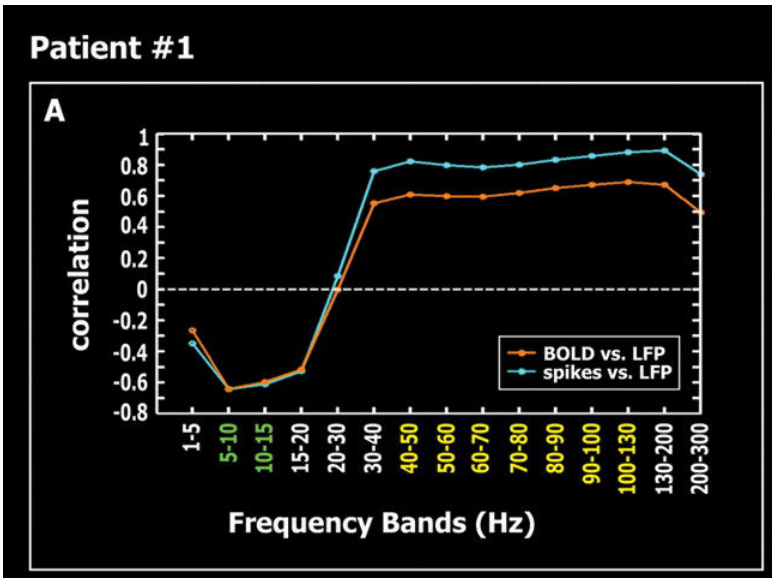

Figure 6.7. Correlation of BOLD with LFP activity in different frequency ranges for one epileptic patient with implanted microwires in A1. Strong positive correlations are found for the γ band with spiking activity. From Mukamel et al. (2005).

Only one other human study has looked at the relation of the fMRI BOLD signal to intracranial recordings (Brovelli et al. 2005). Depth electrodes were implanted in motor cortex of one epileptic patient, and a complex set of motor tasks were performed. β suppression (15-30 Hz) and γ_{high} enhancement (60-200 Hz) was found for motor activity. Comparing to ROIs obtained in a separate cohort of normal subjects, only the γ_{high} enhancement showed a tight spatial colocalization with the BOLD ROIs. It was also the only ECoG band to dissociate the different conditions of their task. They conclude that "among the different intracranial EEG responses, only the high gamma frequency (60-200 Hz) oscillatory activity both dissociates attention/memory from motor intention and spatially colocalizes with the fMRI-identified premotor substrates of these to functions."

These studies, and those of Logothetis et al. (2001) and Niessing et al. (2005), point to one of the advantages of the γ_{high} band for cortical mapping. All of these studies indicate that γ_{high} is the strongest electrophysiological correlate of blood flow, showing stronger correlations than the traditional 40-Hz band (γ_{low}) and, remarkably, even slightly stronger correlations than multi-unit spiking activity. The study by Brovelli et al. (2005) also indicates that γ_{high} shows greater task specificity (ability to dissociate task-related differences).

Why would γ_{high} show and even stronger correlation with hemodynamic measures than MUA? I believe that γ_{high} represents the summation of MUA and synaptic activity via fast receptors, namely glutamate AMPA and $GABA_A$ receptors (see discussion in Edwards et al. 2005). The fast ionic currents of GABAergic signaling via $GABA_A$ contribute directly to the γ_{high} band, and cost metabolic energy to restore the ionic gradients. Thus, GABAergic signaling, γ_{high} activity and metabolic demand correlate positively. However, as an inhibitory signal, GABAergic

input *decreases* single-unit firing. This would result in γ_{high} being slightly more correlated with metabolic and hemodynamic measures than MUA alone.

Summary

All of the studies covered in this section have some flaws. The Darrow and Graf (1945) study involved correlations with manipulations of respiration and temperature. The Logothetis study has a similar drawback in that it used correlations from V1 in response to visual stimuli. It would be preferable to see correlations of ongoing EEG and blood flow measures without specific manipulations or stimulation. Logothetis et al. (2001) used anesthetized animals, as did Niessing et al. (2005). The PET studies typically used across-subjects correlations, but within-subjects correlations would be strongly preferable. The simultaneous EEG-fMRI studies are severely compromised by noise, and scalp EEG has low spatial resolution, making correlations difficult to establish for circumscribed cortical areas. The human intracranial studies (Mukamel et al. 2005; Brovelli et al. 2005) used a different set of subjects for the fMRI measures. A study of simultaneous ECoG and fMRI in unanesthetized humans is still lacking (the study by Darrow and Graf (1945) has done this in animals and remains in some ways the best overall study; unfortunately, none of the studies in this section cite this pioneering study).

Despite these methodological problems, all of these studies converge on the same answer and together they provide strong support for the EEG activation pattern proposed in Chapter 2: that is, for the association that emerged in the 1930s that high and low frequencies represent cortical activation and inactivation, respectively. The crossover between high, "activation" frequencies and low, "inactivation" frequencies occurs between 15-30 Hz, depending on the study. This is the β band by modern convention, and confirms the point made in Chapter 4 that the β band is not a clear sign of activity or inactivity.

Few studies directly examine cerebral metabolism (rCMRglu), but increased metabolism can safely be inferred from increased blood flow. Given that our evolutionary ancestors (animal and human) evolved under conditions where starvation was a real and constant threat, the efficient use of metabolic energy is absolutely critical in cortical function. This is probably why an idling state (represented by α) evolved in the first place, in order to allow inactive regions to conserve energy. I believe that energy usage is the most cogent definition of "activity" or "activation" in terms of what is most critical to the organism evolutionarily. I therefore consider the EEG "activation" pattern to be very strongly supported by the observations of this chapter. We can now proceed on firmer ground to map the human cortex on the basis of its electrical activity. The next chapter applies this major principle of the EEG spectrum to human language mapping.

Chapter 7: Towards human language mapping

Human language can be studied only indirectly in animal models, and therefore linguistic neuroscience depends critically on methods of human neuroimaging. The blood-flow and metabolic techniques of the previous chapter (PET, fMRI, etc.) suffer from a very low temporal resolution (the fastest frequency band that can be tracked is below 1 Hz!), but scalp EEG and MEG suffer from poor spatial resolution. Human intracranial studies are a rare and invaluable opportunity to maximize both. Studies that penetrate the cortex with a microelectrode are extremely rare in humans, so studies of MUA can not be expected to be definitive. Thus, imaging of human language may depend critically on our ability to extract a meaningful measure of cortical activation from surface electrical recordings (ECoG). This thesis has argued at length that such a measure exists ("EEG activation") and that, in particular, the γ_{high} band offers a robust and powerful measure of cortical activation. This chapter further demonstrates the power of the γ_{high} band by examining cortical activations in a complex language task. Although this study is not complete, it already provides one of the best windows into human language function available, in terms of combining high spatial and temporal resolution.

Experiment 3: Verb generation task in epilepsy patients

The verb generation task (Petersen et al. 1988; 1989) is a semantic association task where a noun is presented and the subject must respond with an associated verb. In the variation used here, the noun is a synthesized auditory stimulus presented via speakers and the patient overtly responds by speaking into a microphone. 50 distinct nouns were each presented twice for a total of 100 trials. They were presented with an SOA of 4.1-4.2 s, allowing the patient time to choose a verb and respond. The verbal reaction time (RT), measured from stimulus (noun) onset to response (verb) onset was ~1.6 s. For the major patient of this section (grid patient 1, or "GP1"),

the mean (and range) was 1.49 s (0.87-3.45 s). A handful of trials were rejected due to a very late response (difficulty coming up with a verb).

Five adult epilepsy patients, with only 1 shown in this chapter[12], were studied several days after surgery for implantation of subdural electrodes. The 3 patients analyzed were consenting adults (all females, 24-37 years old) of normal intelligence and with no auditory or language deficits. They were highly cooperative in performing the verb generation task and a variety of other sensory and motor tasks. We excluded all electrodes exhibiting epileptic activity (usually medial temporal lobe focus with some activity seen in the anterior or inferior temporal lobe). Only recordings from ostensibly normal cortex are included and we know of no reason why the activations obtained below should be atypical due to the epileptic condition.

ECoG recordings were from an 8×8 grid of electrodes (2.3 mm contact diameter) embedded in a silastic sheet with center-to-center spacing of 1 cm. The electrode grid is implanted subdurally over the lateral surface of the left hemisphere, contacting frontal, parietal, and temporal lobes. The electrodes are used clinically to monitor for seizure activity in search for the epileptogenic foci, and to deliver electric shocks in ESM language and motor mapping. Additional electrodes are embedded in silastic strips (also with 2.3 mm contact diameter and 1 cm spacing) that curl beneath the orbitofrontal or inferior temporal lobes or extend posteriorly into parietal areas. The electrodes are localized on the patients' high-resolution MRI scan using information from intraoperative photographs, x-rays and/or CT scans, and known constraints (such as 1 cm spacing and that the electrodes must reside on the cortical surface). Further details of the recording methods are given in Appendix 1. The methods of data processing and time-frequency analyses, which are the same as in Experiment 2, are given in Appendices 1 and 2.

[12] 2 have not been analyzed at this time, but a preliminary look the others indicates that the results of this chapter are confirmed in their data.

Time-frequency analyses use a Gaussian filter bank and the Hilbert transform. For a given electrode, analysis begins with the original, continuous recording, S(t), and results in the analytic amplitude time-series, $AA^{cf}(t)$, for a frequency band centered at cf. $AA^{cf}(t)$ has the same length (~7 mins), sampling rate (2003 Hz), and units (μV) as the original signal S(t). Event-related analyses using $AA^{cf}(t)$, are called "event-related spectral amplitudes" (ERSAs), and show the analytic amplitude at each frequency (cf) as a function of time relative to event onset. ERSAs are made for the stimulus (noun) and the response (verb), time-locking to their respective onsets.

However, the "cognitive" interval between the sensory/perceptual processing and the overt motor response is of variable length and does not have a distinct and known onset. This is the interval where the semantic processing occurs and cannot be studied with a typical event-related analysis. I have used two solutions for this problem. First, taking advantage of the excellent SNR of the γ_{high} band, I examine the single-trial analytic amplitudes. When sorted by reaction time, the relative timing of the γ_{high} activations are clearly seen (Figure 7.1).

Second, I make "realigned" ERSAs that warp the duration of each single-trial to match the median duration. The sensory and motor intervals are left unaltered, so this "warping" only affects the intermediate cognitive interval. The sensory/perceptual interval is defined as pre-stimulus baseline through 500 ms post-stimulus. The motor interval is defined as 250 ms prior to speech onset through the end of the trial. It is only the period from 500 ms post-stimulus to 250 ms pre-response that is expanded/contracted to match the median duration. A realigned ERSA is made for each electrode, averaging from 7-14 Hz for the α band or 70-160 Hz for the γ_{high} band. These are used to make movies of activation topography across time (Figure 7.2).

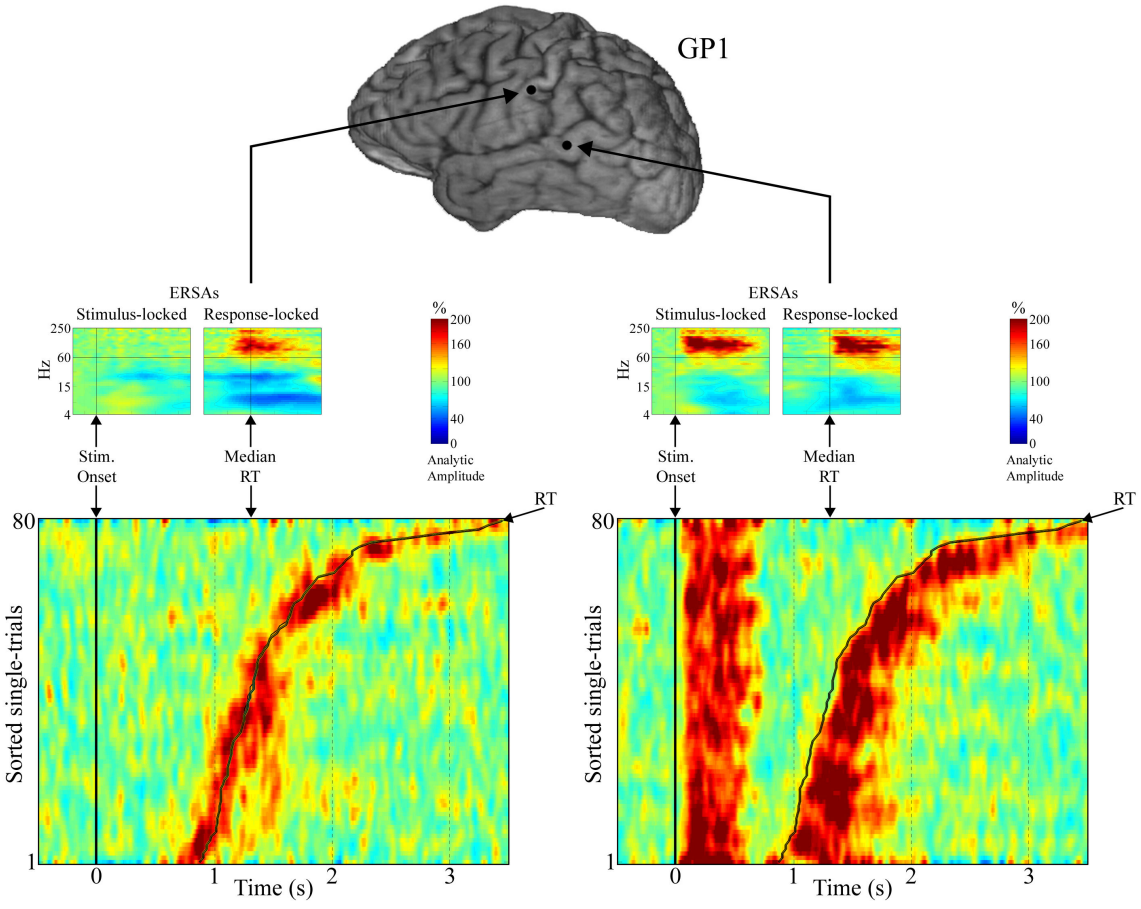

Figure 7.1. Stimulus-locked and response-locked activity from grid patient 1 (GP1). The plots on the bottom show single-trial γ_{high} analytic amplitude, with the single-trials sorted in ascending order of reaction time (RT, measured at voice onset). The auditory stimulus onset (noun) occurs at 0 s and is indicated with a vertical black line. The voice onset time is indicated with a curved black line. The median RT is 1.3 s, with a range of 0.87-3.45 s. The single-trial activity has been smoothed with a 4 trial moving window. Above the single trials are shown the ERSAs time-locked to the stimulus and response. The electrode on the left (pre-central gyrus) shows only response-locked γ_{high} activation, beginning ~200 ms prior to voice onset. Prominent α and β ERD are also seen. The electrode on the right (STG) only responds to auditory stimulation, lasting for ~650 ms after stimulus onset. Because the subject's own voice is an auditory stimulus, this electrode also responds immediately after voice onset (self-stimulatory auditory response).

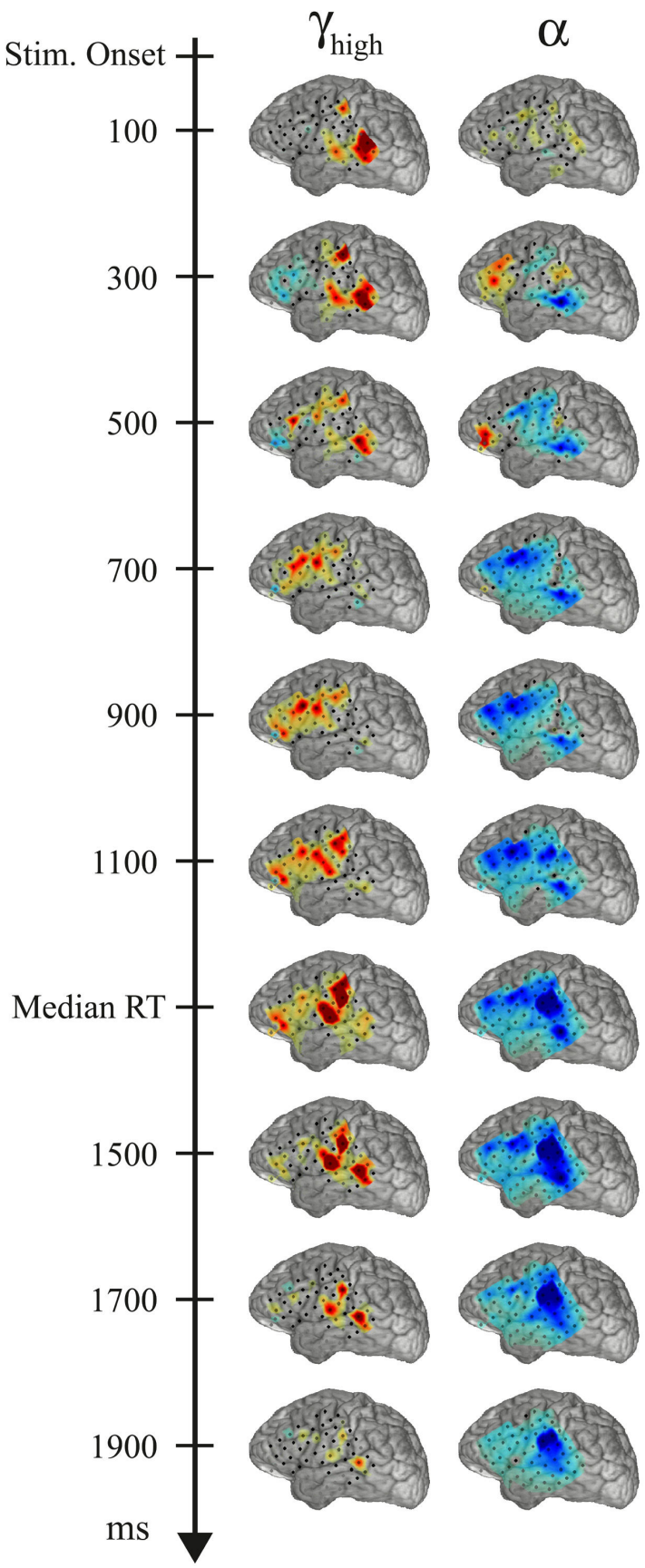

Figure 7.2. Tracking cortical activations during the verb generation task. Topography of γ_{high} (70-160 Hz) and α (7-14 Hz) analytic amplitudes are shown as a function of time. These are snapshots from time-topography movies made by realigning the single-trials to the median RT. Only the interval from 500 ms to 1050 ms is affected by this warping. Before 500 ms is strictly stimulus-locked and after 1050 ms is strictly response-locked. Dots indicate electrode positions, with gray or missing dots for epileptic or rejected electrodes. The anterior-inferior quadrant of the grid showed some epileptic activity (focus in the medial temporal lobe) and so these electrodes should be interpreted with caution.

There are two overall patterns in the results of Figure 7.2. First, the γ_{high} exhibits increases in amplitude and α exhibits decreases in amplitude, consistent with the overall EEG activation pattern. At every latency, α is inversely correlated with γ_{high}, even when different sectors of the grid show enhancement vs. suppressions (at 300 ms for example). Second, the α suppression is less focal than the γ_{high} enhancement, although some topographical specificity is definitely seen for the α band. To a first approximation, the α is a spatially and temporally blurred version of the γ_{high} activity, and flipped in sign.

At closer inspection, the following sequence emerges:

100 ms. Auditory activations are seen in three regions. First, the posterior STG and peri-Sylvian regions that are commonly activated by all auditory stimuli (this patient was also tested with clicks, tones, and syllables). Second, the mid-STG that is activated primarily for auditory speech stimuli (syllables and words). Third, there is a region of activation in the precentral gyrus (!). This region also responds preferentially to speech stimuli, showing virtually no activation to tones. It is also strongly active as a speech motor area (it is just superior to the purely motor electrode shown in Figure 7.1), and I refer to it as the "precentral audio-motor region". This region has been seen in all of the epilepsy patients recorded so far, and is therefore one of our most consistent findings. This same region has recently been identified in fMRI (Wilson et al. 2004), where it was called "superior PMv" (superior, ventral pre-motor). Superior PMv responds preferentially to speech stimuli and is also involved in the speech production (Wilson et al. 2004) (and Stephen Wilson personal communication).

300 ms. Auditory activations persist, and the frontal sector of the grid is suppressed, as indicated by γ_{high} suppression and α enhancement. The significance of this result is unknown.

500 ms. Auditory activations begin to return to baseline, and the earliest signs of IFG activation (~Broca's area) emerge.

700 ms. Auditory activations have ended and multiple electrodes of the IFG show activation.

900 ms. IFG activations persist, with the most anterior-inferior electrodes now showing activity as well.

1100 ms. Now 200 ms prior to the verbal response, the most anterior-inferior electrodes of the IFG are more strongly active, and will peak just before the response. These are therefore implicated in more motor aspects of function, as opposed to other IFG areas that peaked during the semantic processing interval (~550-900 ms). However, unlike the precentral motor areas, these electrodes were not active for a very simple speech output task (patient repeated "aa-ee" every ~5 s).

1300 ms. This is the median RT and motor areas centered on the precentral gyrus show very strong activations. Speech output requires face, mouth, tongue, neck, and diaphragm musculature and therefore activates much of the motor map (or "homunculus").

1500 ms. Motor activations persist, and now the posterior STG and peri-Sylvian auditory electrodes show a strong activation. As in Fig. 7.1, this activation begins with voice onset and is therefore a self-stimulatory response from the sound of the patient's own voice. Interestingly, neither the mid-STG auditory region nor the precentral audio-motor region appears to show a very strong self-stimulatory response.

1700 ms. Motor activations persist but are returning to baseline. Posterior auditory areas are also still active.

1900 ms. All activations are nearly over, but the α suppression is still strong and outlasts the γ_{high} activity by several hundred ms.

Although the results presented here are somewhat preliminary and are only shown for the first patient, several additional patients have been tested. These show mostly consistent results, but also show intersubject variability in the location of language activations (Ojemann et al. 1989). For example, one patient with a more posterior grid placement showed more ~Wernicke's

activation and less IFG activation. One patient with a large lesion involving primary and secondary auditory cortices of the left hemisphere showed no auditory activations at all, except at the precentral audio-motor region (!). This suggests that auditory input to this region is not coming from primary auditory cortex, but from its own nucleus of the thalamus. This patient showed typical IFG activations during the language interval. IFG activations are among the most consistent activations found in the PET and fMRI literature using verb generation tasks (Fig. 7.3), strongly implicating this region in semantic language functions. The STG auditory activations and the pre- and post-central motor activations are the other most consistent findings, both in our patients and the imaging literature[13]. These activations are shown here for the first time with their respective time courses.

[13] Another highly consistent activation in the imaging literature for the verb generation task is in the supplementary motor area (SMA) within the medial surface of the hemisphere. Unfortunately, we lack coverage of this area.

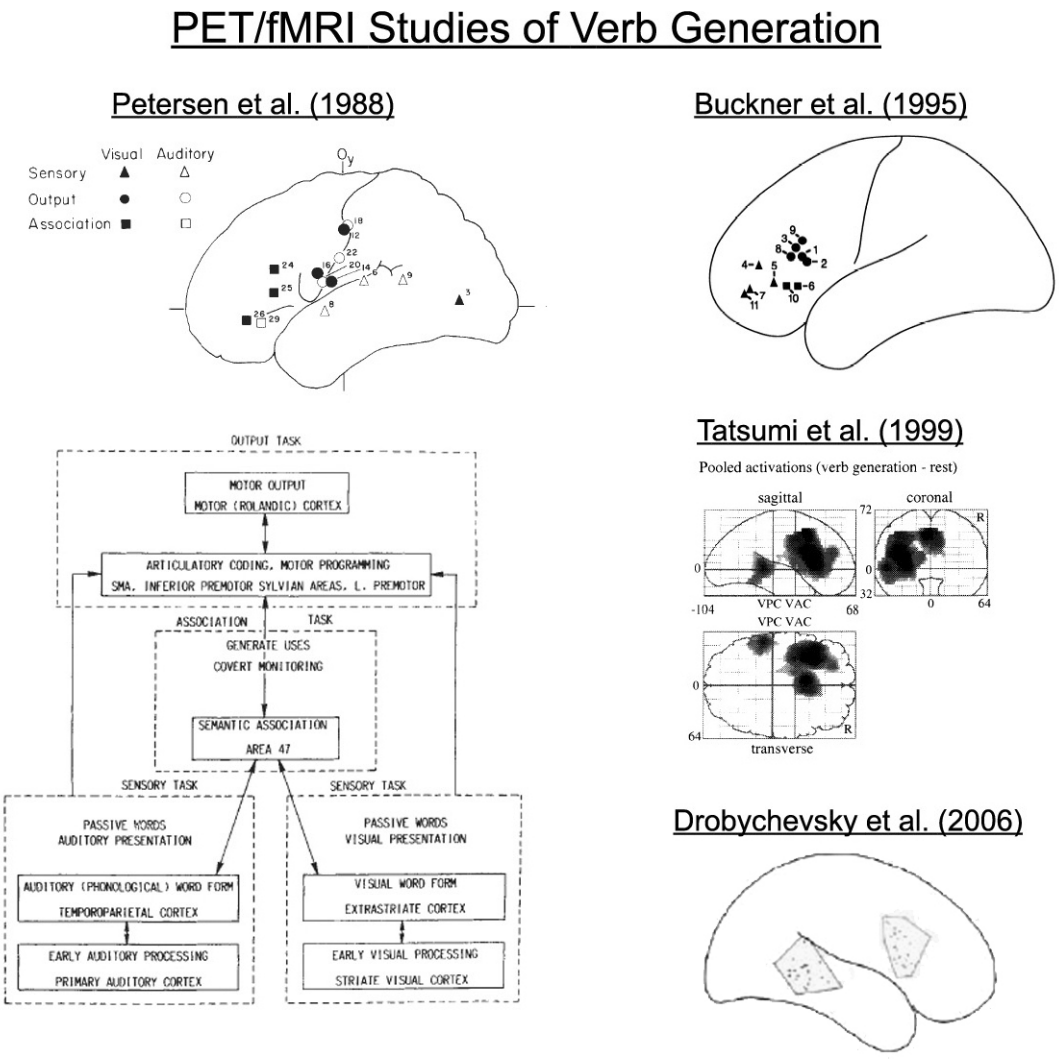

Figure 7.3. PET and fMRI evidence in the verb generation task. **Left:** First imaging study (PET) of the verb generation task showing auditory activation of the STG, semantic association activations of the IFG, and speech motor output activations around the central sulcus. Their model of processing stages involved in the verb generation task is shown below. (Petersen et al. 1988). The results of Experiment 3 support this model (the auditory half), and suggest latency ranges for these different stages of processing. **Right:** Additional PET (Buckner et al. 1995; Tatsumi et al. 1999) and fMRI (Drobyshevsky et al. 2006) studies that also find IFG activations for the verb generation task, with STG activations found when auditory stimuli are used. The later two studies also indicate ~Wernicke's activations.

High-gamma and brain mapping

The γ_{high} band (~60-300 Hz, but strongest and most typically studied ~70-160 Hz) has emerged from ECoG studies as the best electrical measure of cortical activation for use in brain mapping. These advantages are summarized here:

1. Temporal specificity. The envelope of γ_{high} shows the most rapid temporal modulations, and in this sense shows the greatest temporal resolution, or specificity, of any ECoG frequency band. This is partly a mathematical necessity just because it is the highest frequency band (see Appendix 2), but is borne out empirically as shown for example in the auditory study of Crone et al. (2001a) (Figure 5.6).
2. Spatial specificity. The topographical distribution of γ_{high} ERS is repeatedly found to be more focal than the ERD response of α and lower frequencies, and more concentrated around sites thought to be critically involved in the task. In this sense, it shows greater spatial resolution, or specificity.
3. Correspondence to hemodynamic measures. The focal regions of γ_{high} ERS are also found consistently to correspond to hemodynamic and metabolic measures of activity. This not only connects it more strongly to the larger brain mapping literature, but connects it in my opinion to the most essential definition of "activity" (metabolic demand, given that energy usage is of critical evolutionary importance). The correspondence of γ_{high} and blood flow is even stronger than that for MUA activity. The envelope of the γ_{high} appears to nearly represent the envelope of metabolically-expensive signaling activities in gray matter (including MUA activity, with which it also correlates strongly).
4. Task specificity. Several examples show that the patterns of γ_{high} activations nicely differentiate the different stimulus or task conditions in ways that make sense based

on other lines of evidence. For example, the various conditions of the complicated motor task above by Brovelli et al. (2005).

5. Signal-to-noise ratio. Because myogenic activity is not an issue for cortical recordings, we and other authors have usually found that the strongest and most statistically-significant activations, relative to the variability in the baseline, are found in the γ_{high} band. Recall the demonstration by Crone et al. (2001a) of a 400% increase in γ_{high} power relative to the baseline power (Figure 5.6).
6. No confound of ERPs. In several hundred electrodes that I have analyzed, almost none of them showed any significant inter-trial coherence (ITC) in the γ_{high} band. ITC is a measure of phase-alignment across trials that leads to the formation of an ERP. γ_{high} activity is therefore almost purely "induced", and is not overlapped by any common ERPs. This makes the signal much more tractable for analyses and understanding, and relates also to its better SNR.

These advantages have major implications for the basic research goals of cognitive neuroscience, and for the clinical mapping goals of the neurosurgeon (Chapter 1). The same advantages of the γ_{high} band will also make it the best frequency band to use in brain-computer interface (BCI) applications. Because of the importance of the γ_{high} band, I will consider the mechanism of γ_{high} "ERS" in the next chapter. Echoing a previous challenge to the desynchronization model of α blocking (Motokawa 1943b), I will argue against synchronization as the basis of γ_{high} "ERS".

Chapter 8: Rayleigh distributions and the mechanism of "desynchronization"

This chapter will explore the basic mechanism of α "desynchronization" (suppression of α amplitude), which has played a major role in this thesis. This will lead to a conceptual framework for also understanding γ_{high} "ERS". Recall from Chapter 2 that the desynchronization hypothesis was first given by Adrian and Matthews (1934a; 1934b). Other authors of the 1930's echoed this idea. For example, in one of the most eloquent statements of this hypothesis, Gerard (1936) states: "Probably the shift from synchrony to asynchrony and back is most important in accounting for the commonly seen fluctuations in these rhythms and for their sharp change under the impact of afferent impulses… as if a great many feeble rhythms gradually shifted out of phase with one another… Such effects can be attributed entirely to changes in the time relations between units without invoking an alteration of any individual beat."

The desynchronization hypothesis became widely accepted and Pfurtscheller's (1977) term "event-related desynchronization" (ERD) added to its dominance. There is, however, another major possibility for the observed decrease of α amplitude – that such effects can be attributed entirely to changes of single-unit output, without invoking any alteration of the time relations between units. The major insight for this was provided by Motokawa's statistical-mechanical theory of the EEG (Motokawa and Mita 1942; Motokawa 1943a; 1943b). The outstanding work of Motokawa has been forgotten and I begin this chapter with some original historical scholarship concerning his research.

Motokawa's statistical-mechanical theory of the EEG

Koiti Motokawa was Japan's first major EEG scientist, publishing over 20 papers on the EEG between 1941 and 1949. Other than Motokawa's, only a small handful of minor EEG

reports appeared out of Japan prior to the 1950s. Motokawa published only in Japanese journals with low readership outside Japan, and wrote in German until 1947. Perhaps for these reasons, his work was forgotten (at least outside of Japan). However, he made several highly original contributions that deserve recognition. As discussed in Chapter 3 (Figure 3.4), he was the first to show time-amplitude plots of α blocking (Motokawa 1941; Motokawa and Mita 1941). In one interesting report, he used a specially designed bed that could be rotated in 3 dimensions to give the first demonstration of α blocking to vestibular stimulation (Motokawa et al. 1943). Most importantly for the present purpose, his "statistical-mechanical" theory of the EEG included a major conceptual contribution to the understanding of α blocking.

Figure 8.1. Photograph of Koiti Motokawa, a pioneer physiologist at the Tohoku University in Japan. Kindly provided with permission for use by Prof. Hajime Mushiake.

Motokawa developed his statistical-mechanical theory of the EEG in a series of three papers appearing in 1942-3 (Motokawa and Mita 1942; Motokawa 1943a; 1943b). This was a highly mathematical treatment with the major purpose of explaining the distribution of α wave amplitudes during the resting state, and the suppression of α amplitudes during an active state. Examples of Motokawa's α amplitude histograms are shown in Figure 8.2. To anticipate, these histograms were found to follow what is today known as a Rayleigh distribution, and he was able to predict this distribution from his theory!

Figure 8.2. **Top left:** Scalp EEG recording method for these studies (from Motokawa 1944). α amplitude was measured ~peak-to-peak by hand, as shown in Figure 3.4. **Bottom left:** Histograms of α amplitudes during a) mental passivity, and b) mental activity (from Motokawa and Mita 1942). In accordance with the EEG activation pattern, the amplitudes shift to the left (smaller amplitudes) during activity. **Right:** Distribution of α amplitudes in resting vs. excited conditions (from Motokawa 1943b with labeling added). The empirical distributions are fit with the theoretical distribution derived in his statistical-mechanical theory (today's "Rayleigh" distribution).

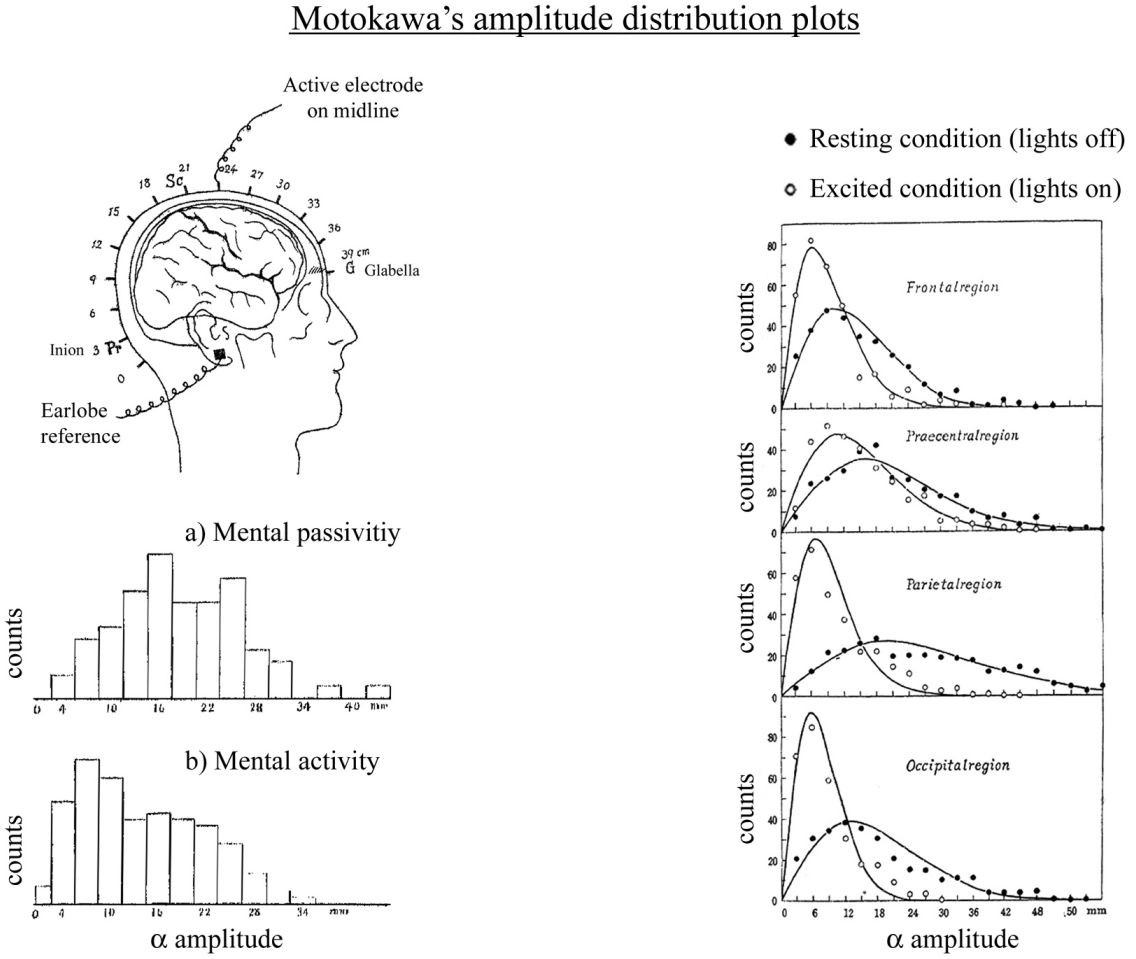

In developing his statistical-mechanical theory, Motokawa was amongst the first EEG authors to clearly integrate dipole theory into his thinking. He was definitely the first in the EEG literature to give dipoles a mathematical representation, using vectors in the complex plane (as modern engineers and physicists would do). He assumed that the pyramidal cells of the cortex, with their long and parallel apical dendrites, could act as electrical dipoles[14] and were the major generators of the EEG. This is in accord with the modern view, and along with Adrian and a couple of others, he deserves historical credit for this major insight into EEG biophysics. Using dipolar theory, he developed an original conceptual/biophysical model of the α rhythm.

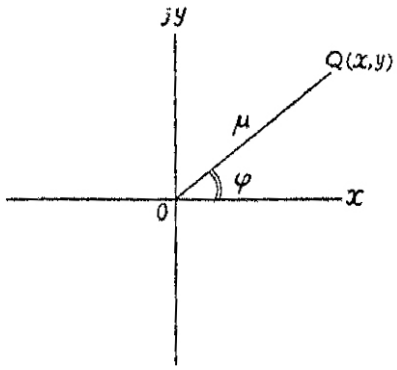

Abb. 4. Zahlenebene für die elektrische Schwankung einer Nervenzelle in der Grosshirnrinde. μ: Amplitude. φ: Phasenwinkel.

Figure 8.3. Motokawa's (1943a) illustration of a vector in the complex plane. The figure caption reads (my translation from German): "Plot of the electrical oscillation of a nerve cell in the cerebral cortex. μ: amplitude. φ: phase angle"

Motokawa's model of the α rhythm focused on the contributions of individual pyramidal cells. He assumed that each pyramidal cell generates α oscillations of some amplitude and phase. Per his dipolar theory, this means that the electrical dipole of each single cell alternately points towards the cortical surface or towards the white matter (with the alternation every ~50 ms). Equivalently, the representing vector is rotating around in the complex plane at ~10 Hz. This

[14] A dipole is simply a separation of charge, and this results in an electrical field that can be detected at a distance. In the pyramidal cell, the separation of charge is between the apical and basal dendrites. A contemporary treatment would note that it is really a separation of "sources" and "sinks" that generates the electrical fields of the EEG, but that this acts as a "virtual" separation of charge in that the consequences for the electrical field are the same.

occurs because the pyramidal cells are alternately depolarized at their apical dendrites and then at their basal dendrites (switching every ~50 ms). It is this *asymmetrical* depolarization that generates an electrical dipole, and the vacillation of the asymmetry from apical to basal dendrites results in a "dynamical dipole". He states that, physiologically, this would occur by sequential excitation of one pole of the cell and then the other. Motokawa's reasoning here is correct, and today we would specify that apical depolarization gives surface-negativity and basal depolarization surface-positivity (Creutzfeldt 1974; Bindman and Lippold 1981; Mitzdorf 1985).

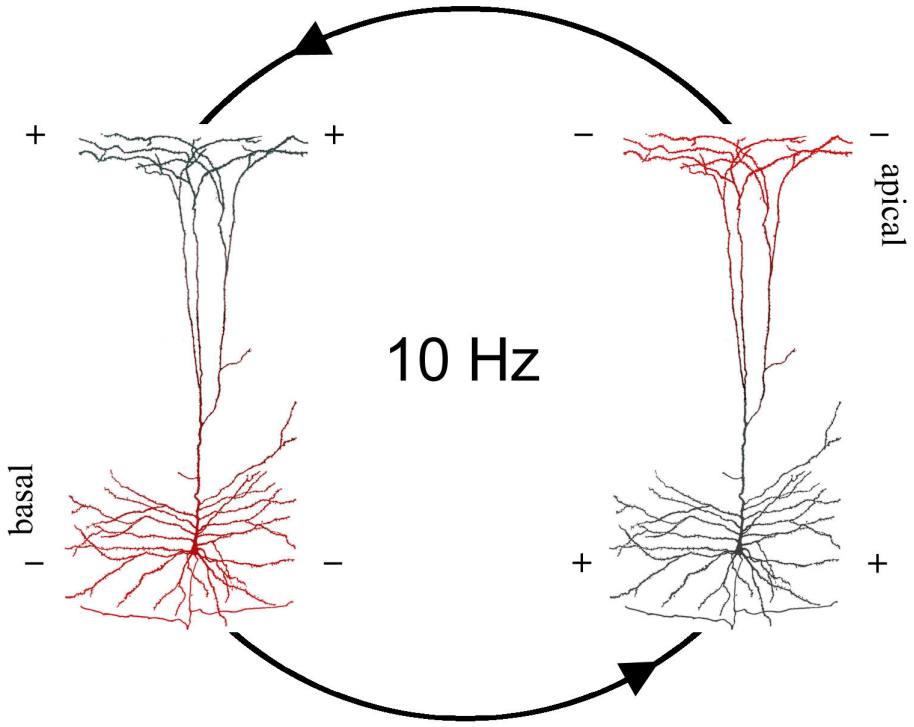

Figure 8.4. Illustration of Motokawa's model of single-cell behavior during the α rhythm. The pyramidal cell is from Ramón y Cajal (1899; in DeFelipe and Jones 1988). Red is used to indicate depolarization (excitation). According to Motokawa, the depolarization vacillates between poles of the cell at the frequency of the α rhythm (10 Hz). I have inserted + and – signs to indicate where positive and negative potentials would be recorded per modern biophysical theory (basal/apical depolarization gives surface positivity/negativity).

Motokawa's radical assumption concerned the phase relations across the *population* of these oscillating single-cells. Most authors (of his time and ours) implicitly or explicitly assume that population waveforms (i.e. the EEG that we record) require synchrony of the underlying unit waveforms for their existence. On the contrary, Motokawa assumed that for each single cell "the phase is entirely random", that is "the phase angle can take all values from 0 to 2π with equal likelihood…" There are no inherent phase relations between cells, and these phase angles can be assigned independently for each single-cell. If there is no phase synchrony between cells, and the phases are distributed uniformly around the phase circle, shouldn't the resulting sum be zero? The answer is no (!), rather the amplitude of the resulting sum will stochastically vary according to the Rayleigh distribution (as shown in the next section). Motokawa and Mita (1942) derived the Rayleigh distribution according to the above assumptions and using the summation of vectors in the complex plane. They arrive at the following formula for the probability that the α-wave amplitude falls between A and A+dA (i.e. within one bin of a histogram):

$$W = 2 \cdot h^2 \cdot A \cdot \exp(-h^2 \cdot A^2) \cdot dA,$$

where W is the probability ("Wahrscheinlichkeit") and h is a parameter. This defines a discrete Rayleigh distribution (by modern terminology) with scale parameter $\beta = 1/(h \cdot \sqrt{2})$. He states that the mode = $1/(h \cdot \sqrt{2})$ and the mean = $\sqrt{\pi}/(2 \cdot h)$, as is correct for a Rayleigh where the mode equals β and the mean equals $\beta \cdot \text{sqrt}(\pi/2)$. In Motakawa (1943a), he further derives an equation for h based on the square-root of N (the number of single-cells), cell densities, average dipole moments, and average spatial angles. Although an impressive accomplishment, this derivation of h will not be given here. Rather, we will focus on the reason for finding the Rayleigh distribution of α amplitudes in the EEG.

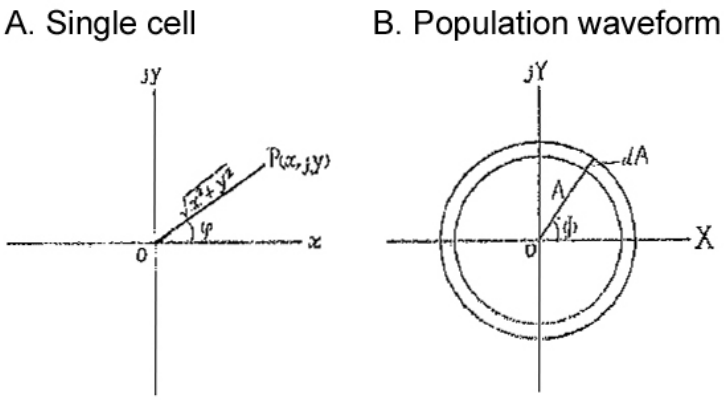

Figure 8.5. A. Representation of the oscillation of a single-cell as a vector in the complex plane (from Motokawa and Mita 1942). He uses small letters for single cells, thus ϕ is the phase angle, and x and y are the real and imaginary components of the vector. The amplitude is the length of this vector, a=sqrt(x^2+y^2). **B.** Similar vector representation for the population waveform (i.e. the EEG waveform that we actually record). He uses capital letters for the population, thus Φ is the phase angle, and X and Y are the real and imaginary components of the vector. The length of the vector, A, at some point in time is one observation of α amplitude. Many such observations across time give the histograms shown in Figure 8.2. The two circles in **B** enclose one bin of such a histogram (the bin from A to A+dA). The essence of Motokawa's theory is that the single-cell vectors in **A** are distributed randomly around the phase circle. The summation of these vectors gives the population vector in **B**. Under the assumption of phase randomness in the unit vectors (ϕ~Uniform), the amplitudes (lengths) of the population vectors will be distributed according to the Rayleigh distribution (A~Rayleigh). The "~" is a modern designation of "distributed according to" and I use "sqrt" to stand for the square-root.

The Rayleigh distribution

Was Motokawa's derivation correct in arriving at the Rayleigh distribution? Yes, and this section will illustrate this derivation. The Rayleigh distribution is a 2-D realization of the 3-D Maxwell-Boltzman distribution used in statistical mechanics. The Maxwell-Boltzmann

distribution gives the distribution of speeds of gas molecules in an ideal gas. It arises because the x, y, and z components of the molecular velocities are independently and normally distributed (each has mean zero and a non-zero variance, with a higher variance corresponding to a higher temperature). A molecule's speed is equal to $\text{sqrt}(x^2+y^2+z^2)$, and the distribution of molecular speeds is the Maxwell-Boltzmann distribution. The Rayleigh distribution arises by similar assumptions using 2-D vectors. Motokawa mentions Brownian motion and the collective behavior of gas molecules in (Motokawa and Mita 1942), and mentions the "Maxwellian law of velocity" in (Motokawa 1943a). Thus, Motokawa's "statistisch-mechanische" theory of the EEG was aptly named indeed!

Any modern introduction to the Rayleigh distribution will teach that it arises in the following situation. If the X and Y components of a set of 2-D vectors are independently and normally distributed, then the lengths of the vectors, $A=\text{sqrt}(X^2+Y^2)$, will be distributed according to a Rayleigh. More formally, if $X\sim\text{Normal}(0,\sigma)$ and $Y\sim\text{Normal}(0,\sigma)$, then $A\sim\text{Rayleigh}(\beta)$, where β is the "scale parameter" of the Rayleigh distribution and $\beta=\sigma$. Note that the Normal distribution (or Gaussian distribution) is a two-parameter distribution, where the first parameter gives the mean and the second parameter the variance. The Rayleigh distribution is a one-parameter distribution, where the scale parameter (β) determines both the mean and the variance. The mean of the distribution is equal to $\beta\cdot\text{sqrt}(\pi/2)$ and the variance of the distribution is equal to $\beta^2\cdot\text{sqrt}(2-\pi/2)$. The mode, or peak, of a Rayleigh distribution is equal to β. By analogy to the Maxwell-Boltzmann distribution, both of these parameters (β and σ) would correspond to the temperature of the gas.

We now look at the summation of unit waveforms to give a population waveform, and show that this results in a Rayleigh distribution of population amplitudes. I begin with a simple

example involving only 10 Hz sinusoids, and later generalize to arbitrary signals. It will be recalled that a sine wave can be represented as a vector in the complex plane. The amplitude of the sine wave is the length of the vector, and the phase of the sinusoid (usually taken at time 0) becomes the phase angle of the vector (usually the positive X axis defines a phase of 0, the positive Y axis a phase of $\pi/2$, and so on). The example in Figure 8.6 shows N=16 unit sine waves (red) that add to make the population sine wave (blue). Note that the summation of 10 Hz sinusoids can only result in a 10 Hz sinusoid (there is no possibility of "leakage" into other frequency bands).

It is known from other examples in physics that the amplitude of the population waveform is proportional to $\sqrt{N}$. For example, a stadium with N people cheering will not summate to silence despite the random phase relations between sound waveforms of individual voices. Rather, a "roar of the crowd" with sound amplitude proportional to $\sqrt{N}$ is obtained. Here we see a nice insight into why this relation holds. By expanding the equation for linear[15] coherence (C), we obtain the equation $A = N \cdot C \cdot \bar{a}$. Coherence varies from 0 to 1, where 0 indicates precise non-alignment of vectors around the phase circle and 1 indicates precise alignment. With random placement of vectors, neither of these extremes is likely to hold (for example, 2 vectors would need to be precisely 180° out of phase to cancel). Instead, the modal coherence obtained is $1/\sqrt{N}$. Since $A = N \cdot C \cdot \bar{a}$, this gives a modal population amplitude $A_m = N \cdot (1/\sqrt{N}) \cdot \bar{a} = \sqrt{N} \cdot \bar{a}$. Note that the relation $A = N \cdot C \cdot \bar{a}$ is an identity that holds no matter what the distribution of unit phases and amplitudes, and regardless of whether the Rayleigh distribution is found for A.

[15] Linear coherence, as opposed to phase coherence, is used throughout.

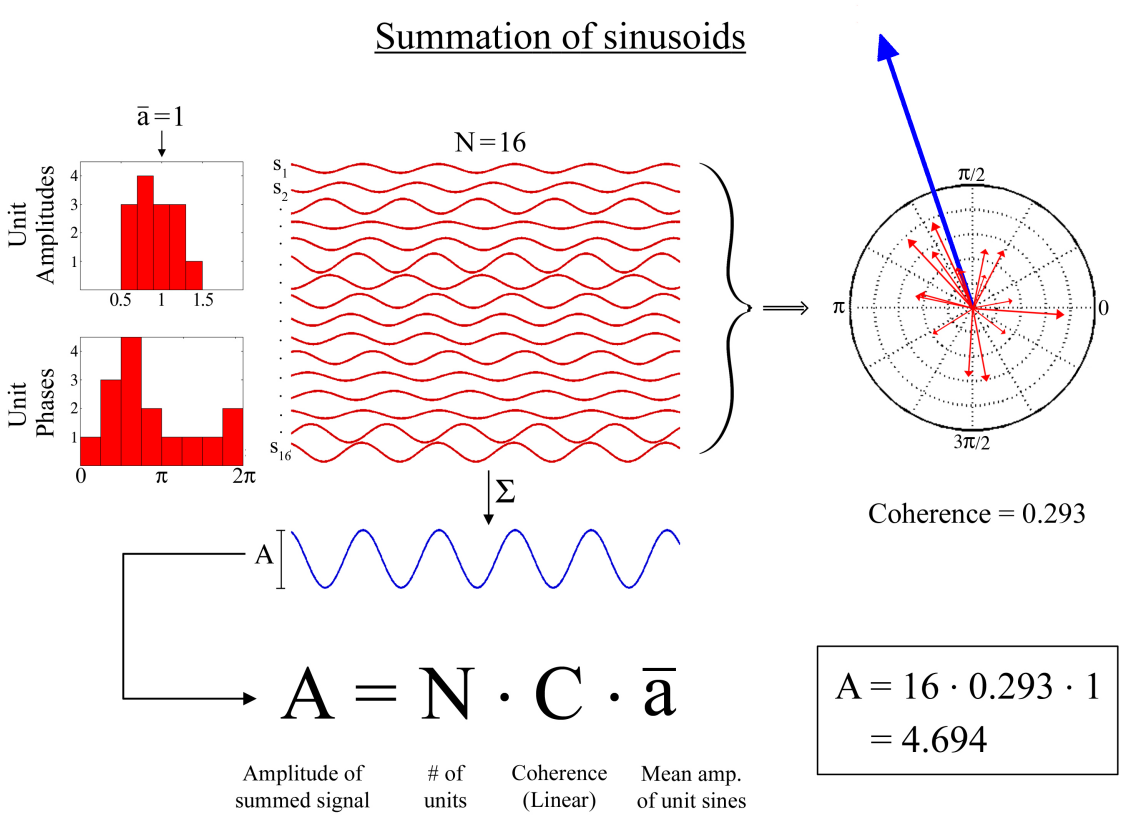

Figure 8.6. Example of the summation of unit waveforms (red, small letters) resulting in a population waveform (blue, capital letters). The unit waveforms are designated as $s_1,s_2\ldots s_N$. and their vector representations (red arrows) as $\mathbf{z_1},\mathbf{z_2}\ldots\mathbf{z_N}$. The population waveform is designated as S, and its vector representation (blue arrow) as **Z** (bold letters indicate complex numbers throughout). In this example, there are N=16 unit sine waves in the population. The unit amplitudes are distributed uniformly from 0.5-1.5 (a~Uniform(0.5,1.5)) with a mean of 1 ($\bar{a}$=1). The phases are distributed uniformly from 0 to 2π (ϕ~Uniform(0,2π)). But note that any given sample of 16 points taken randomly from 0-2π will not be exactly uniform. In this particular instance, there is a slight concentration of unit phases in the interval π/2 to π. This results in a non-zero coherence (C) and therefore a non-zero amplitude (A) of the population sine. In this example, the coherence (C) was 0.293 and A was 4.694 according to the identity $A=N\cdot C\cdot\bar{a}$. Note that 4.694 is approximately equal to $\sqrt{N}\cdot\bar{a} = 4\cdot 1 = 4$, as expected.

Summing N sines M times

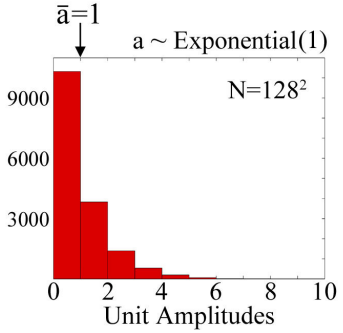

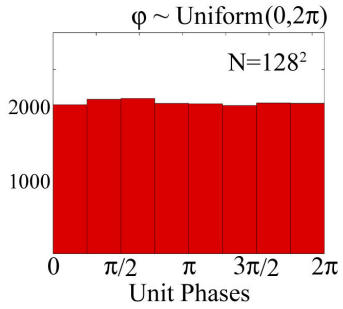

for k=1:M

Generate N sines and sum.

$$Z_k = \sum_{i=1}^{N} z_i$$

$$Z_k = X_k + j \cdot Y_k$$

$$A_k = \mathrm{abs}(Z_k) = \sqrt{X_k^2 + Y_k^2}$$

$$A_k = N \cdot \bar{a} \cdot C_k$$

end

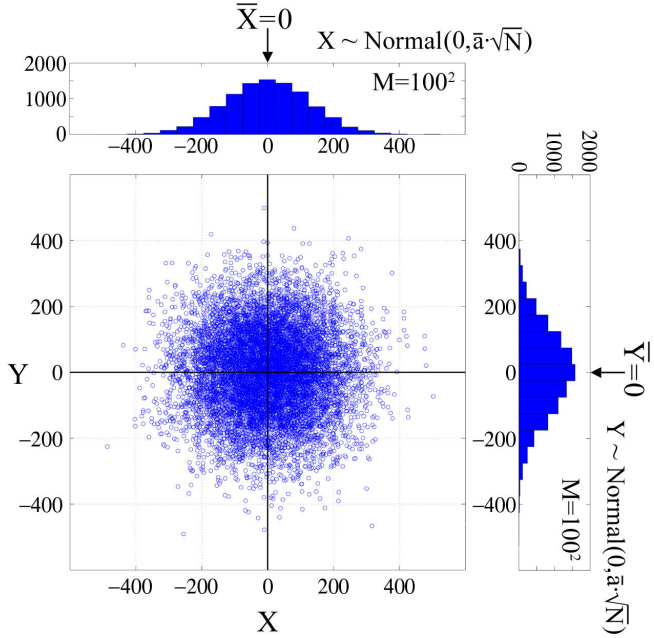

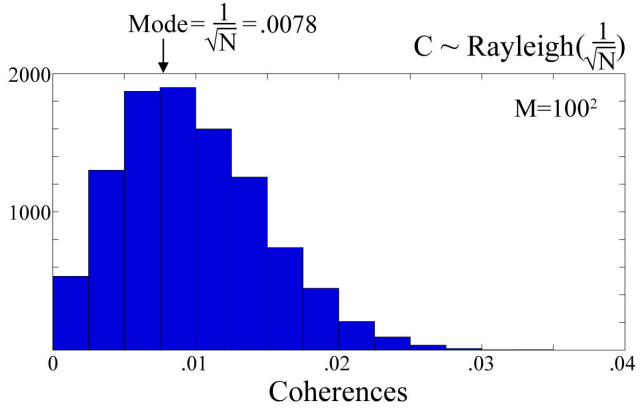

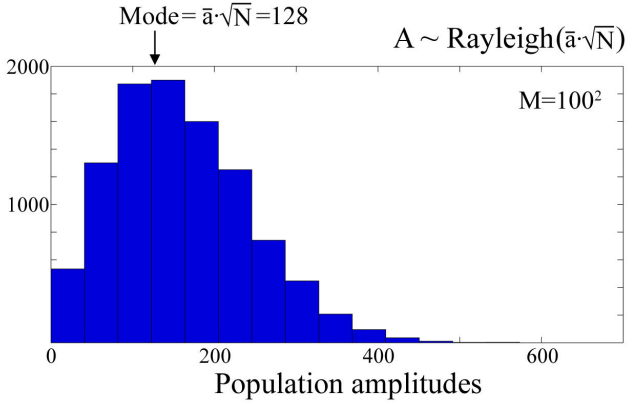

Figure 8.7 (previous page)**.** Derivation of the Rayleigh distribution for population amplitudes. Again, unit values are represented with small letters and red, and population values with capital letters and blue. In this case, the unit amplitudes (a) were distributed exponentially with a mean of 1: a~Exponential(1). Although I consider this a roughly realistic distribution, only the mean amplitude ($\bar{a}$) matters in the long run. The unit phases are distributed randomly from 0 to 2π: ϕ~Uniform(0,2π). There are $N=128^2$ units in this example. For each of M iterations, these N units are summed together to give a population waveform as in the previous example. Each population vector (**Z**, blue arrow in the previous figure) becomes a dot in the scatter plot to the right. There is one population vector per iteration, and therefore M dots in the scatter plot. Because the unit phases (ϕ) were uniformly distributed, this results (proof not given) in a normal distribution for the real (X) and complex (Y) parts of the population vectors: X~Normal(0, $\bar{a}\cdot\sqrt{N}$) and Y~Normal(0, $\bar{a}\cdot\sqrt{N}$). These are the marginal distributions shown for the scatter plot. X and Y are also independently distributed, and so the conditions are met for a Rayleigh distribution of population amplitudes (A), where $A = \text{sqrt}(X^2+Y^2)$. Thus, A~Rayleigh($\bar{a}\cdot\sqrt{N}$) and the peak (mode) of the distribution is at $\bar{a}\cdot\sqrt{N}$ (128 in this example). Because the identity $A=N\cdot C\cdot\bar{a}$ holds for each iteration, it follows that the coherences (C) also obey a Rayleigh distribution: C~Rayleigh($1/\sqrt{N}$). In this example, the modal coherence is 1/128 = 0.0078.

Motokawa's challenge to the desynchronization hypothesis

According to the relation $A = N\cdot C\cdot\bar{a}$, we see that there are two possibilities for reducing the population amplitude (A). Either the coherence across the population (C) can be decreased, or the mean unit amplitude ($\bar{a}$) can be decreased (note that a change in N is equivalent to a change in $\bar{a}$, so this factor can be ignored as a distinct hypothesis for affecting A). Taking Gerard's (1936) version of the desynchronization hypothesis, whereby only the time relations between units are

changed, this implicates a change in C but no change in ā. Motokawa would take the exact opposite stance, that C remains at chance levels ($1/\sqrt{N}$) and only ā changes. Although Motokawa did not use C in his mathematical treatment and did not show the relation $A = N \cdot C \cdot \bar{a}$, he was thinking along these same lines.

We return to Motokawa's model of the α rhythm (Figure 8.4), whereby each single cell is generating its own α rhythm due to asymmetrical depolarization. Motokawa postulated that there are no particular phase relations across the unit α rhythms, and the population (EEG) α rhythm is due only to the non-zero coherence that arises by chance. That is, the EEG α rhythm is the roar of the crowd with an amplitude proportional to $\sqrt{N} \cdot \bar{a}$. Since no particular synchrony holds in the "synchronized" state, a desynchronization is not called for. Motokawa (1943b) states: "Adrian posits asynchrony during mental activity and synchrony during mental rest… by our theory, asynchrony, or randomness of phase, occurs already in mental rest, so that complete chaos does not appear *de novo*." Rather, the population amplitude diminishes because the unit amplitudes diminish. According to his biophysical theory, this requires a decrease in the dipole moments and therefore a decrease in the asymmetrical depolarization of single cells. In a state of excitation, the cell is expected to become bombarded with inputs and become depolarized strongly, but more or less evenly, across the entire surface of its membrane (Figure 8.8). This would mean a reduced *asymmetry* of depolarization, and therefore a reduced dipole moment. To summarize (my translation from German):

> "From the perspective of our theory, the blocking of the α-waves is easiest understood as a reduction of the dipole moments… On the basis of our electrophysiological knowledge, we can understand the mechanism of the electrical oscillations of the nerve cells – that the cell membrane at either pole of the cell body is alternately depolarized with a certain period. Considering that a functioning rhythmic structure can easily be put in a tonic or persistent state of excitation through stimulation, one might think that the depolarization of the

nerve cells by an external or internal stimulus spreads over the entire surface of the cell body and the prior electrical asymmetry decreases, which directly implies the aforementioned reduction of the dipole moment." –Motokawa (1943b).

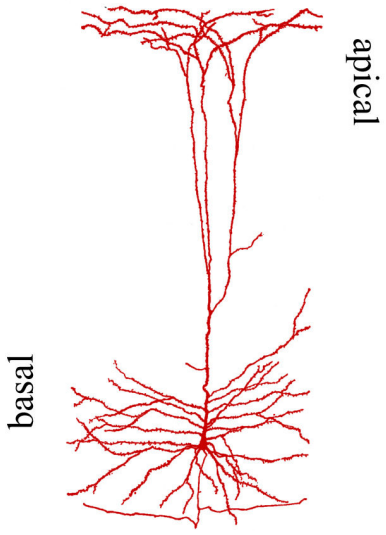

Figure 8.8. State of pyramidal cell (same as Figure 8.4) during α blocking. The cell is depolarized strongly (indicated by red) all over the membrane. However, there is no asymmetry of depolarization at either the apical or basal ends. Thus, no net dipole would result from this cell.

Rayleigh distributions for broadband signals

Motokawa and Mita (1942) noted that their analysis applies equally well to vectors obtained through a Fourier analysis. Within any given frequency band, the complex vectors summate in the same manner as shown for simple 10 Hz sinusoids above. This is given further demonstration in Appendix 2, where it is shown that this analysis also applies to vectors obtained through the Hilbert transform in a time-frequency analysis. Thus, the 10 Hz frequency band of a broadband signal can be approached in the same manner as outlined above for 10 Hz sinusoids. In particular, the equation $A=N\cdot C\cdot \bar{a}$ holds for each frequency band.

Broadband signals can be categorized in terms of the slope of their power spectrum in log-log coordinates, defining different "colors" of noise (white, pink, brown, black; see Appendix 2, Figure A2.1). Colored noise summates to produce the same color of noise if the phase relations

are random at each frequency band. Each individual frequency band summates separately, so there is no "leakage" across frequency bands. Thus, if there is no synchrony above chance across the population, the result of dark brown noise in the EEG waveform implies that each single unit is generating dark brown noise. This could be tested simply by obtaining power spectra for intracellular waveforms. However, I suspect that there is above-chance coherence between cells at lower frequencies, and this would fall to chance in the γ band. Thus, I would predict brown noise for an intracellular power spectrum, but dark brown noise for the ECoG. In any case, the different hypotheses for "ERD" are testable (albeit not easily).

A final assessment

Unfortunately there is one error in Motokawa's analysis. The distributions of α amplitudes were assembled over time, but successive time points are not independent. The Rayleigh distribution that is obtained across time is still a sign of underlying randomness of phase. However, this is a random and uniform distribution of phase *across* time (both for the underlying units and for the population waveform). This does not imply that *at any given time point* the distribution of underlying unit phases is random and uniform. Unfortunately, we cannot sample a single time-point more than once in real data, so we cannot see if it would show a Rayleigh distribution. It is not possible to obtain M independent realizations of the summation process as was done in Figure 8.7. Thus, the Rayleigh distribution obtained across time is consistent with underlying randomness of unit phases, but does not guarantee it. I do not currently know of any way to demonstrate unit phase relations from histograms of population amplitudes. However, there may be one way to test Motokawa's assertion of unit phase randomness using a technique not known in his time. Namely, simultaneous intracellular recordings of multiple cortical cells with coherence analyses would shed some light on this issue.

Despite this flaw, we have gained much from Motokawa's insights and the analyses shown above. I consider his model of the α rhythm essentially accurate, with the only caveat that some coherence across the population probably holds. His model of α desynchronization as due to ~uniform depolarization of single cells is certainly at least partly correct. He also appears to be basically correct that the distribution of EEG amplitudes conforms to a Rayleigh, and his analysis correctly shows this to be a simple consequence of randomness of phase (but with the flaw concerning the temporal dimension). In working out the implications of his ideas, we have arrived at the identity (which holds regardless of the Rayleigh analysis): $A = N \cdot C \cdot \bar{a}$. This relation makes clear the competing hypotheses for α desynchronization: there can either be a decrease of unit amplitudes ($\downarrow\bar{a}$) or a decrease of coherence across the population ($\downarrow C$). Probably a combination of these two holds.

In the γ_{high} band, coherence across units is expected to be much lower and probably very close to chance levels. At 100 Hz, a temporal scatter of ±5 ms obliterates all synchrony (phase distributed ~uniformly from 0-2π). At 250 Hz, a scatter of only ±2 ms is necessary. Thus, we do not expect an $\uparrow C$ to play a major role in the γ_{high} band. Rather an $\uparrow\bar{a}$ would most likely make the dominant contribution to the observed $\uparrow A$. That is, γ_{high} "ERS" does not require synchronization.

I consider our observed γ_{high} increases to consist almost entirely of the "roar of the crowd". The cells in an active cortical area will experience a bombardment of synaptic inputs and show an increase in firing. Fast synaptic potentials (due to AMPA glutamate receptors and $GABA_A$ receptors) and spiking activity together contribute to the γ_{high} band (see discussion in Edwards et al. 2005). A strong increase in these types of activity will lead to a strong increase in γ_{high} activity, regardless of the synchrony between these activities. A strong increase in these activities would also lead to increased metabolic and blood flow demand due to the need to

restore the resting ionic gradients (Ames 2000; Attwell and Laughlin 2001; Lennie 2003). This explains the strong association between γ_{high} activity and blood flow (Chapter 6). Note that if the γ_{high} increase were due to an increase in synchrony (↑C), it would be difficult to explain the strong correlation with blood flow. I therefore predict that the single cells are generating stronger γ_{high} during activation (↑ā), and this would be reflected in time-frequency analyses of intracellular potentials in response to activating stimuli.

This may seem at odds with the work on γ synchrony and temporal binding (Singer 1993; Buzsáki 1994), and I do believe that synchrony holds within cell assemblies. But each ECoG electrode records from a great many cell assemblies, and these will not be in phase coherence with each other[16]. Thinking of the phase histograms above, units from any one cell assembly may show very tight coherence with phases restricted to only one bin of the histogram. However, if assemblies are related by only chance coherence (phase distributed randomly around the phase circle) then the total population of unit phases will also be uniformly distributed. Thus, in the final analysis, I accept the temporal binding hypothesis for cell assemblies, but maintain that γ_{high} of the ECoG is the "roar of the crowd" in the sense that its amplitude is just $\sqrt{N}\cdot\bar{a}$.

Summary of thesis

This thesis has largely been a tale of two frequency bands. Fluctuations in the lower frequencies (below ~20 Hz) are "waves of rest" and indicate a state of cortical idling or inactivation. Suppression of spontaneous fluctuations in these low frequencies to activating stimuli has been seen innumerable times since Beck's original observation in his doctoral thesis of 1891. By Motokawa's analysis, this is caused by a strong, but even, depolarization over the pyramidal cell membrane and the consequent reduction of dipole amplitude. Because membrane

[16] In fact, by the temporal binding hypothesis, their separate identities as separate cell assemblies practically *requires* them to exhibit a lack of synchrony.

depolarization is metabolically costly, α is inversely correlated with metabolic measures of activation. Others posit a desynchronization across the population of cells, but no real physiological explanation has been offered by this camp.

On the other end of the EEG spectrum (above ~30 Hz) are "waves of activity", and these were first shown by Ector's (1936) ECoG studies in rabbits to be a specific sign of cortical activation useful for cortical mapping. Ectors even reported activity in today's γ_{high} range (>60 Hz), but it has really only been appreciated since the human ECoG work of Crone et al. (1998, 2001a). γ_{high} has recently emerged as the most powerful method of mapping the cortex on the basis of its electrical activity, as experiments in this thesis also show. Although synchrony and binding in the γ range are tantalizing notions that very likely hold in cell assemblies, the simplest explanation for the power of γ_{high} is that it reflects the "roar" of millions of synaptic and firing events of a focally active cortical area. These same events incur a costly metabolic demand and lead to a strong correlation of γ_{high} with metabolic and hemodynamic measures of activation. But metabolic and hemodynamic measures do not come anywhere close to offering the temporal resolution of γ_{high} for tracking activation. Time-frequency analyses of human ECoG patients can be expected to contribute enormously to cognitive neuroscience in the near future. It appears that the 1800s quest for an electrocortical means of mapping has found its best answer in the γ_{high} band. I am also optimistic that a modified statistical-mechanical theory of the EEG that extends Motokawa's work on the Rayleigh distribution will allow for insights into more than just "activation" on the basis of ECoG.

Appendix 1: ECoG methods

The UCB-UCSF intracranial project

This appendix gives the details of the methods used to record ECoG from human neurosurgical patients. These recordings were done in collaboration with two neurosurgeons, Dr. Mitchel S. Berger and Dr. Nicholas M. Barbaro, at the University of California, San Francisco (UCSF). This was a collaborative project between these and other individuals at UCSF and various members of the laboratory of Robert T. Knight at UC Berkeley (UCB). The system used was assembled on a mobile cart by myself, Richard Fechter (clinical engineer at UCSF), and Clay Clayworth (lab manager and technician, Knight Lab, UCB) with important help from Leon Y. Deouell (former post-doctoral researcher, Knight Lab, UCB), Maryam Soltani (graduate student, Knight Lab, UCB), Ryan T. Canolty (graduate student, Knight Lab, UCB), Dr. Heidi E. Kirsch (neurologist and epileptologist at UCSF), and Sarang S. Dalal (graduate student in the lab of Srikantan S. Nagarajan at UCSF).

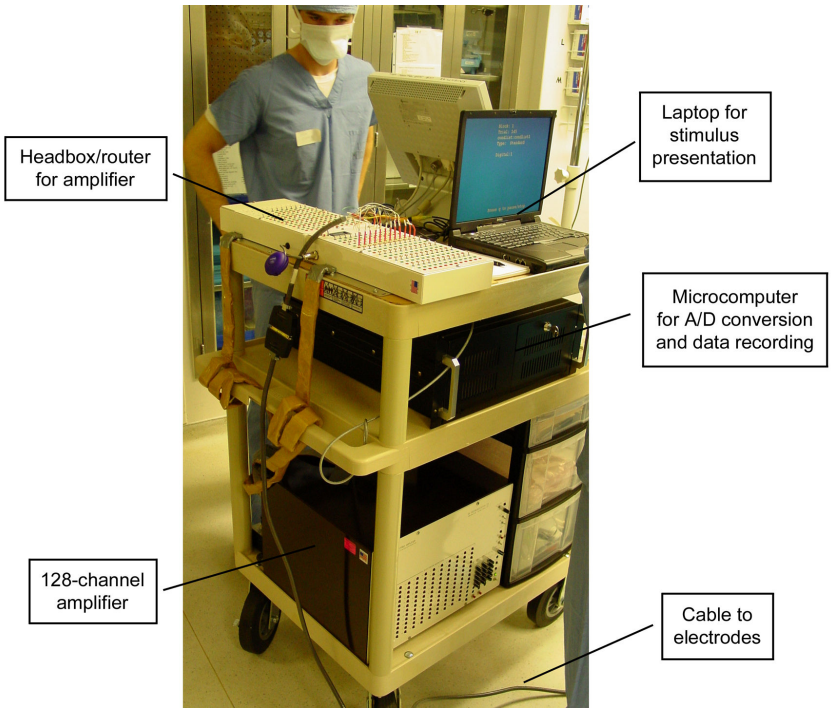

Figure A1.1. Photograph of myself with the mobile cart and ECoG recording system taken in Dr. Berger's operating room (UCSF) in September, 2002, shortly after the system was assembled.

All ECoG recordings used this mobile system. The amplifier (SA Instrumentation Company) had 128-channels, a gain of 10k (5k was used in a couple of recent patients), and a filter bandpass of 0.01-250 Hz in most patients. The most recent patients (1 tumor patient and 3 epilepsy patients) were recorded with a broader filter setting of 0.01-1000 Hz (-3 dB cutoffs). The amplifier output was routed to a microcomputer with an analog-to-digital (A/D) conversion card and recorded at a sampling rate of 2003 Hz (16-bit resolution) using Datapac 2000 software (RUN Technologies).

Stimulus timing was carefully marked by recording stimulus events as "channels" with the same sampling rate in Datapac. For visual stimuli, a white square was put in the corner and a photodiode placed over it. This sends an analog output current directly to a channel of the A/D card and gives exact stimulus timing in the ECoG record. For auditory stimuli, the output to the speakers was split and one copy sent directly to a channel of the A/D card. Again, this gives exact stimulus timing in the ECoG record. For speech production and motor events, a microphone was routed through a simple analog mixer and sent directly to a channel of the A/D card. Again, this gives exact timing with no delay at the same sampling rate as the ECoG data.

This project involves two distinct patient populations. The first are tumor patients with ECoG recordings done during neurosurgery ("acute" recordings) with Dr. Mitchell S. Berger. The results from Experiments 1 and 2 (Chapters 4 and 5) concern data from these recordings. The second are epilepsy patients with ECoG recordings performed several days after neurosurgery ("chronic" recordings) with Dr. Nicholas M. Barbaro. The results in Chapter 7 concern data from these recordings. Both patient populations were comprised of adults (age range 19-57 y.o.) who consented at least one day prior to recordings during a consultation with the neurologist or neurosurgeon. All studies involved no additional risk to the patients and were approved by the Committee on Human Research (both at UCSF and UCB).

Recordings in tumor patients

All patients were undergoing surgery for resection of gliomas in the left-hemisphere, and therefore at risk of damage to language areas. After opening the craniotomy, the patient is brought out of general anesthesia (propofol remifentanyl combination) for awake language mapping. This procedure takes up to 1 hour and uses electrical shocks during simple language tasks to identify regions critical for language ("eloquent" cortex) (Penfield and Roberts 1959; Ojemann 1979; Ojemann et al. 1989). The trajectory and extent of the subsequent resection is tailored to these results (for more details on the neurosurgical procedure, see Berger 1996; Maciunas et al. 1996). Because electrical stimulation mapping (ESM) involves risk of inducing seizure, electrodes are placed on the cortical surface in order to monitor for after-discharges. Electrodes are ~4-10 carbon ball electrodes (just under 3 mm contact diameter) and are referenced to similar electrodes placed near the margin of the craniotomy, typically on the dura.

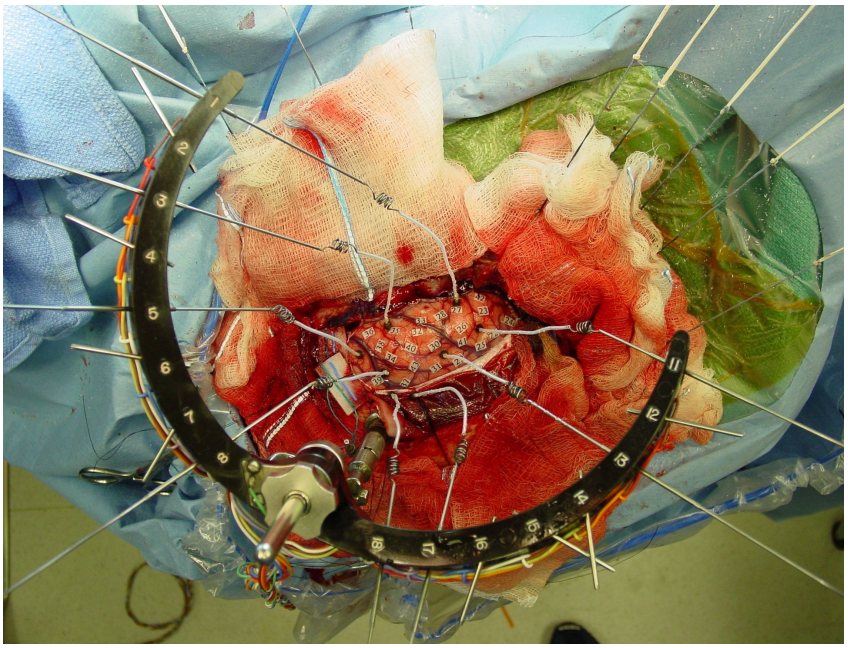

Figure A1.2. Photograph of craniotomy and electrode setup for one tumor patient. The black, horseshoe-shaped apparatus is the "cortical crown" and it is affixed to the skull. Electrodes are mounted in the crown and placed on the cortical surface. The numbers on the crown are the

electrode numbers given in the ERSA figures of Chapters 4 and 5. The small white squares on the cortical surface are numbered tags used in the language mapping procedure.

Major sulcul and gyral landmarks are identifiable on the photograph (up-close pictures are also taken). Because the location of the craniotomy is know by the neurosurgeon, the photograph alone can be used to determine the locations of the electrodes, at least in terms of the overall gyral position. The outline of the craniotomy is drawn on a template brain during surgery (the figures for all tumor patients show this template brain with the outlined craniotomy redrawn digitally) and gyral locations are usually obtained from the neurosurgeon. Most electrodes in the tumor patients were further localized with the help of an intraoperative localization device coregistered to the patient's pre-operative MRI scan. This "frameless stereotactic device" (Stealthstation, Medtronic) uses a set of fiducials, infrared sensors, and a pointing device to achieve accurate localization relative to the MRI (see Berger 1996; Maciunas et al. 1996). The anatomical localizations were primarily carried out by another graduate student, Maryam Soltani. All ECoG data from tumor patients were collected by Maryam Soltani and myself, with occasional assistance from others listed in the acknowledgements (most often Sarang Dalal).

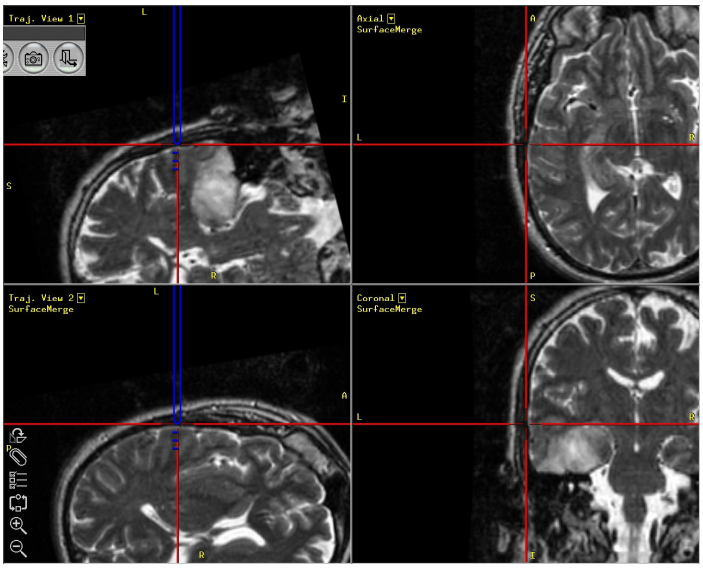

Figure A1.3. "MRI snapshot" taken with the intraoperative localization device. This shows the location of electrode 7 of Patient 3 presented in Figures 4.8 and 4.10. The tumor can be seen in the coronal slices (upper left and lower right) in the inferior and medial temporal lobe.

Our recordings use the same electrodes already in place for these clinical purposes. At the end of the language mapping, we connect to the electrodes and record ECoG for ~5 mins. Our recordings are passive and do not involve any electrical stimulation and therefore add no additional risk to the patient. We have not observed any epileptiform activity in any of our records, and electrodes over the tumor (as confirmed by MRI localization) were not included. All of our patients showed at least 1-2 electrodes with no event-related activity, indicating that the reference electrode was "silent" with respect to these events (auditory stimuli). Given the small number of electrodes used in these recordings, we preferred not to use the common-average reference (more discussion below).

Auditory stimuli were presented in the operating room (OR) using speakers placed on the ground ~0.5 m from the patient's head. There were no known auditory deficits in any of the patients, and the patient's hearing was not significantly compromised by the surgical draping (covering the left ear) as normal conversation was possible throughout. Beeps of the heart rate monitor were turned off during the language mapping procedure and remained off during our experimental session. Background noise level in the OR was estimated at 50-55 dB SPL.

Recordings in epilepsy patients

All epilepsy patients were undergoing surgery by Dr. Nicholas Barbaro to treat intractable epilepsy. Two surgeries are carried out separated by about 1 week. In the first surgery, a number of electrodes are implanted and in the second they are removed and epileptogenic tissue is resected. The electrodes consist of surface ECoG electrodes embedded in silastic (clear plastic) sheets and strips, and linear arrays of depth electrodes that penetrate to the medial temporal lobe (hippocampus or amygdala). The cables from the electrodes emerge from the craniotomy and surgical headdress and are used in the ensuing week for recordings and stimulation in the post-operative recovery room. The recordings are studied by the attending epileptologists and

neurological staff to identify foci of high seizure activity and onset. These are also used to deliver electrical shocks in a language mapping procedure similar to the ESM procedure for tumor patients. Motor areas are also identified by ESM (typically for mouth, face, or hand). At the time of writing this thesis, we have collected ECoG from 7 epilepsy patients, but have not made any systematic comparisons between ECoG and ESM results.

For our experimental paradigms, we bring the mobile ECoG cart described above into the patient's room several days after the initial surgery. The cables from the electrodes remain connected to the clinical monitoring system at all times. The signal from the cable is split and recorded separately on our system (using Datapac, sampling rate of 2003 Hz, etc.). No stimulation is performed while we are recording. Our recordings involve no additional risk to the patients and are approved by the Committee on Human Subjects. All patients consent to the procedure and may opt to end the experiments at anytime. Our experimental epilepsy ECoG recordings have been done by Ryan Canolty, myself, and Sarang Dalal, and a nurse or member of the neurological staff is always present throughout.

Our main results involve recordings from an 8×8 grid of electrodes implanted on the lateral surface of the left hemisphere[17]. The electrodes are 4 mm platinum-iridium disks (2.3 mm contact diameter, impedance of roughly 1-5 kΩ) with center-to-center spacing of 1 cm. Similar electrodes also embedded in silastic with 1 cm spacing are used in strips of electrodes that curl under the orbitofrontal cortex, inferior temporal lobe, or posteriorly over parietal cortex. No results are presented from the depth electrodes that penetrate to the medial temporal lobe.

[17] Although right hemisphere grids are also implanted, the grid is most often called for when language mapping is planned and so left hemisphere grids are more common.

The procedure for localizing the electrodes was developed mostly by Sarang Dalal and carried out by myself and Sarang Dalal (manuscript in preparation). All patients had a high-resolution T1 MRI scan. Following brain extraction (deletion of non-brain tissue from the MRI) using BET2 (www.fmrib.ox.ac.uk/analysis/research/bet/) (Jenkinson et al. 2005), a 3D reconstruction was made in MRIcro (www.sph.sc.edu/comd/rorden/mricro.html) (Rorden and Brett 2000). A lateral snapshot of this 3D rendering is used for all figures showing anatomy from these patients (as seen in Figures 7.1 and 7.2). Thus, the overall goal of the procedure was to identify the electrode locations on the MRI scan. This also allows MNI and Talairach coordinates to be obtained.

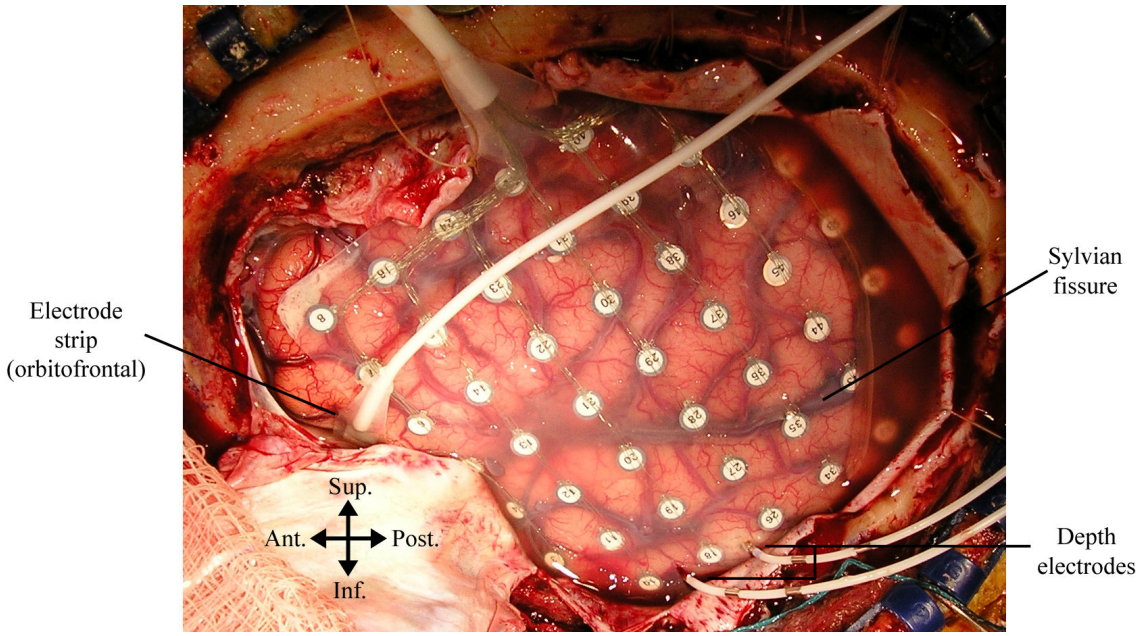

Figure A1.4. Intraoperative photograph taken during the first surgery prior to the placement of the electrode grid. This is from the patient shown in Chapter 7. The main 8×8 grid of electrodes is embedded in clear silastic, allowing major sulci and gyri to be identified.

In addition to the MRI scan, each patient has an x-ray and/or CT scan and intraoperative photographs of the electrode placement. The photograph provides the most certain localizations

for visible electrodes as their position relative to major sulci and gyri is clearly seen. The x-ray and/or CT scan are especially useful for electrode strips and depth electrodes that cannot be seen in the intraoperative photograph. The localization of electrodes on the MRI scan is further aided by the constraints that the electrodes must land on the surface of the cortex at a distance of 1 cm (give or take a couple of mm) from each other. We estimate that the error of the localization procedure is no more than ~0.5 cm for the electrodes visible on the intraoperative photograph, and ~1 cm for the others.

Data preprocessing and artifacts

All data were imported into Matlab (MathWorks Inc.) for processing. Stimulus timing was extracted from the speaker channel (auditory tasks) or photodiode channel (visual tasks), and response timing from the microphone channel (both tapping and speech responses). Some tasks used a key-press response and digital codes were used for response timing (stimulus timing was always obtained precisely from the analog channels). For sensory/perceptual tasks, the first several stimuli were rejected to allow the cortical responses to stabilize. In many patients, volume adjustments were required at the beginning of an auditory block and these trials were also rejected. In addition to these "experimental" rejections, a set of rejections were done based on artifacts in the ECoG data.

Data rejection was done for each channel separately on the continuous record. First, time points of amplifier saturation were identified as those with an absolute value greater than 340 μV (beyond which the linear range of the amplifier is exceeded). Another criterion for saturation is based on the fact that the voltage trace goes "flat" during these periods. Time-points where all frequency bands (from 8-250 Hz excluding 60 and 180 Hz) were lower than their first percentile in amplitude (i.e., in the time-series of analytic amplitude were rejected for saturation. Recovery from saturation was identified in a similar straightforward manner. Second, we sought to reject

artifacts, such as spikes or rapid disconnects of electrode contact that would cause a large, transient increase across all frequency bands. Given that amplitude in the high (>25 Hz) and low (<20 Hz) frequencies are inversely correlated, it is highly unusual for all frequency bands to simultaneously exhibit an abnormally high amplitude. The time-series of each frequency band was converted to a z-score (subtract mean and divide by the standard deviation) and the z-score value of the 99^{th} percentile was subtracted. Thus, only time-points of very high amplitudes remained at a positive z-score value. Adding this across frequency bands identified time-points where all or most frequency bands were simultaneously at an abnormally large amplitude (using the z-score allows each frequency band to contribute equally, given differences in their absolute amplitudes).

These automatic rejections were usually checked by visual inspection and a few additional epochs of rejection were added by selection in EEGLAB (Delorme and Makeig 2004). Note that small artifacts may escape detection by the above methods, but these are the very same artifacts which make negligible contributions to the event-related averages. Taken to an extreme, all time-points are contaminated by *some* degree of artifact or noise; it is the time-points of amplifier saturation or excessively large artifacts that I sought to eliminate. The above procedure was found to be very satisfactory for this purpose. Some averages were checked without artifact rejection (not shown) and this did not change the results in any way affecting our main conclusions. The rejections help against the worry that the important results in the γ_{high} band, where signal levels are minutely small, could be excessively influenced by just one or two outlier events. Even if one or two outlier events of *physiological* origin were accidentally excluded, this may even be preferable as we want our results to represent the typical physiological response. Artifact rejections for Experiment 1 (Chapter 4) were done by a somewhat different method given in Edwards et al. (2005).

For making ERPs only, data was filtered above 2.3 Hz to exclude slow drifts and heart beat artifact. For time-frequency analyses, this is not necessary as the filtering is essentially built in to the method. Frequency bands below 3 Hz are usually not studied, however, due to the presence of these artifacts. Large artifacts are also present at 60 Hz and its odd harmonics (180 Hz, 300 Hz, etc.) and occasionally the even harmonics (120 Hz, etc.). These frequency bands are usually ignored. However, ECoG recordings are not contaminated by ocular or muscle artifacts, which make a major contribution to scalp EEG and swamp the ability to detect γ_{high}.

For the epilepsy recordings only, data was re-referenced to a common-average reference (CAR). The CAR consists of the mean across all electrodes, using only non-rejected sample points (so as not to contaminate the average). Flipping the sign of the CAR is an approximation to the activity that was contributed by the reference electrode, as this is the only activity that is common at all recording electrodes. Subtracting the CAR is thus an approximation to subtracting the contributions of the reference electrode. Of course, this ideal is not entirely achieved, and another way to conceptualize this re-referencing is that it subtracts the "spatial DC" from the recorded activity (by definition, the "spatial DC" is the mean activity level across all electrodes or points in space). Crone et al. (2001a) also use the CAR for their epilepsy recordings and provide a good discussion of its justification.

For the tumor patients, where only 4-10 electrodes were recorded, the original reference was kept. The assumptions of the CAR are very poorly met with this few electrodes. The original reference was almost always on the margin of the craniotomy on the dura and there were always at least one or two recording electrodes that showed no event-related activity (as would result from an "active" reference). The analyses for Experiment 2 (Chapter 5) were checked with a CAR re-referencing, and the results were not drastically altered in any way affecting the main conclusions.

Appendix 2: Time-frequency methods

All time-frequency analyses were done with a Gaussian filter bank and the Hilbert transform. For a given electrode, this begins with the original, continuous ("raw") signal, S(t). S(t) is in units of μV. Capital letters are used by the convention of Chapter 8 to represent population waveforms (ECoG recordings are population waveforms, representing the linear summation of the voltage contributions from thousands of single cells). The t in parentheses indicates that S is a function of time, i.e. it is in the "time domain". S(t) is typically several minutes long (one block) and at a sampling rate of 2003 Hz, it is therefore a very long time series. Let's call the total number of time points T.

The spectrum

The first step is to take the FFT and thereby enter the frequency domain. The result is the spectrum, $\mathbf{Z}(f)$. Thus, $\mathbf{Z}(f) = \text{fft}(S(t))$. This is a set of complex numbers of the same length as S(t). That is, if F is the total number of frequencies in $\mathbf{Z}(f)$, then F = T. **Z** is in bold font to indicate that it consists of complex numbers. All complex variables will be represented here (as in Chapter 8) with bold letters. Complex numbers can be represented as vectors in the complex plane, as already discussed in Chapter 8 (see Figures 8.3, 8.5, and 8.6 for examples of complex numbers as vectors). Therefore, each element of $\mathbf{Z}(f)$ has an amplitude and a phase. The amplitude is the length of the vector, and the phase is the angle of the vector with respect to the positive X-axis (ordinate). Let A(f) be the amplitude at each frequency and Φ(f) be the phase at each frequency. Then, $A(f) = |\mathbf{Z}(f)|$ and $\Phi(f) = \text{angle}(\mathbf{Z}(f))$. The | | operation gives the absolute value of a complex number, or equivalently the length of the vector. A(f) is the amplitude spectrum, and Φ(f) is the phase spectrum. These are both real (not complex) numbers. A(f) is bounded below at 0, as a

vector cannot have a negative length, and unbounded above. It is in units of μV, the same units as S(t). Φ(f) ranges from 0 to 2π in units of radians.

Power is amplitude squared, so the power spectrum is obtained by squaring each element of the amplitude spectrum. Thus, $P(f) = A(f)^2$ and is in units of μV^2. The slope of the power spectrum in log-log coordinates (plotting log(P(f)) vs. log(f)) defines a category of colored noise. A slope of 0 is white noise, -1 is pink noise, -2 is brown noise, and -3 or lower is black noise (Schroeder 1991). The slope of the amplitude spectrum in log-log coordinates (plotting log(A(f)) vs. log(f)) works just as well. A slope of 0 is white noise, -0.5 is pink noise, -1 is brown noise, and -1.5 or lower is black noise (Figure A2.1). I typically find values between -1 and -2 for human ECoG data and therefore ECoG is approximately "dark brown" noise.

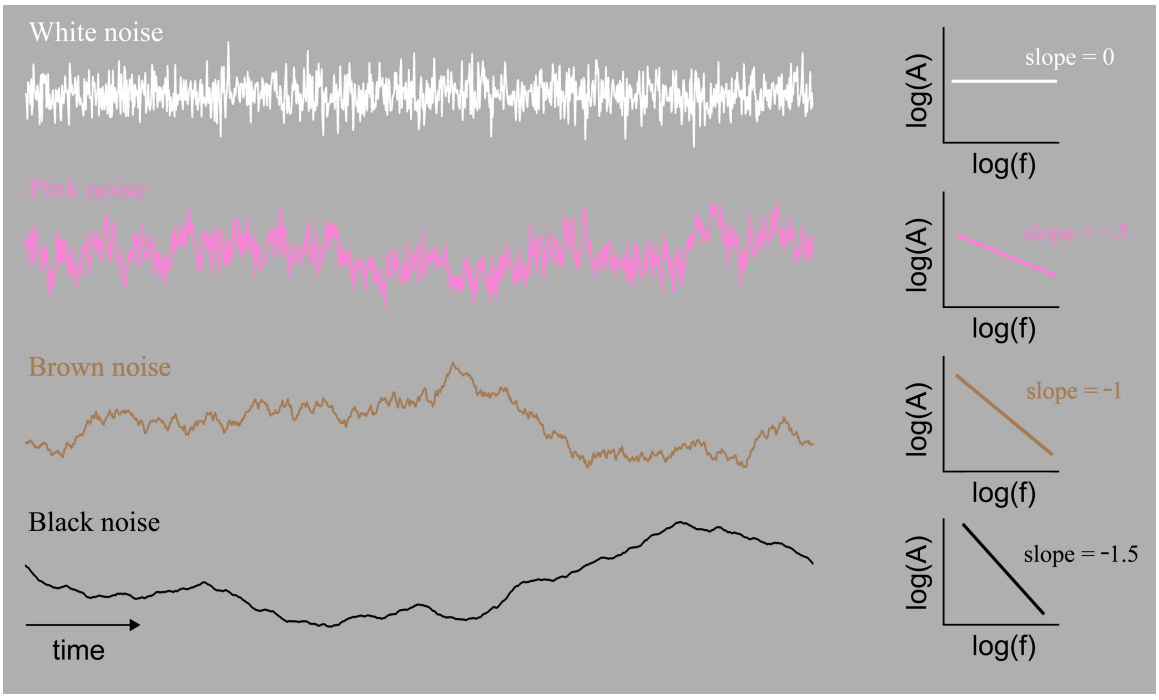

Figure A2.1. Illustration of colored noise generated in Matlab. The log-log amplitude spectrum is given to the right with the corresponding slopes. Note that there is increasing redundancy across time (temporal autocorrelation) with decreasing slope.

Obtaining the amplitude spectrum or power spectrum is a spectral analysis (or frequency analysis). But no time information is yet known, and what we seek is the time varying spectrum. The need for time-frequency analysis is given a beautiful exposition in Cohen (1995): "Time varying spectra are common in ordinary life. During sunset the frequency composition of the light changes quickly and dramatically. In saying that the sky is getting redder we are conveying a time-frequency description because we are describing how the frequencies are changing in time… Standard musical notation is a time-frequency representation since it shows the player what notes, or frequencies, should be played as time progresses." I defer to Cohen (1995) and others in making the following important point. The Fourier transform is not just an arbitrary method of frequency analysis. It has deep mathematical roots in the properties of real numbers and practically defines what it means to enter the frequency domain. It is commonly stated in the EEG literature that the Fourier transform only applies to perfectly periodic signals. There is only a narrow sense in which this criticism holds, and I might call this the "fallacy of citing the Fourier fallacy". *All* of the information in the original time domain signal, S(t), is contained in the frequency domain spectrum, **Z**(f), obtained by the Fourier transform. **Z**(f) is therefore a complete representation, regardless of whether S(t) is a periodic signal or not.

The Hilbert transform with a Gaussian filter bank

Another fallacy in the EEG literature is to criticize one or another method of time-frequency analysis. The major competing methods are the ST-FFT[18], wavelets, and Hilbert transform methods. On p. 136 of Cohen (1995), he arrives impressively at one equation that "*all* time-frequency representations can be obtained from". This remarkable result even applies to Wigner distributions and modified Wigner distributions. Examination of this equation reveals that the Fourier transform is an integral part, showing again that it is not just an arbitrary analysis

[18] Note that the ST-FFT ("short-time" or "moving-window" FFT) is a method of time-frequency analysis, whereas the FFT is a method of frequency analysis only (no time information).

method. When viewed from the unified perspective of Cohen (1995), the debate concerning ST-FFT vs. wavelets vs. Hilbert becomes moot. They can all be made equivalent by appropriate selection of parameters. This point is also made in the often-cited paper on the Hilbert transform by Flanagan (1980), and in the EEG literature by the exceptionally clear work of Andreas Bruns (2004). Probably the major confusion in the pseudo-debate results from the fact that the ST-FFT method is usually used with a linear frequency scale with the same bandwidth at all frequencies, whereas wavelets are usually used with a logarithmic frequency scale with the same relative bandwidth ("constant-Q", or same ratio of bandwidth to center frequency) at all frequencies. However, the ST-FFT can also be run with different window lengths for each frequency band and thereby achieve a constant-Q set of bandwidths. And wavelets can also be run such that the length of the wavelet in time is held constant (rather than the number of cycles), giving equal bandwidths for each frequency band. Either of these can also be used with a semi-logarithmic scale somewhere in between the linear and logarithmic scales. The Hilbert transform can also be used with any arbitrary frequency spacing and set of bandwidths.

Combining the two fallacies mentioned above, it is sometimes stated that the ST-FFT is a poor method of time-frequency analysis because the FFT only applies to periodic signals. This "criticism" misses the point in two regards!

Given the theoretical equivalence of the ST-FFT, wavelets, and Hilbert methods, the major deciding factor between methods is the computational time required. As Bruns (2004) notes, the Hilbert can be implemented with only one FFT per channel, and one inverse-FFT per frequency band. Thus (and I have confirmed with tests in Matlab), the Hilbert method is the fastest and is therefore chosen for all of my time-frequency analyses. It is also the easiest to program, requiring only a few lines of code, as it amounts to a simple windowing operation in the frequency domain. It is also the easiest to understand and work with in my opinion.

The Hilbert transform can be run on any time-domain signal, S(t), and the result is called the *analytic signal*, **AS**(t). The analytic signal is thus a complex signal in the time domain. The analytic signal has a very nice set of mathematical properties, as discussed in Flanagan (1980) and Cohen (1995). As a series of complex numbers, each element of **AS**(t) can be represented as a vector in the complex plane, and so **AS**(t) can be thought of as a time-series of vectors with the same sampling rate as the original signal S(t). The length of the vectors defines the *analytic amplitude*, AA(t). Thus, AA(t) = |**AS**(t)|. The angle of the vectors defines the *instantaneous phase*, IΦ(t). Thus, IΦ(t) = angle(**AS**(t)). AA(t) is bounded below at 0 and unbounded above, in units of μV (the same units as S(t)). It is the envelope of the original signal, S(t). IΦ(t) ranges from 0 to 2π in units of radians. The vectors of **AS**(t) typically rotate around the complex plane as time progresses, and the instantaneous rate of this rotation - the derivative of the IΦ(t) - is the instantaneous frequency, IF(t). Conveniently, the real part of the analytic signal is the original signal (indicating again that we have not lost any information in going into the frequency domain with the FFT):

$$S(t) = \text{real}(\mathbf{AS}(t)).$$

Although I will not go far into the mathematics of the Hilbert transform, its implementation is very straightforward. The negative frequencies of the spectrum are set to zero, the amplitude of the positive frequencies are doubled to compensate, and the inverse-FFT is taken. We define a Hilbert frequency domain function, h(f), where h(f)=0 for negative f, h(f)=2 for positive f, and h(f)=1 for the DC frequency. The Hilbert transform on the signal S(t) is:

$$\mathbf{Z}(f) = \text{fft}(S(t)).$$

$$\mathbf{Z'}(f) = \mathbf{Z}(f) \cdot h(f).$$ [The · is element-by-element multiplication].

$$\mathbf{AS}(t) = \text{ifft}(\mathbf{Z'}(f)).$$ [ifft is the inverse-FFT].

If the Hilbert transform is run on each of a set of bandpass filtered signals, this becomes an efficient time-frequency method. Because the Hilbert transform can be run on any arbitrary time-domain signal, there are no restrictions on how to construct the filter bank. However, as discussed in Singh and Theunissen (2003), a Gaussian filter bank has a nice set of properties and in certain respects offers an optimal trade off of time and frequency resolution. It is also easy to implement as a windowing operation in the frequency domain. We define a Gaussian frequency domain window, $G^{cf}(f)$, for each center frequency (cf). This is the familiar Gaussian shaped function centered around some frequency cf (the mean) and with some bandwidth σ (the standard deviation). A set of such Gaussian windows, one for each cf, constitutes a Gaussian filter bank. Our only questions in setting up the Gaussian filter bank are: Which set of center frequencies (cfs) should be used? And, what bandwidth (σ) should be used for each cf? These questions are addressed in a subsequent section.

I first illustrate the combined use of the Gaussian filter bank and Hilbert transform for some center frequency. I arbitrarily choose a center frequency of 40 Hz for this example, cf = 40. It would be computationally inefficient to first filter the signal, and then apply the Hilbert transform. This would require 2 uses of the fft and 2 uses of the ifft. Instead, these two steps are combined into one frequency domain operation. One frequency domain window, $H^{40}(f)$, is made from the element-by-element multiplication of $G^{40}(f)$ and h(f): $H^{40}(f) = G^{40}(f) \cdot h(f)$. The superscript "40" indicates that we are working with cf = 40 Hz. We can now obtain the analytic signal for the 40 Hz band as follows:

$\mathbf{Z}(f) = \text{fft}(S(t))$.

$\mathbf{Z^{40}}(f) = \mathbf{Z}(f) \cdot H^{40}(f)$. [This is element-by-element multiplication].

$\mathbf{AS^{40}}(t) = \text{ifft}(\mathbf{Z^{40}}(f))$.

From this, the filtered signal could be obtained if desired: $S^{40}(t) = \text{real}(\mathbf{AS}^{40}(t))$. The analytic amplitude at 40 Hz (the envelope of the filtered signal) is the absolute value: $AA^{40}(t) = |\mathbf{AS}^{40}(t)|$. Both of these signals have the same sampling rate (2003 Hz) and units (μV) as the original signal. If phase analyses are to be done, then $I\Phi^{40}(t) = \text{angle}(\mathbf{AS}^{40}(t))$. Repeating this operation for each center frequency completes the time-frequency analysis.

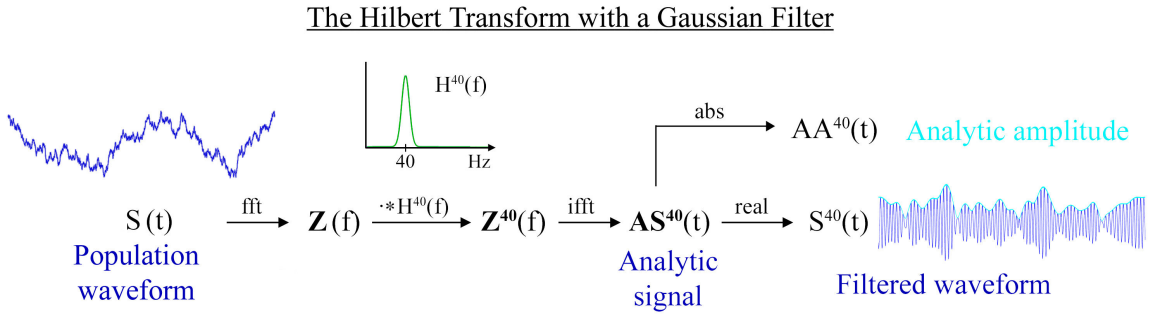

Figure A2.2. Illustration of the steps involved in using the Hilbert transform together with a Gaussian filter. In this example, the center frequency (cf) is 40 Hz. The original population waveform that is recorded is S(t). **Z**(f) is the spectrum of S(t). $\mathbf{AS}^{40}(t)$ is the analytic signal at 40 Hz. The real part of $\mathbf{AS}^{40}(t)$ is the filtered waveform at 40 Hz, $S^{40}(t)$. The absolute value of $\mathbf{AS}^{40}(t)$ is the analytic amplitude for 40 Hz, $AA^{40}(t)$.

The ERSA

Event-related averages of the analytic amplitude can be performed in exactly the same manner as for making traditional ERPs. I call the result the "Event-related spectral amplitude" (ERSA). The ERSA is in units of μV, with one row per center frequency and one column per time point. For display purposes only, I convert to units of % relative to the pre-event baseline. One of the ERSAs from Experiment 2 is shown here in detail in order to explain the plotting conventions (Figure A2.3).

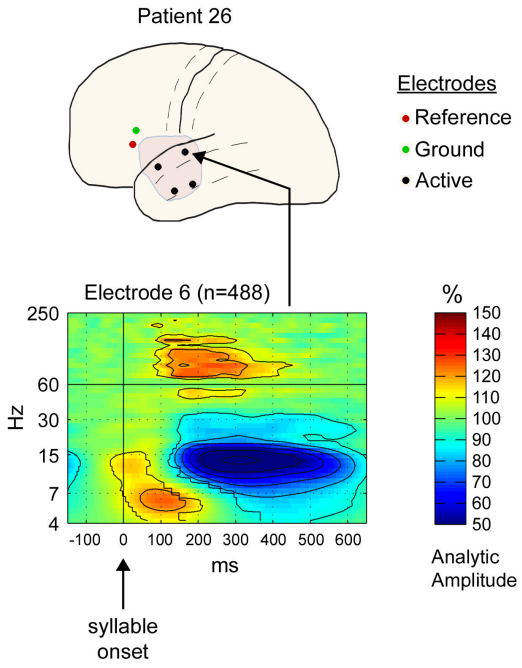

Figure A2.3. ERSA from one electrode in response to syllables. The location of the electrode is shown in the above template brain (Appendix 1). The number of events contributing to the event-related average is indicated in parentheses (n=488) above the ERSA. Time (ms) is on the ordinate, with syllable onset at 0 ms. The frequency scale for the abscissa is logarithmic, with labels at ~boundaries of traditional Greek-letter bands (θ: 4-7 Hz, α: 7-15 Hz, β: 15-30 Hz, γ_{low}: 30-60 Hz; γ_{high}: 60-250 Hz). The line at 60 Hz clearly demarcates the boundary between low and high γ, but also indicates the location of 60 Hz electrical interference. Results at 60 Hz should be ignored; note the gap in the island of γ activity at 60 Hz. Color indicates analytic amplitude in units of %, as indicated in the color bar to the right. 100% (green) is the mean analytic amplitude of the pre-stimulus baseline for each frequency. Contours are drawn on the ERSA at levels indicated by the hash-marks in the colorbar (50%, 60%, etc.) except at 100%. However, these contours are only drawn for pixels that are statistically significant ($p<0.02$, see below for methods). Thus, all pixels within the contours are statistically significant. The event-related averaging and statistical assessment were all done in original units of μV. The units of % are obtained after averaging *for display purposes only*.

The relation of population amplitude to unit amplitudes

In this section, I develop the summation ideas of Chapter 8 in the framework of frequency analysis and time-frequency analysis. This expands the theoretical insights of Motokawa's statistical-mechanical theory, and the usefulness of the equation $A = N \cdot C \cdot \bar{a}$ developed in that section. It also provides a major justification for choosing amplitude rather than power. As in Chapter 8, small letters will represent unit variables and capital letters will represent population-level variables.

The population waveform that we actually record, S(t), is the linear summation of N unit waveforms: $S(t) = s_1(t) + s_2(t) + \ldots + s_N(t)$. Because summation and the FFT are linear operations, the population spectrum, $\mathbf{Z}(f)$, is the summation of the unit spectra:

$$\mathbf{Z}(f) = \mathbf{z_1}(f) + \mathbf{z_2}(f) + \ldots + \mathbf{z_N}(f).$$

In any summation of complex numbers, the real and imaginary parts summate separately:

$$X(f) = x_1(f) + x_2(f) + \ldots + x_N(f).$$

$$Y(f) = y_1(f) + y_2(f) + \ldots + y_N(f).$$

$$\mathbf{Z}(f) = X(f) + i \cdot Y(f). \; [i = \sqrt{-1} \text{ (the basic imaginary number)}].$$

However, the population amplitude spectrum, A(f), is not the simple summation of the unit amplitude spectra: $A(f) \neq a_1(f) + a_2(f) + \ldots + a_N(f)$! Rather, the population amplitude spectrum depends on the coherence between the units in the same way as for summing sine waves (Figure 8.6 above): $A(f) = N \cdot C(f) \cdot \bar{a}(f)$. Here C(f) is the linear coherence as a function of frequency and $\bar{a}(f)$ is the mean amplitude spectrum across the units.

This analysis shows that the principles developed in Chapter 8 for 10 Hz sine waves apply to any frequency band of the spectrum. Motokawa and Mita (1942) noted that their analysis

applies equally well to vectors obtained through a Fourier analysis, and were therefore well aware of this fact. Accordingly, if the unit phase spectra, $\phi_1(f)$, $\phi_2(f)$, …, $\phi_N(f)$, exhibit a uniform distribution at a given frequency, then the population amplitudes at that frequency, A(f), will be distributed according to the Rayleigh. Thus, Motokawa's analysis for 10 Hz sinusoids applies equally well to the 10 Hz frequency of broadband signals.

It should be noted that the population power spectrum, P(f), is not expected to relate to the unit spectra in such a straightforward manner. A Rayleigh distribution of powers is not expected (or obtained empirically) and I do not know of any simple distribution that does fit. This simplicity of understanding the amplitude spectra vs. the power spectra is one reason to choose amplitude over power. It recognizes the fact that the EEG is a summation process.

I next show that the same analysis applies to the analytic signal of the Hilbert transform. This follows from the fact that all of the operations involved in the Hilbert transform are linear operations. Figure A2.4 illustrates this example for a center frequency of 40 Hz: cf = 40. If we had all of the unit waveforms ($s_1(t)$, $s_2(t)$… $s_N(t)$) and obtained their analytic signals at 40 Hz, then the summation of these unit analytic signals would equal the population analytic signal, $\mathbf{AS}^{40}(t)$. The population analytic amplitude, $AA^{40}(t)$, is related to the unit analytic amplitudes by the usual equation: $AA^{40}(t) = N \cdot C^{40}(t) \cdot \bar{a}\bar{a}^{40}(t)$. Here, $\bar{a}\bar{a}^{40}(t)$ is the mean of the unit analytic amplitudes at 40 Hz. Note that the coherence at 40 Hz, $C^{40}(t)$, is a function of time. This would be obtained from the unit instantaneous phases, also functions of time.

Figure A2.4 (next page)**.** The summation of unit waveforms (generated as brown noise) and all of the operations of the Gaussian filter and Hilbert transform are linear. Therefore, the population analytic signal ($\mathbf{AS}^{40}(t)$) can be arrived at equivalently by several routes.

Summation of unit waveforms: Hilbert transform

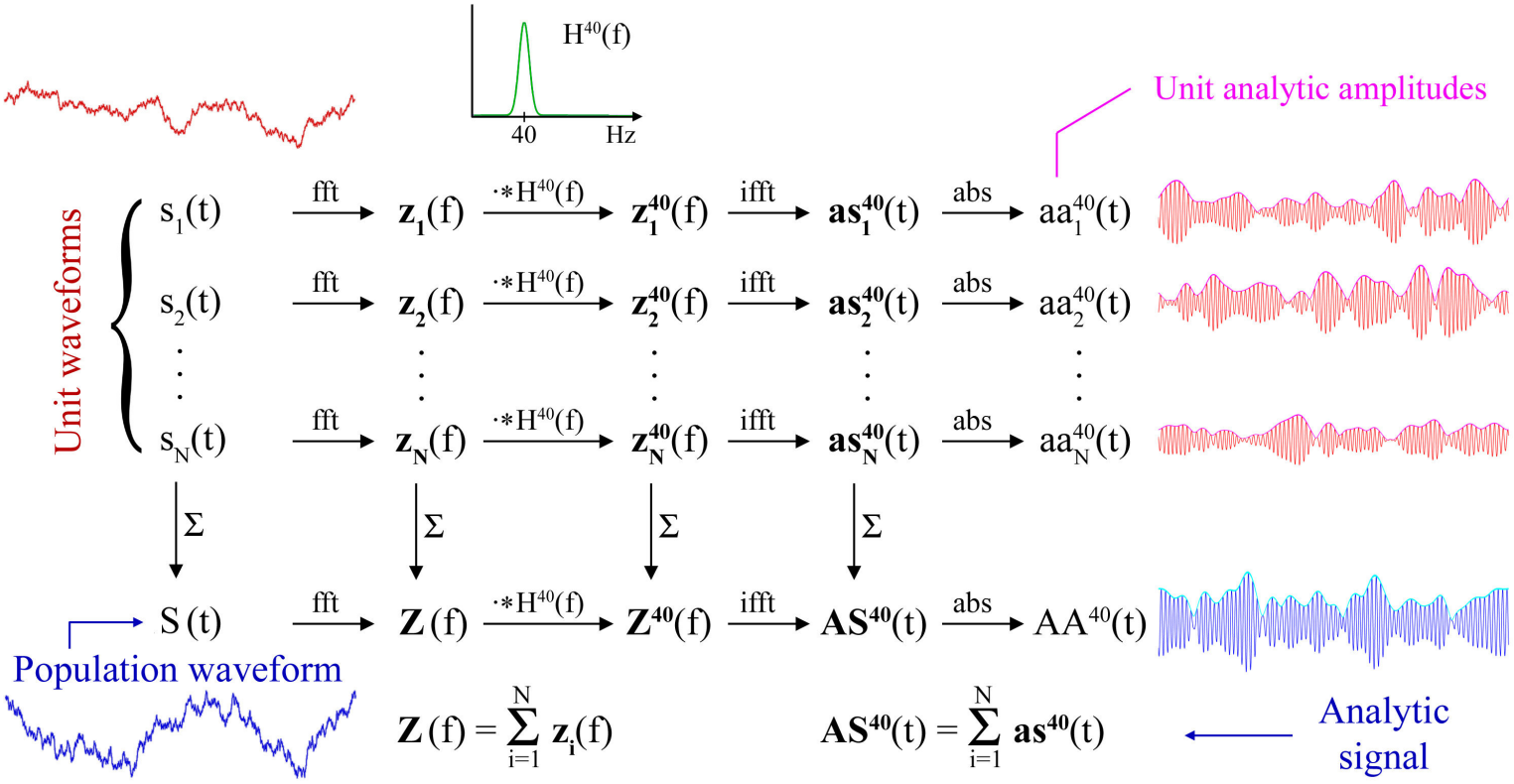

We therefore find a neat framework for working with analytic *amplitudes*. We can arrive at the population analytic amplitude by any number of routes, because all of the operations involved are linear. However, taking the square at any point to obtain power would be a non-linear transform and this framework would no longer hold. Accordingly, the distribution of analytic amplitudes is expected to follow a Rayleigh (and does, at least for γ range frequencies), but the distribution of power is not as easily understood.

This section is concluded by examining Motokawa's flaw. Recall that he obtained his αamplitudes by measuring peak-to-peak at each peak. This is a rough approximation to the analytic amplitude obtained with the Hilbert transform (the envelope of the signal)[19]. By either method, one obtains a distribution of amplitudes *across time*. Working with a center frequency of 10 Hz (cf=10): $AA^{10}(t) = N \cdot C^{10}(t) \cdot \bar{a}\bar{a}^{10}(t)$. Thus, in one long block of data of length T, there are T values in $AA^{10}(t)$. Our distribution is not of M independent realizations of the summation process (as in Figure 8.7), but rather of T values across time. These are not independent due to time dependencies. This could be practically avoided by taking measures at long intervals from each other, but this actually isn't the essential flaw. The essential flaw is that a Rayleigh distribution no longer implies that the underlying units are randomly distributed in phase. By the conditions for obtaining a Rayleigh distribution of vector lengths, the real and imaginary parts of the vectors must be independently and normally distributed. In this case, the vectors are the vectors in the analytic signal, $\mathbf{AS}^{10}(t)$. In order for $|\mathbf{AS}^{10}(t)|$ to be distributed by a Rayleigh, this means $X^{10}(t)$ and $Y^{10}(t)$ have to be independently and normally distributed. But these are population variables not unit variables! Because the instantaneous phase rotates around the complex plane across time, the distribution of $I\Phi^{10}(t)$ is likely to be distributed ~uniformly for

[19] The peak-to-peak amplitude is double the analytic amplitude, and Motokawa's equation for the Rayleigh distribution includes this extra factor of 2.

large T. This is the reason that $X^{10}(t)$ and $Y^{10}(t)$ are normally distributed[20] across time, not because of the underlying unit relations. To summarize:

$I\Phi^{10}(t)$~Uniform$(0,2\pi)$. Therefore,

$X^{10}(t)$~Normal, and $Y^{10}(t)$~Normal. Therefore,

$AA^{10}(t)$~Rayleigh.

Empirically, we indeed obtain a Rayleigh distribution of analytic amplitudes (at least for γ frequencies) and now we have a good explanation as to why. This is an important result. Several authors have commented that we need to begin looking at distributions of EEG measures rather than just means. However, very little work has actually been done in this direction. One recent paper (Canolty et al. 2006) fit a Gamma distribution to γ_{high} analytic amplitudes of the ECoG. Although a good fit was obtained, several distributions fit nearly or just as well (Nakagami, Weibull, etc.), and the Rayleigh usually fits as well or better. The better fit for the Rayleigh is found in most cases despite the fact that the Rayleigh is only a 1-parameter distribution and the Gamma is a 2-parameter distribution (as are the Nakagami, Weibull, etc.). We have a theoretical explanation for why the Rayleigh distribution arises in our data, but I know of no explanation for the Gamma or other distribution. For frequencies below the γ range, the Rayleigh no longer fits the empirically obtained distributions as well (it does fit well enough that we can easily understand how Motokawa obtained a Rayleigh distribution empirically for α amplitudes). Indeed, the Rayleigh fails systematically in a predictable direction as the frequency band becomes lower. It would appear that there is some 2-parameter, modified-Rayleigh distribution that does hold at all frequency bands (this modified-Rayleigh distribution will be distinct from the Gamma, Weibull, and Nakagami, as I have already tried these). Therefore, many open questions remain.

[20] I actually do not currently know how the assumption of independence works in to this analysis. This will require some more thought, but in any case the Rayleigh is obtained empirically.

1) $X^{cf}(t)$ and $Y^{cf}(t)$ are supposed to be normally and independently distributed for the Rayleigh to obtain. Are they independent, and if not, what is the consequence of their dependence?
2) How do we deal with the issue of time-dependencies when obtaining our distributions across time?
3) Why are γ analytic amplitudes fit well by the Rayleigh, but lower frequencies are not fit as well? Does this have to do with greater time-dependencies for lower frequencies? Or with greater dependencies across units for lower frequencies? That is, perhaps lower frequencies do exhibit above-chance coherence across units, but γ frequencies do not.
4) Can these issues be resolved with an improved mathematical analysis that identifies a 2-parameter modified-Rayleigh distribution that fits the distributions for all frequency bands?

I am optimistic that such progress can be made, and that it will lead to a modified statistical-mechanical theory of the EEG. This would yield powerful insights into unit-population relations and possibly realize the hope of Motokawa that distributions of population-level measures can inform us about unit-unit relations. Note again that many important insights have already been gained from a consideration of Motokawa's original statistical-mechanical theory. For example, the equation $A(f) = N \cdot C(f) \cdot \bar{a}(f)$ holds regardless of whether the Rayleigh distribution holds, and gives an important insight into the different possibilities for the observed "ERD" or "ERS" in the EEG.

Filter bandwidths

Returning to practical issues in the construction of the ERSA, the filter bandwidths of the Gaussian filter bank must be chosen. The analytic amplitude time-series, $AA^{cf}(t)$, is the same length T as the original signal and at the same sampling rate (2003 Hz). However, the sampling rate is not the real temporal resolution, in the sense of the uncertainty principle. Given the tradeoff between time and frequency resolution demanded by the uncertainty principle, the more narrow the filter bandwidth the lower the time resolution. Using the symbols of Singh and Theunissen (2003) in this section, the uncertainty principle is:

$$\sigma_f \cdot \sigma_t \geq 1/4\pi.$$

σ_f is the bandwidth parameter (visualized as the blur or spread in the frequency domain that determines the frequency resolution) and σ_t is the duration parameter (visualized as the blur or spread in the time domain that determines the temporal resolution). Essentially, this equation says that the product of time resolution and frequency resolution can never go lower than $1/4\pi$ (the units are in radians).

For a Gaussian filter bank, σ_f is just the standard deviation parameter of the Gaussian shaped filter function in the frequency domain (different for each center frequency in the filter bank). Conveniently, "the time window that corresponds to the Gaussian filter in the filter bank is also a Gaussian function with standard deviation parameter (also the effective duration of the window[21]) given by: $\sigma_t = 1/(2\pi\sigma_f)$" (Singh and Theunissen 2003).

Thus, one reason to use the Gaussian filter bank is that it connects very easily to the uncertainty principle that fundamentally governs all time-frequency analyses. The settings of the analysis can literally be constructed from first principles! Using the ideas and equations

[21] This equation shows how to set up the equivalent ST-FFT analysis with a Gaussian-tapered moving window in the time domain. It also indicates the length of "Morlet" (Gaussian-tapered) wavelets to use.

developed in Singh and Theunissen (2003) for a Gaussian filter bank and "modulation spectra", I have been able make precise and principled decisions for the several settings that must be decided. For example, how far apart should center frequencies be spaced within the filter bank? There is a certain minimum spacing below which no further information is obtained (in fact, the same standard deviation parameters of the Gaussian filters). At what temporal sampling interval should p-values be tested? With the problem of multiple-testing, we do not want to test α modulation every 1/2003 sec! In fact, it is in some respects meaningless to discuss modulation of a 10 Hz carrier frequency any faster than 10 Hz (what would 40 Hz modulation of a 10 Hz carrier wave look like?). Thus, we only need to sample the 10 Hz envelope at 20 Hz by the Nyquist principle. Although I always use the full sampling rate of 2003 Hz for averaging and displaying, there is no need to go beyond the Nyquist of the fastest meaningful modulation frequency for testing p-values. This saves a tremendous number of multiple hypothesis tests.

Unfortunately, it would require a lengthy and mathematically-involved discussion to show exactly how and why I arrived at my final settings, but the basic principles are to be found in (Flanagan 1980; Cohen 1995; Singh and Theunissen 2003). My settings are thus only briefly outlined. I used a logarithmic frequency scale for all displays as it allows clear visualization of both lower and higher frequencies. My filter bandwidths grow semi-logarithmically with increasing center frequency. Constant filter bandwidths are typically used in the ST-FFT approach with a single moving window used for all frequency bands. Constant "Q", or ratio of filter bandwidth to center frequency, is usually used in the wavelets approach where each wavelet has the same number of cycles. My settings are precisely in between these two, and I have found this to offer a good compromise between time and frequency resolution for human ECoG. I was assisted in this choice by the optimization analyses and discussion given by Lewicki (2002) for the time-frequency analysis of auditory signals. My filter bandwidths begin at $\sigma = 0.39$ Hz for a

center frequency of 1 Hz and grow semi-logarithmically from there. Thus, at cf = 40 Hz, σ_f = 2.46 Hz. At cf = 100 Hz, σ_f = 3.84 Hz. And so on. Precisely, in a plot of log(f) vs. log(σ_f), I use a y-intercept (1 Hz, since log(1)=0) of 0.39 and a slope of 0.5. Here, a slope of 0 would correspond to a fixed bandwidth at all center frequencies, and a slope of 1 would correspond to a fixed ratio of bandwidth to center frequency (constant-Q).

Statistical assessment in the time-frequency plane

For all ERSAs, we want to know whether changes seen after the stimulus or around some other event are greater than what is expected by chance fluctuations in the baseline. I have tested a number of methods to address this issue, and found that the non-parametric resampling method used for the ERSP by Makeig and colleagues (Makeig et al. 2002; Delorme and Makeig 2004) is very satisfactory. Data points are drawn at random from the baseline periods in the single-trials to create a reference ("surrogate") distribution. Each element of the reference distribution is the average of the same number of single-trials as used for the actual ERSA. Typically, 2000 surrogate averages are obtained for each frequency band. The actual value under test (all values remain in units of μV for these statistical tests) is compared to the reference distribution for the appropriate frequency band. Raw p-values are obtained as percentile positions in the reference distribution. However, as discussed in the above section this is not done for every time point, but at a new sampling interval appropriate for the center frequency and filter bandwidth under question. Nonetheless, many thousands of such hypothesis tests are done for each subject given the large number of points in the time-frequency plane. To correct for multiple-comparisons, I use the False Discovery Rate approach (Benjamini and Hochberg 1995). This approach has a number of advantages over no correction on the one hand (too liberal) and Bonferroni correction on the other hand (too conservative), and is particularly appropriate for exploratory data analyses (Nichols and Hayasaka 2003). All p-values indicated in the ERSAs are the FDR-corrected p-

values. They are indicated by the contour lines drawn on the ERSA, which are only drawn for significant ($p<0.02$) points. Thus, all values within the contour lines are statistically significant. It is not uncommon to find some significant points in the baseline. This is almost always found to occur when there is a considerable slope in the baseline, for example if the amplitude is still recovering from the previous event (see the α band in Figure A2.2, for example). Because there is a consistent trial-tot-trial amplitude variation in this situation, significant p-values are expected.

References

Swedenborg E (1740-1741). Oeconomia regni animalis. Amsterdam, Changuion.

Gall FJ, Spurzheim J (1810-1819). Anatomie et Physiologie du Système Nerveux en Général, et du Cerveau en Particulier. Paris, F. Schoell.

Flourens M-J-P (1824). Recherches Expérimentales sur les Propriétés et les Fonctions du Système Nerveux dans les Animaux Vertébrés. Paris, J. B. Ballière.

Bouillaud J-B (1825). Recherches cliniques propres à démontrer que la perte de la parole correspond à la lésion des lobules antérieurs du cerveau et à confirmer l'opinion de M. Gall, sur le siège de l'organ du langage articulé. Archives génerale de médecine (Paris) **8**: 25-45.

du Bois-Reymond EH (1848-1884). Untersuchungen über thierische Elektricität. Berlin, G. E. Reimer.

Broca P (1861). Remarques sur le siège de la faculté du langage articulé suivies d'une observation d'aphémie (perte de la parole). Bulletins de la Société Anatomique (Paris) **6**: 330-357, 398-407.

Fritsch G, Hitzig E (1870). Über die elektrische Erregbarkeit des Grosshirns. Archiv für Anatomie und Physiologie **37**: 300-32.

Caton R (1875). The electric currents of the brain. British medical journal **2**: 278.

Ferrier D (1875a). Experiments on the brain of monkeys. Proceedings of the Royal Society of London **161**: 409-30.

Ferrier D (1875b). The Croonian Lecture: Experiments on the brain of monkeys (Second series). Philosophical transactions of the Royal Society of London **165**: 433-88.

Ferrier D (1876). The functions of the brain. London, Smith-Elder & Co.

Caton R (1877). Interim report on investigation of the electric currents of the brain. British medical journal **Suppl. 1**: 62-5.

Danilevsky VY (1877). Investigations into the Physiology of the Brain (Doctoral thesis in Russian), University of Kharkov.

Ferrier D (1886). The functions of the brain. New York, G. P. Putnam's Sons.

Caton R (1887). Researches on electrical phenomena of cerebral grey matter. Ninth International Medical Congress **3**: 246-49.

Munk H (1890). Über die Funktionen der Grosshirnrinde. Berlin, A. Hirschwald.

Beck A (1891). Oznaczenie lokalizacyi z mozgu i rdzeniu za pomoca zjawisk elektrycznych (Determination of localization in the brain and spinal cord by means of electrical phenomena), Doctoral thesis presented October 20, 1890. Polska Akademija Umiejetnosci. Series II. **1**: 186-232.

Danilevsky VY (1891). Zur Frage über die elektromotorische Vorgänge im Gehirn als Ausdrück seines Tätigkeitszustandes. Zentralblatt für Physiologie **5**: 1-4.

Mills CK (1891). On the localization of the auditory centre. Brain **14**: 465-72.

Goltz F (1892). Der Hund ohne Grosshirn. Siebente Abhandlung über die Verrichtungen des Grosshirn. Archiv für die gessamte Physiologie **51**: 570-614.

Ramón y Cajal S (1899). Studies on the human cerebral cortex II: Structure of the motor cortex of man and higher mammals. Revista Trimestral Micrográfica **4**: 117-200.

Mott FW (1907). Bilateral lesion of the auditory cortical centre: complete deafness and aphasia. British medical journal **2**: 310-15.

Bernstein J (1912). Elektrobiologie, die Lehre von den elektrischen Vorgängen im Organismus auf moderner Grundlage dargestellt. Braunschweig, F. Vieweg.

Pravdich-Neminsky VV (1913). Ein Versuch der Registrierung der elektrischen Gehirnerscheinungen. Zentralblatt für Physiologie **27**: 951-60.

Cybulski N, Jelenska-Macieszyna (1914). Action currents of the cerebral cortex (in Polish). Bull int Acad Cracovie **Series B**: 776-81.

Forbes A, Thacher C (1920a). Electron tube amplification with the string galvanometer. American journal of physiology **51**: 177-8.
Forbes A, Thacher C (1920b). Amplification of action currents with the electron tube in recording with the string galvanometer. American journal of physiology **52**: 409-71.
Gasser HS, Newcomer HS (1921). Physiological action currents in the phrenic nerve: an application of the thermionic vacuum tube to nerve physiology. American journal of physiology **57**: 1-26.
Gasser HS, Erlanger J (1922). A study of the action current of nerve with the cathode ray oscillograph. American journal of physiology **62**: 496-524.
Pravdich-Neminsky VV (1925). Zur Kenntnis der elektrischen und der Innervationsvorgänge in den funktionellen Elementen und Geweben des tierischen Organismus. Elektrocerebrogramm der Saugetiere. Pflügers Archiv für gesamte Physiologie **209**: 362-82.
Adrian ED (1926). The impulses produced by sensory nerve endings. Journal of physiology **61**: 49-72.
Adrian ED, Zotterman Y (1926). The impulses produced by sensory nerve endings. Part 2: The response of a single end-organ. Journal of physiology **61**: 151-71.
Höber R (1926). Physikalische Chemie der Zelle und der Gewebe. Leipzig, W. Engelmann.
Bramwell E (1927). A case of cortical deafness. Brain **50**: 579-80.
Berger H (1929). Über das Elektrenkephalogramm des Menschen. Archiv für Psychiatrie und Nervenkrankheiten **87**: 527-70.
Lashley KS (1929). Brain Mechanisms and Intelligence. Chicago, University of Chicago Press.
Berger H (1930). Über das Elektrenkephalogramm des Menschen. II. Journal für Psychologie und Neurologie **40**: 160-79.
Penfield W (1930). The radical treatment of traumatic epilaepsy and its rationale. Canadian Medical Association journal **23**: 189-97.
Berger H (1931). Über das Elektrenkephalogramm des Menschen. III. Archiv für Psychiatrie und Nervenkrankheiten **94**: 16-60.
Adrian ED (1932). The mechanisms of nervous action. Philadelphia, University of Pennsylvania Press.
Berger H (1932a). Über das Elektrenkephalogramm des Menschen. IV. Archiv für Psychiatrie und Nervenkrankheiten **97**: 6-26.
Berger H (1932b). Über das Elektrenkephalogramm des Menschen. V. Archiv für Psychiatrie und Nervenkrankheiten **98**: 231-54.
Dietsch G (1932). Fourier-Analyse von Elektrencephalogrammen des Menschen. Pflügers Archiv für die gesammte Physiologie **230**: 106-12.
Berger H (1933a). Über das Elektrenkephalogramm des Menschen. VI. Archiv für Psychiatrie und Nervenkrankheiten **99**: 555-74.
Berger H (1933b). Über das Elektrenkephalogramm des Menschen. VII. Archiv für Psychiatrie und Nervenkrankheiten **100**: 301-20.
Berger H (1933c). Über das Elektrenkephalogramm des Menschen. VIII. Archiv für Psychiatrie und Nervenkrankheiten **101**: 452-69.
Adrian ED (1934). Electrical activity of the nervous system. Archives of neurology and psychiatry **32**: 1125-36.
Adrian ED, Matthews BHC (1934a). The interpretation of potential waves in the cortex. Journal of physiology **81**: 440-71.
Adrian ED, Matthews BHC (1934b). The Berger rhythm: potential changes from the occipital lobes in man. Brain **57**(4): 355-85.
Berger H (1934). Über das Elektrenkephalogramm des Menschen. IX. Archiv für Psychiatrie und Nervenkrankheiten **102**: 538-57.

Tönnies JF (1934). Die unipolare Ableitung elektrischer Spannungen vom menschlichen Gehirn. Die Naturwissenschaften **22**: 411-4.
Adrian ED, Yamagiwa K (1935). The origin of the Berger rhythm. Brain **58**(3): 323-51.
Berger H (1935). Über das Elektrenkephalogramm des Menschen. X. Archiv für Psychiatrie und Nervenkrankheiten **103**: 444-54.
Durup G, Fessard A (1935). L'électoencéphalogramme de l'homme. Observations psycho-physiologiques relatives à l'action des stimuli visuels et auditifs. L'année psychologique **36**: 1-35.
Ectors L (1935). Étude oscillographique des activités sensitives et motrice du cortex cérébral chez l'animal éveillé. Comptes rendus des séances de la Société de biologie et des ses filiales **120**: 1339-43.
Foerster O, Altenburger H (1935). Elektrobiologische Vorgänge an der menschlichen Hirnrinde. Deutsche Zeitschrift für Nervenheilkunde **135**: 277-88.
Gibbs FA, Davis H, Lennox WG (1935). The electro-encephalogram in epilepsy and in conditions of impaired consciousness. Archives of neurology and psychiatry **34**: 1133-48.
Jasper HH, Carmichael L (1935). Electrical potentials from the intact human brain. Science **81**: 51-3.
Kornmüller AE (1935). Die bioelektrischen Erscheinungen architektonischer Felder der Grosshirnrinde. Biological reviews of the Cambridge Philosophical Society **10**: 383-426.
Loomis AL, Harvey EN, Hobart G (1935a). Potential rhythms of the cerebral cortex during sleep. Science **81**(2111): 597-8.
Loomis AL, Harvey EN, Hobart G (1935b). Further observations on the potential rhythms of the cerebral cortex during sleep. Science **82**(2122): 198-200.
Range RW (1935). Der Einfluß von Narcotika auf die Tätigkeit der Großhirnrinde des Kaninchens. Journal für Psychologie und Neurologie **46**: 364-70.
Rohracher H (1935). Die gehirnelektrischen Erscheinungen bei geistiger Arbeit. Zeitschrift für Psychologie **136**: 308-24.
Berger H (1936). Über das Elektrenkephalogramm des Menschen. XI. Archiv für Psychiatrie und Nervenkrankheiten **104**: 678-89.
Ectors L (1936). Étude de l'activité électrique du cortex cérébral chez le lapin non narcotisé ni curarisé. Archives internationales de physiologie **43**: 267-98.
Gerard RW (1936). Factors controlling brain potentials. Cold Spring Harbor symposia on quantitative biology **4**: 292-304.
Jasper HH (1936). Cortical excitatory state and synchronism in the control of bioelectric autonomous rhythms. Cold Spring Harbor symposium on quantitative biology **4**: 320-38.
Jasper HH, Andrews HL (1936). Human brain rhythms: I. Recording techniques and preliminary results. Journal of general psychology **14**: 98-126.
Loomis AL, Harvey EN, Hobart G (1936). Electrical potentials of the human brain. Journal of experimental psychology **19**: 249-79.
Walter WG (1936). The location of cerebral tumors by electro-encephalography. Lancet **2**: 305-8.
Bagchi BK (1937). The adaptation and variability of response of the human brain rhythm. Journal of psychology **3**: 463-85.
Berger H (1937a). Über das Elektrenkephalogramm des Menschen. XII. Archiv für Psychiatrie und Nervenkrankheiten **106**: 165-87.
Berger H (1937b). Über das Elektrenkephalogramm des Menschen. XIII. Archiv für Psychiatrie und Nervenkrankheiten **106**: 577-84.
Blake H, Gerard RW (1937). Brain potentials during sleep. American journal of physiology **119**: 692-703.
Davis H, Davis PA, Loomis AL, Harvey EN, Hobart G (1937). Changes in human brain potentials during the onset of sleep. Science **86**(2237): 448-50.

Hoagland H, Rubin MA, Cameron DE (1937). The electroencephalogram of schizophrenics during insulin hypoglycemia and recovery. American journal of physiology **120**: 559-70.
Loomis AL, Harvey EN, Hobart G (1937). Cerebral states during sleep as studied by human brain potentials. Journal of experimental psychology **21**: 127-44.
Marinesco G, Sager O, Kreindler A (1937). Etudes éléctroencéphalographiques: le sommeil et le coma. Bulletin de l'Académie de Médecine de Roumainie **2**: 454-8.
Penfield W, Boldrey E (1937). Somatic motor and sensory representation in the cerebral cortex of man as studied by electrical stimulation. Brain **60**: 389-443.
Rheinberger MB, Jasper HH (1937). The electrical activity of the cerebral cortex in the unanesthetized cat. American journal of physiology **119**: 186-96.
Rohracher H (1937). Die gehirnelektrischen Erscheinungen bei Sinnesreizen. Zeitschrift für Psychologie **140**: 274-308.
Walter WG (1937). The electro-encephalogram in cases of cerebral tumour. Proceedings of the Royal Society of Medicine **30**: 579-98.
Berger H (1938). Über das Elektrenkephalogramm des Menschen. XIV. Archiv für Psychiatrie und Nervenkrankheiten **108**: 407-31.
Davis H, Davis PA, Loomis AL, Harvey EN, Hobart G (1938a). Human brain potentials during the onset of sleep. Journal of neurophysiology **1**: 24-38.
Davis PA, Davis H, Thompson JW (1938b). Progressive changes in human electroencephalogram under low oxygen tension. American journal of physiology **123**: 51-2.
Drohocki Z, Drohocka J (1938). L'électrocorticogramme pendant l'établissement de la narcose a l'uréthane. Comptes rendus des séances de la Société de biologie et des ses filiales **129**: 895-8.
Grass AM, Gibbs FA (1938). A Fourier transform of the electroencephalogram. Journal of neurophysiology **1**: 521-6.
Jasper HH, Andrews HL (1938). Electro-encephalography: III. Normal differentiation between occipital and pre-central regions in man. Archives of neurology and psychiatry **39**: 96-115.
Rubin MA (1938). The distribution of the alpha rhythm over the cerebral cortex of normal man. Journal of neurophysiology **1**: 313-23.
Davis H, Davis PA (1939). The electrical activity of the brain. Its relation to physiological states and to states of impaired consciousness. Research publications of the Association for Research in Nervous and Mental Disease **19**: 50-80.
Davis PA (1939). Effects of acoustic stimuli on the waking human brain. Journal of neurophysiology **2**: 494-9.
Drohocki Z (1939). Elektrospektrographie des Gehirns. Klinische Wochenschrift **18**: 536-8.
Drohocki Z, Drohocka J (1939a). Étude électroencéphalographique de la localization pharmacologique des narcotiques. Archives internationales de pharmacodynamie et de thérapie **62**: 265-80.
Drohocki Z, Drohocka J (1939b). L'utilisation du test électroencéphalographique pour la localisation pharmacologique de l'évipan. Comptes rendus des séances de la Société de biologie et des ses filiales **131**: 1287-91.
Himwich HE, Hadidian Z, Fazekas JF, Hoagland H (1939). Cerebral metabolism and electrical activity during insulin hypoglycemia in man. American journal of physiology **125**: 578-85.
Hoagland H, Himwich HE, Campbell E, Fazekas JF, Hadidian Z (1939). Effects of hypoglycemia and pentobarbital sodium on electrical activity of cerebral cortex and hypothalamus (dog). Journal of neurophysiology **2**: 276-88.
Jung R (1939). Das Elektrencephalogramm und seine klinische Anwendung. I. Methodik der Ableitung, Registrierung und Deutung des EEG. Nervenarzt **12**: 569-91.

Davis PA (1941). Effect on the electroencephalogram of alterations in blood sugar level. American journal of physiology **133**: P259-60.
Jasper HH (1941). Electroencephalography. Epilepsy and cerebral localization; a study of the mechanism, treatment and prevention of epileptic seizures. Penfield W and Erickson TC. Springfield, Ill., Baltimore, Md., C. C. Thomas**:** 380-454.
Jung R (1941). Das Elektrencephalogramm und seine klinische Anwendung. II. Das EEG des Gesunden, seine Variationen und Veränderungen und deren Bedeutung für das pathologische EEG. Nervenarzt **14**: 57-70, 104-17.
Motokawa K (1941). Die elektrenkephalographische Untersuchung des Entstehungsmechanismus der periodischen Nachbilder. Tohoku journal of experimental medicine **40**: 48-77.
Motokawa K, Mita T (1941). Die elektrenkephalographische Untersuchung über den Adaptionsmechanismus des Zentralnervensystems. Japanese journal of medical sciences. III. Biophysics **7**: 213-33.
Penfield W, Erickson TC (1941). Epilepsy and cerebral localization; a study of the mechanism, treatment and prevention of epileptic seizures. Springfield, Ill., Baltimore, Md.,, C. C. Thomas.
Motokawa K, Mita T (1942). Das Wahrscheinlichkeitsprinzip über die gehirnelektrischen Erscheinungen des Menschen. Japanese journal of medical sciences. III. Biophysics **8**: 63-77.
Motokawa K (1943a). Eine statistisch-mechanische Theorie über das Elektrenkephalogramm. Tohoku journal of experimental medicine **45**: 278-96.
Motokawa K (1943b). Über den Mechanismus der Entstehung und Hemmung der alpha-Wellen des Hirnpotentials. Tohoku journal of experimental medicine **45**: 297-308.
Motokawa K, Tuziguti K, Huzimori B (1943). Die Körperlage und das Elektrenkephalogramm des Menschen. Japanese journal of medical sciences. III. Biophysics **9**: 121-34.
Walter WG (1943). An automatic low frequency analyzer. Electronic engineering **16**: 9-13.
Motokawa K (1944). Die Verteilung der elektrischen Aktivität auf der Grosshirnrinde des normalen Menschen. Tohoku journal of experimental medicine **46**: 382-95.
Walter WG, Dovey VJ (1944). Electroencephalography in cases of sub-cortical tumor. Journal of neurology, neurosurgery and psychiatry **7**: 57-65.
Darrow CW, Graf CG (1945). Relation of electroencephalogram to photometrically observed vasomotor changes in the brain. Journal of neurophysiology **8**: 449-61.
Jasper HH (1948). Charting the sea of brain waves. Science **108**: 343-7.
Moruzzi G, Magoun HW (1949). Brain stem reticular formation and activation of the EEG. Electroencephalography and clinical neurophysiology **1**: 455-73.
Penfield W, Rasmussen T (1950). The cerebral cortex of man; a clinical study of localization of function. New York,, Macmillan.
Bancaud J, Bloch V, Paillard J (1953). Contribution EEG à l'étude des potentiels évoqués chez l'homme au niveau du vertex. Revue neurologique **89**: 399-418.
Gastaut Y (1953). Les pointes négatives évoquées sur le vertex. Leur signification psychophysiologique et pathologique. Revue neurologique **89**: 382-99.
Perl ER, Galambos R, Glorig A (1953). The estimation of hearing threshold by electroencephalography. Electroencephalography and clinical neurophysiology **5**(4): 501-12.
Abe M (1954). Electrical responses of the human brain to acoustic stimulus. Tohoku journal of experimental medicine **60**(1): 47-58.
Penfield W, Jasper HH (1954). Epilepsy and the functional anatomy of the human brain. Boston, Little.
Darrow CW, Vieth RN, Wilson J (1957). Electroencephalographic blocking and adaptation. Science **126**(3263): 74-5.

Jasper HH (1958). The ten twenty electrode system of the international federation. Electroencephalography and clinical neurophysiology **10**: 371-5.
Penfield W, Roberts L (1959). Speech and brain-mechanisms. Princeton, N.J.,, Princeton University Press.
Chatrian GE, Petersen MC, Lazarte JA (1960). Responses to clicks from the human brain: some depth electrographic observations. Electroencephalography and clinical neurophysiology **12**: 479-89.
Jus A, Jus C (1960). Étude de l'extinction par répétition de l'expression EEG du réflexe d'orientation et de l'action du frein externe sur les réactions EEG aux différents stimuli chez l'homme. Electroencephalography and clinical neurophysiology. Supplement **13**: 321-33.
Brazier MAB (1961). A history of the electrical activity of the brain; the first half-century. New York, Macmillan.
Cooley JW, Tukey JW (1965). An algorithm for the machine calculation of complex Fourier series. Mathematics of computation **19**: 297-301.
Kasamatsu A, Hirai T (1966). An electroencephalographic study on the zen meditation (Zazen). Folia psychiatrica et neurologica japonica **20**(4): 315-36.
Pillsbury JA, Meyerowitz S, Salzman LF, Satran R (1967). Electroencephalographic correlates of perceptual style: field orientation. Psychosomatic medicine **29**(5): 441-9.
Cohen D (1968). Magnetoencephalography: evidence of magnetic fields produced by alpha-rhythm currents. Science **161**(843): 784-6.
Celesia GG, Puletti F (1969). Auditory cortical areas of man. Neurology **19**(3): 211-20.
Gloor P, Ed. (1969). Hans Berger on the electroencephalogram of man. Electroencephalography and clinical neurophysiology. New York, Elsevier.
Giannitrapani D (1970). EEG changes under differing auditory stimulations. Archives of general psychiatry **23**(5): 445-53.
Puletti F, Celesia GG (1970). Functional properties of the primary cortical auditory area in man. Journal of neurosurgery **32**(2): 244-7.
Cohen D (1972). Magnetoencephalography: detection of the brain's electrical activity with a superconducting magnetometer. Science **175**(22): 664-6.
Luria AR (1973). The working brain: an introduction to neuropsychology. London, Allen Lane.
Putney RT (1973). Conditioned alpha blocking re-examined with the measurement of individual wave amplitudes. Electroencephalography and clinical neurophysiology **34**(5): 485-93.
Creutzfeldt OD (1974). Neuronal basis of EEG-waves. Handbook of electroencephalography and clinical neurophysiology. Creutzfeldt OD. Amsterdam, Elsevier. **2, part C:** 5-55.
Milstein V (1974). Alpha wave phase and alpha attenuation. Electroencephalography and clinical neurophysiology **37**(2): 167-72.
Brenner D, Williamson SJ, Kaufman L (1975). Visually evoked magnetic fields of the human brain. Science **190**(4213): 480-2.
Celesia GG (1976). Organization of auditory cortical areas in man. Brain **99**(3): 403-14.
Reite M, Zimmerman JE, Edrich J, Zimmerman J (1976). The human magnetoencephalogram: some EEG and related correlations. Electroencephalography and clinical neurophysiology **40**(1): 59-66.
Pfurtscheller G (1977). Graphical display and statistical evaluation of event-related desynchronization (ERD). Electroencephalography and clinical neurophysiology **43**(5): 757-60.
Pfurtscheller G, Aranibar A (1977). Event-related cortical desynchronization detected by power measurements of scalp EEG. Electroencephalography and clinical neurophysiology **42**(6): 817-26.
Ojemann GA (1979). Individual variability in cortical localization of language. Journal of neurosurgery **50**(2): 164-9.

Pfurtscheller G, Aranibar A (1979). Evaluation of event-related desynchronization (ERD) preceding and following voluntary self-paced movement. Electroencephalography and clinical neurophysiology **46**(2): 138-46.

Flanagan JL (1980). Parametric coding of speech spectra. Journal of the Acoustical Society of America **68**(2): 412-9.

Bindman L, Lippold OCJ (1981). The neurophysiology of the cerebral cortex. London, Arnold.

Buchsbaum MS, Kessler R, King A, Johnson J, Cappelletti J (1984). Simultaneous cerebral glucography with positron emission tomography and topographic electroencephalography. Progress in brain research **62**: 263-9.

Mitzdorf U (1985). Current source-density method and application in cat cerebral cortex: investigation of evoked potentials and EEG phenomena. Physiological reviews **65**(1): 37-100.

DeFelipe J, Jones EG (1988). Cajal on the cerebral cortex. New York, Oxford University Press.

Fox PT, Raichle ME, Mintun MA, Dence C (1988). Nonoxidative glucose consumption during focal physiologic neural activity. Science **241**(4864): 462-4.

Petersen SE, Fox PT, Posner MI, Mintun M, Raichle ME (1988). Positron emission tomographic studies of the cortical anatomy of single-word processing. Nature **331**(6157): 585-9.

Creutzfeldt OD, Ojemann GA, Lettich E (1989). Neuronal activity in the human lateral temporal lobe. I. Responses to speech. Experimental brain research **77**(3): 451-75.

Ojemann GA, Ojemann JG, Lettich E, Berger MS (1989). Cortical language localization in left, dominant hemisphere. An electrical stimulation mapping investigation in 117 patients. Journal of neurosurgery **71**(3): 316-26.

Petersen SE, Fox PT, Posner MI, Mintun M, Raichle ME (1989). Positron emission tomographic studies of the processing of single words. Journal of cognitive neuroscience **1**: 153-70.

Ogawa S, Lee TM, Kay AR, Tank DW (1990). Brain magnetic resonance imaging with contrast dependent on blood oxygenation. Proc Natl Acad Sci U S A **87**(24): 9868-72.

Schroeder MR (1991). Fractals, chaos, power laws : minutes from an infinite paradise. New York, W.H. Freeman.

Bandettini PA, Wong EC, Hinks RS, Tikofsky RS, Hyde JS (1992). Time course EPI of human brain function during task activation. Magnetic resonance in medicine **25**(2): 390-7.

Démonet J-F, Chollet F, Ramsay S, Cardebat D, Nespoulous J-L, Wise R, Rascol A, Frackowiak R (1992). The anatomy of phonological and semantic processing in normal subjects. Brain **115 (Pt 6)**: 1753-68.

Kwong KK, Belliveau JW, Chesler DA, Goldberg IE, Weisskoff RM, Poncelet BP, Kennedy DN, et al. (1992). Dynamic magnetic resonance imaging of human brain activity during primary sensory stimulation. Proc Natl Acad Sci U S A **89**(12): 5675-9.

Ogawa S, Tank DW, Menon R, Ellermann JM, Kim SG, Merkle H, Ugurbil K (1992). Intrinsic signal changes accompanying sensory stimulation: functional brain mapping with magnetic resonance imaging. Proc Natl Acad Sci U S A **89**(13): 5951-5.

Pfurtscheller G, Neuper C (1992). Simultaneous EEG 10 Hz desynchronization and 40 Hz synchronization during finger movements. Neuroreport **3**(12): 1057-60.

Zatorre RJ, Evans AC, Meyer E, Gjedde A (1992). Lateralization of phonetic and pitch discrimination in speech processing. Science **256**(5058): 846-9.

Makeig S (1993). Auditory event-related dynamics of the EEG spectrum and effects of exposure to tones. Electroencephalography and clinical neurophysiology **86**(4): 283-93.

Pfurtscheller G, Neuper C, Kalcher J (1993). 40-Hz oscillations during motor behavior in man. Neuroscience letters **164**(1-2): 179-82.

Singer W (1993). Synchronization of cortical activity and its putative role in information processing and learning. Annual reviews of physiology **55**: 349-74.

Berger MS, Deliganis AV, Dobbins J, Keles GE (1994). The effect of extent of resection on recurrence in patients with low grade cerebral hemisphere gliomas. Cancer **74**(6): 1784-91.

Buzsáki G (1994). Temporal coding in the brain. Berlin ; New York, Springer-Verlag.

Démonet J-F, Price C, Wise R, Frackowiak RS (1994). Differential activation of right and left posterior sylvian regions by semantic and phonological tasks: a positron-emission tomography study in normal human subjects. Neurosci Lett **182**(1): 25-8.

Finger S (1994). Origins of neuroscience : a history of explorations into brain function. New York, Oxford University Press.

Jokeit H, Makeig S (1994). Different event-related patterns of gamma-band power in brain waves of fast- and slow-reacting subjects. Proc Natl Acad Sci U S A **91**(14): 6339-43.

Benjamini Y, Hochberg Y (1995). Controlling the False Discovery Rate - a Practical and Powerful Approach to Multiple Testing. Journal of the Royal Statistical Society Series B-Methodological **57**(1): 289-300.

Berger MS (1995). Functional mapping-guided resection of low-grade gliomas. Clinical neurosurgery **42**: 437-52.

Buckner RL, Raichle ME, Petersen SE (1995). Dissociation of human prefrontal cortical areas across different speech production tasks and gender groups. Journal of neurophysiology **74**(5): 2163-73.

Cohen L (1995). Time-frequency analysis. Englewood Cliffs, N.J, Prentice Hall PTR.

Fiez JA, Raichle ME, Miezin FM, Petersen SE, Tallal P, Katz WF (1995). PET studies of auditory and phonological processing - effects of stimulus characteristics and task demands. Journal of cognitive neuroscience **7**(3): 357-75.

Makeig S, Elbert T, Braun C (1995). Magnetic event-related spectral perturbations. Biomagnetism: fundamental research and clinical applications. Baumgartner C. Amsterdam, Elsevier, IOS Press**:** 257-61.

Sinkkonen J, Tiitinen H, Naatanen R (1995). Gabor filters: an informative way for analysing event-related brain activity. Journal of neuroscience methods **56**(1): 99-104.

Tallon C, Bertrand O, Bouchet P, Pernier J (1995). Gamma-range activity evoked by coherent visual stimuli in humans. European journal of neuroscience **7**(6): 1285-91.

Berger MS (1996). Minimalism through intraoperative functional mapping. Clinical neurosurgery **43**: 324-37.

Binder JR, Frost JA, Hammeke TA, Rao SM, Cox RW (1996). Function of the left planum temporale in auditory and linguistic processing. Brain **119 (Pt 4)**: 1239-47.

Maciunas RJ, Berger MS, Copeland B, Mayberg MR, Selker R, Allen GS (1996). A technique for interactive image-guided neurosurgical intervention in primary brain tumors. Neurosurgery clinics of North America **7**(2): 245-66.

Ojemann JG, Miller JW, Silbergeld DL (1996). Preserved function in brain invaded by tumor. Neurosurgery **39**(2): 253-8; discussion 258-9.

Skirboll SS, Ojemann GA, Berger MS, Lettich E, Winn HR (1996). Functional cortex and subcortical white matter located within gliomas. Neurosurgery **38**(4): 678-84; discussion 684-5.

Tallon-Baudry C, Bertrand O, Delpuech C, Pernier J (1996). Stimulus specificity of phase-locked and non-phase-locked 40 Hz visual responses in human. Journal of neuroscience **16**(13): 4240-9.

Zatorre RJ, Meyer E, Gjedde A, Evans AC (1996). PET studies of phonetic processing of speech: review, replication, and reanalysis. Cerebral cortex **6**(1): 21-30.

Crone NE, Miglioretti DL, Gordon B, Lesser RP (1998). Functional mapping of human sensorimotor cortex with electrocorticographic spectral analysis. II. Event-related synchronization in the gamma band. Brain **121 (Pt 12)**: 2301-15.

Jacobson GP, Henderson J, Smith BJ, Elisevich KV (1998). High resolution recording of late cortical surface potentials N1 and gamma band response (GBR). Journal of the American Academy of Audiology **9**(2): 87-94.

Sadato N, Nakamura S, Oohashi T, Nishina E, Fuwamoto Y, Waki A, Yonekura Y (1998). Neural networks for generation and suppression of alpha rhythm: a PET study. Neuroreport **9**(5): 893-7.

Hoge RD, Atkinson J, Gill B, Crelier GR, Marrett S, Pike GB (1999). Linear coupling between cerebral blood flow and oxygen consumption in activated human cortex. Proc Natl Acad Sci U S A **96**(16): 9403-8.

Pfurtscheller G (1999). EEG event-related desynchronization (ERD) and event-related synchronization (ERS). Electroencephalography : basic principles, clinical applications, and related fields. Niedermeyer E and Lopes da Silva F. Baltimore ; London, Williams & Wilkins**:** 958-67.

Tatsumi IF, Fushimi T, Sadato N, Kawashima R, Yokoyama E, Kanno I, Senda M (1999). Verb generation in Japanese--A multicenter PET activation study. Neuroimage **9**(1): 154-64.

Ames A, 3rd (2000). CNS energy metabolism as related to function. Brain research reviews **34**(1-2): 42-68.

Bertrand O, Tallon-Baudry C (2000). Oscillatory gamma activity in humans: a possible role for object representation. International journal of psychophysiology **38**(3): 211-23.

Binder JR, Frost JA, Hammeke TA, Bellgowan PS, Springer JA, Kaufman JN, Possing ET (2000). Human temporal lobe activation by speech and nonspeech sounds. Cerebral cortex **10**(5): 512-28.

Curio G (2000). Linking 600-Hz "spikelike" EEG/MEG wavelets ("sigma-bursts") to cellular substrates: concepts and caveats. Journal of clinical neurophysiology **17**(4): 377-96.

Finger S (2000). Minds behind the brain : a history of the pioneers and their discoveries. Oxford ; New York, Oxford University Press.

Rorden C, Brett M (2000). Stereotaxic display of brain lesions. Behavioural neurology **12**(4): 191-200.

Tervaniemi M, Medvedev SV, Alho K, Pakhomov SV, Roudas MS, Van Zuijen TL, Näätänen R (2000). Lateralized automatic auditory processing of phonetic versus musical information: a PET study. Human brain mapping **10**(2): 74-9.

Attwell D, Laughlin SB (2001). An energy budget for signaling in the grey matter of the brain. Journal of cerebral blood flow and metabolism **21**(10): 1133-45.

Crone NE, Boatman D, Gordon B, Hao L (2001a). Induced electrocorticographic gamma activity during auditory perception. Brazier Award-winning article, 2001. Clinical neurophysiology **112**(4): 565-82.

Crone NE, Hao L, Hart J, Jr., Boatman D, Lesser RP, Irizarry R, Gordon B (2001b). Electrocorticographic gamma activity during word production in spoken and sign language. Neurology **57**(11): 2045-53.

Logothetis NK, Pauls J, Augath M, Trinath T, Oeltermann A (2001). Neurophysiological investigation of the basis of the fMRI signal. Nature **412**(6843): 150-7.

Goldman RI, Stern JM, Engel J, Jr., Cohen MS (2002). Simultaneous EEG and fMRI of the alpha rhythm. Neuroreport **13**(18): 2487-92.

Lewicki MS (2002). Efficient coding of natural sounds. Nature neuroscience **5**(4): 356-63.

Makeig S, Westerfield M, Jung TP, Enghoff S, Townsend J, Courchesne E, Sejnowski TJ (2002). Dynamic brain sources of visual evoked responses. Science **295**(5555): 690-4.

Foucher JR, Otzenberger H, Gounot D (2003). The BOLD response and the gamma oscillations respond differently than evoked potentials: an interleaved EEG-fMRI study. BMC Neurosci **4**: 22-.

Laufs H, Kleinschmidt A, Beyerle A, Eger E, Salek-Haddadi A, Preibisch C, Krakow K (2003). EEG-correlated fMRI of human alpha activity. Neuroimage **19**(4): 1463-76.

Lennie P (2003). The cost of cortical computation. Current biology **13**(6): 493-7.
Moosmann M, Ritter P, Krastel I, Brink A, Thees S, Blankenburg F, Taskin B, Obrig H, Villringer A (2003). Correlates of alpha rhythm in functional magnetic resonance imaging and near infrared spectroscopy. Neuroimage **20**(1): 145-58.
Nichols T, Hayasaka S (2003). Controlling the familywise error rate in functional neuroimaging: a comparative review. Statistical methods in medical research **12**(5): 419-46.
Ray S, Jouny CC, Crone NE, Boatman D, Thakor NV, Franaszczuk PJ (2003). Human ECoG analysis during speech perception using matching pursuit: a comparison between stochastic and dyadic dictionaries. IEEE transactions on biomedical engineering **50**(12): 1371-3.
Singh NC, Theunissen FE (2003). Modulation spectra of natural sounds and ethological theories of auditory processing. Journal of the Acoustical Society America **114**(6 Pt 1): 3394-411.
Boatman D (2004). Cortical bases of speech perception: evidence from functional lesion studies. Cognition **92**(1-2): 47-65.
Bruns A (2004). Fourier-, Hilbert- and wavelet-based signal analysis: are they really different approaches? Journal of neuroscience methods **137**(2): 321-32.
Delorme A, Makeig S (2004). EEGLAB: an open source toolbox for analysis of single-trial EEG dynamics including independent component analysis. Journal of neuroscience methods **134**(1): 9-21.
Indefrey P, Cutler A (2004). Prelexical and lexical processing in listening. The cognitive neurosciences. Gazzaniga MS. Cambridge, Mass., MIT Press**:** 759-74.
Oakes TR, Pizzagalli DA, Hendrick AM, Horras KA, Larson CL, Abercrombie HC, Schaefer SM, Koger JV, Davidson RJ (2004). Functional coupling of simultaneous electrical and metabolic activity in the human brain. Human brain mapping **21**(4): 257-70.
Wilson SM, Saygin AP, Sereno MI, Iacoboni M (2004). Listening to speech activates motor areas involved in speech production. Nature neuroscience **7**(7): 701-2.
Brovelli A, Lachaux JP, Kahane P, Boussaoud D (2005). High gamma frequency oscillatory activity dissociates attention from intention in the human premotor cortex. Neuroimage **28**(1): 154-64.
Edwards E, Soltani M, Deouell LY, Berger MS, Knight RT (2005). High gamma activity in response to deviant auditory stimuli recorded directly from human cortex. Journal of neurophysiology **94**(6): 4269-80.
Feige B, Scheffler K, Esposito F, Di Salle F, Hennig J, Seifritz E (2005). Cortical and subcortical correlates of electroencephalographic alpha rhythm modulation. Journal of neurophysiology **93**(5): 2864-72.
Jenkinson M, Pechaud M, Smith S (2005). BET2: MR-based estimation of brain, skull and scalp surfaces. 11th International conference on functional mapping of the human brain.
Liebenthal E, Binder JR, Spitzer SM, Possing ET, Medler DA (2005). Neural substrates of phonemic perception. Cerebral cortex **15**(10): 1621-31.
Mukamel R, Gelbard H, Arieli A, Hasson U, Fried I, Malach R (2005). Coupling between neuronal firing, field potentials, and fMRI in human auditory cortex. Science **309**(5736): 951-4.
Niessing J, Ebisch B, Schmidt KE, Niessing M, Singer W, Galuske RA (2005). Hemodynamic signals correlate tightly with synchronized gamma oscillations. Science **309**(5736): 948-51.
Canolty RT, Edwards E, Dalal SS, Soltani M, Nagarajan SS, Kirsch HE, Berger MS, Barbaro NM, Knight RT (2006). High gamma power is phase-locked to theta oscillations in human neocortex. Science **313**(5793): 1626-8.
Drobyshevsky A, Baumann SB, Schneider W (2006). A rapid fMRI task battery for mapping of visual, motor, cognitive, and emotional function. Neuroimage **31**(2): 732-44.